

Brine Availability Test in Salt (BATS) FY21 Update

Spent Fuel and Waste Disposition

Prepared for:

**US Department of Energy
Office of Nuclear Energy
Office of Spent Fuel and Waste Disposition
Office of Spent Fuel and Waste Science and Technology**

Prepared by:

Sandia National Laboratories

Kris Kuhlman, Melissa Mills, Richard Jayne, Ed Matteo,
Courtney Herrick, Martin Nemer, Yongliang Xiong,
Charles Choens, Matt Paul

Los Alamos National Laboratory

Phil Stauffer, Hakim Boukhalfa, Eric Gultinan, Thom Rahn,
Doug Weaver, Shawn Otto, Jon Davis

Lawrence Berkeley National Laboratory

Jonny Rutqvist, Yuxin Wu, Mengsu Hu,
Sebastian Uhlemann, Jiannan Wang

August 31, 2021

M2SF-21SN010303052 SAND2021-10962 R

DISCLAIMER

This information was prepared as an account of work sponsored by an agency of the U.S. Government. Neither the U.S. Government nor any agency thereof, nor any of their employees, makes any warranty, expressed or implied, or assumes any legal liability or responsibility for the accuracy, completeness, or usefulness, of any information, apparatus, product, or process disclosed, or represents that its use would not infringe privately owned rights. References herein to any specific commercial product, process, or service by trade name, trade mark, manufacturer, or otherwise, does not necessarily constitute or imply its endorsement, recommendation, or favoring by the U.S. Government or any agency thereof. The views and opinions of authors expressed herein do not necessarily state or reflect those of the U.S. Government or any agency thereof.



**Sandia
National
Laboratories**

Sandia National Laboratories is a multimission laboratory managed and operated by National Technology & Engineering Solutions of Sandia LLC, a wholly owned subsidiary of Honeywell International Inc., for the U.S. Department of Energy's National Nuclear Security Administration under contract DE-NA0003525.



ABSTRACT

This report summarizes the 2021 fiscal year (FY21) status of ongoing borehole heater tests in salt funded by the disposal research and development (R&D) program of the Office of Spent Fuel & Waste Science and Technology (SFWST) of the US Department of Energy's Office of Nuclear Energy's (DOE-NE) Office of Spent Fuel and Waste Disposition (SFWD). This report satisfies SFWST milestone M2SF-21SN010303052 by summarizing test activities and data collected during FY21. The Brine Availability Test in Salt (BATS) is fielded in a pair of similar arrays of horizontal boreholes in an experimental area at the Waste Isolation Pilot Plant (WIPP). One array is heated, the other unheated. Each array consists of 14 boreholes, including a central borehole with gas circulation to measure water production, a cement seal exposure test, thermocouples to measure temperature, electrodes to infer resistivity, a packer-isolated borehole to add tracers, fiber optics to measure temperature and strain, and piezoelectric transducers to measure acoustic emissions. The key new data collected during FY21 include a series of gas tracer tests (BATS phase 1b), a pair of liquid tracer tests (BATS phase 1c), and data collected under ambient conditions (including a period with limited access due to the ongoing pandemic) since BATS phase 1a in 2020. A comparison of heated and unheated gas tracer test results clearly shows a decrease in permeability of the salt upon heating (i.e., thermal expansion closes fractures, which reduces permeability).

VERSION INFO

This report is an update of the as-built description of the project and the first phase data, which are found in more details in the FY20 report (SAND2020-9034R). The 2020 report presents the final as-built description of the arrays and the first phase of operational data (BATS phase 1a, January to March 2020) from the BATS field test.

Date	Version
Aug 31, 2021	Version for DOE-NE review (SNL Programmatic review: 1355567)
Sep 7, 2021	Version approved for external release (only formatting differences to Aug 31 version) SAND2021-10962 R

ACKNOWLEDGEMENTS

The project is financially supported by the Disposal R&D program of DOE-NE's SFWST office. We acknowledge assistance from the following: the Nuclear Waste Partnership (NWP); Waste Isolation Pilot Plant (WIPP) underground facilities personnel, who provide underground access, power infrastructure, and drilling support; and the DOE Office of Environmental Management (DOE-EM) Carlsbad Field Office (CBFO) chief scientist, George Basabilvaso, whom the Test Coordination Office (TCO) works for. The authors thank Jason Heath of Sandia National Laboratories (SNL) for providing a careful technical review of the entire document.

CONTENTS

ACRONYMS	viii
1. Background and Test Overview	1
1.1 Motivation for BATS	1
1.2 BATS Phases.....	2
1.3 BATS Field Test Components	3
2. Test Design Details.....	5
2.1 Heater Test Phases and Tracers.....	6
2.2 D – (Tracer Source) borehole.....	6
2.2.1 Gas tracers.....	6
2.2.2 Liquid tracers	7
3. Summary of BATS Data: January 2020 to August 2021	8
3.1 HP – Heater/Packer Boreholes.....	8
3.1.1 Gas stream pressure and flowrate time series	9
3.1.2 Water content time series.....	10
3.1.3 Water isotopic composition time series	13
3.1.4 Gas composition time series	14
3.1.5 Borehole closure gauge time series.....	15
3.1.6 Heater power and temperature time series	15
3.2 AE – Acoustic Emission Time Series	15
3.2.1 Unheated array – 60 versus 40 dB preamplification gain	16
3.3 T – Temperature Time Series.....	19
3.4 E – Apparent Resistivity Results.....	21
3.4.1 ERT monitoring results.....	23
3.4.2 Heating and tracer tests May to July 2021	24
3.5 SM – Liquid Sample Boreholes	27
3.5.1 Air temperature and RH time series.....	27
3.6 SL – Seal Borehole Time Series and Test Results.....	27
3.6.1 Air temperature and RH time series.....	27
3.6.2 Strain and temperature time series	28
3.6.3 Salt, brine, and cementitious material interactions analysis	29
3.7 In-Drift Time Series	29
4. BATS Phase 1b Gas Tracer Tests: January to June 2021.....	31
5. BATS Phase 1c Liquid Tracer Tests: July to August 2021	37
5.1 Water Production Data During Heating.....	37
5.2 AE Observations During May to Aug 2021 Heating Events	42
6. Planned Post-Test Analyses.....	44
6.1 Borehole Precipitate Analysis.....	44
6.2 Salt Sampling via Over-Core	44

7.	Summary.....	45
8.	References	46
A-1.	Appendix: Tabular Data	48

LIST OF FIGURES

Figure 1.	Layout of boreholes and in-drift equipment in N-940 (view looking south).	3
Figure 2.	WIPP underground map. BATS phase 1a location indicated with red circle. BATS 1s shakedown test location indicated with blue star. Drift widths not to same scale as repository layout.	4
Figure 3.	As-built locations and orientations of boreholes in the eastern unheated (top) and the western heated (bottom) arrays.....	5
Figure 4.	Gas tracer test plumbing.	7
Figure 5.	Gas plumbing for BATS phases 1b and 1c (removed hydrocarbon trap and moved existing LI-COR and added second LI-COR compared to BATS phase 1a).	9
Figure 6.	Gas stream mass flowrates up- and down-stream of HP packer for heated (H) and unheated (U) arrays.....	9
Figure 7.	Gas stream pressure and temperature downstream of HP packer.	10
Figure 8.	Raw LI-COR water concentration (Jan to Mar 2020 data are switched, after April 2020, dedicated LI-COR instruments are located before solenoids).	11
Figure 9.	RH up- (red) and down-stream (green) of the heated (left) and unheated (right) desiccant.	11
Figure 10.	Desiccant water production data.....	12
Figure 11.	Water production computed from RH and gas flowrate compared to desiccant-based observations.	12
Figure 12.	Picarro CRDS raw data.....	13
Figure 13.	Heated (left) and unheated (right) array Picarro CRDS data.....	14
Figure 14.	Change in HP borehole diameter measured by LVDT.....	15
Figure 15.	Total number of AE hits and daily rate per array for the unheated array. Top row is 60 dB gain. Bottom row is 40 dB gain.	17
Figure 16.	Energy (left) and frequency (right) content of AE from the unheated array. Top row is 60 dB gain, bottom row is 40 dB gain.	18
Figure 17.	Located events for unheated array for April 26 to May 2 (60 dB gain), blue, and May 3 to May 10 (40 dB gain), red. The image is looking south into unheated array.	19
Figure 18.	Thermocouple and heater power data from heated array.	20
Figure 19.	Thermocouple data from unheated array.....	21
Figure 20.	Data overview showing temperature in the ERT boreholes (top panel), mean injection current (central panel) and mean measured resistance (bottom panel, solid line) as well	

as stacking errors (dashed line). Data gaps due to interruptions in the experiment are highlighted. 22

Figure 21. Raw data time-series for the unheated array. Measured resistances show stable conditions, while changes with regards to the baseline measurements highlight episodes of short-term disturbances. The entire data set (bottom panel) shows a generally increasing resistivity trend. 23

Figure 22. Raw data time-series for the heated array. Measured resistances show stable conditions, while changes with regards to the baseline measurements highlight episodes of heating and brine leakage. The strong change during the middle of the experiment relates to a period where multiple permeability tests were conducted. The entire data set (bottom panel) shows a generally decreasing resistivity trend. 24

Figure 23. 3D resistivity models showing the change in both arrays during heating and tracer tests in Summer 2021. Top panel shows the resistivity variation in the heated plot for 3 different areas within the studied domain, as well as the temperature recorded in the heated borehole. The other temperature sensors failed during this experiment. A-D show 3D changes in resistivity. 26

Figure 24. Air temperature (left) and relative humidity (right) for SM boreholes. 27

Figure 25. Air temperature (left) and relative humidity (right) for SL boreholes during BATS 1a. 28

Figure 26. Strain and temperature inside cement plugs in SL borehole. 29

Figure 27. In-drift air temperature (top left), relative humidity (top right), barometric pressure (bottom left), and air speed (bottom right). 30

Figure 28. Gas tracer test 1 results in unheated array. 32

Figure 29. Gas tracer test 3 results (unheated) in heated array. 33

Figure 30. Gas tracer test 4 results (unheated) in heated array. 34

Figure 31. Gas tracer test 5 results (heated) in heated array. 35

Figure 32. RH observed in SM boreholes during tracer testing activities 36

Figure 33. All gas tracer test source borehole pressure responses. 36

Figure 34. Temperature response of thermocouples in heated array during heated tracer test. 38

Figure 35. Multiparameter flowmeter, LI-COR 850, and RH data during heated gas and liquid tracer tests 40

Figure 36. Picarro CRDS data during heated tracer tests. 41

Figure 37. Total number of AE hits and daily rate per array during May to July 2021 heater test. Orange lines represent heating phases in the borehole; blue lines represent cooling phases. 42

Figure 38. Energy (left) and frequency (right) content of AE from May to July 2021 heater test. 43

Figure 39. Event localizations of May to July 2021 heater test showing sensors, black cones, and event, colored spheres. Color scale shows time progression, with red colors representing May 10 and green representing July 26. 43

LIST OF TABLES

Table 1. Summary of BATS phase 1a boreholes.....	3
Table 2. Gas tracer test statistics.....	31
Table 3. Key events during 2021 heated tracer tests.....	39
Table 4. Desiccant water production data for heated array.....	48
Table 5. Desiccant water production data for unheated array.....	51
Table 6. BATS TCO Events through July 2021	54

ACRONYMS

AE	acoustic emissions	LVDT	linear variable differential transformer
BATS	Brine Availability Test in Salt	MU-3	map unit 3 (WIPP stratigraphic unit) – also MU-1 through MU-5
CBFO	Carlsbad Field Office (DOE-EM WIPP office)	NETL	National Energy Technology Laboratory
COVID-19	coronavirus disease of 2019	NWP	Nuclear Waste Partnership (WIPP operations contractor)
CRDS	cavity ring-down spectrometer	PA	performance assessment
CT	computed tomography	R&D	research and development
DEC	double-ended cylinder	RH	relative humidity
DOE	Department of Energy	SDI	Salt Disposal Investigations (proposed CBFO program)
DOE-EM	DOE Office of Environmental Management	SFWST	Spent Fuel & Waste Science and Technology (DOE-NE program)
DOE-NE	DOE Office of Nuclear Energy	SNL	Sandia National Laboratories
DRZ	disturbed rock zone (equivalent to EDZ)	SRS	Stanford Research Systems
DSS	distributed strain sensing	TCO	WIPP Test Coordination Office
DTS	distributed temperature sensing	TGA	thermogravimetric analysis
EDZ	excavation damaged zone	THMC	thermal-hydrological-mechanical-chemical
EdZ	excavation disturbed zone	UHP	ultra-high purity (99.999%)
ERT	electrical resistivity tomography	US	United States
FY	fiscal year (October-September)	WIPP	Waste Isolation Pilot Plant (DOE-EM site, managed by CBFO)
GWB	G-seep WIPP brine	XRF	X-ray fluorescence
LANL	Los Alamos National Laboratory		
LBNL	Lawrence Berkeley National Laboratory		

BRINE AVAILABILITY TEST IN SALT FY21 UPDATE

This fiscal year 2021 (FY21) report presents data collected from the Brine Availability Test in Salt (BATS) field test. The test is funded by the US Department of Energy's Office of Nuclear Energy (DOE-NE) Spent Fuel and Waste Disposition Program, under the disposal research and development (R&D) program of the Office of Spent Fuel & Waste Science and Technology (SFWST). The test is located underground at the Waste Isolation Pilot Plant (WIPP), a DOE Office of Environmental Management (DOE-EM) site managed by the Carlsbad Field Office (CBFO).

The high-level test plan by Stauffer et al. (2015) places BATS in the context of a multi-year testing strategy, which involves testing a range of processes at multiple scales, eventually culminating in a drift-scale disposal demonstration. The organization of the current phases of the BATS field test is outlined in "*Project Plan: Salt In-Situ Heater Test*" (SNL et al., 2020), and a plan for upcoming years is proposed in "*Brine Availability Test in Salt (BATS) Extended Plan for Experiments at the Waste Isolation Pilot Plant (WIPP)*" (Kuhlman et al., 2021).

An early conceptual design of the BATS field test was laid out in Kuhlman et al. (2017), which includes appendices with detailed references to previous salt field tests and provides context and motivation for the individual test components of BATS. This level-2 milestone report presents new data collected in FY21. More details on the as-built state of the BATS experiment can be found in the FY20 milestone report "*FY20 Update on Brine Availability Test in Salt*" (Kuhlman et al., 2020). This report presents both a high-level summary of all data collected since January 2020 and a more detailed discussion of specific tracer test activities conducted in FY21.

1. Background and Test Overview

1.1 Motivation for BATS

The focus of the BATS field test is brine availability in salt. These field tests are the first part of a wider systematic multi-year field investigation campaign to improve the existing long-term repository safety case for disposal of heat-generating radioactive waste in salt. BATS seeks to better understand how much brine can flow into an excavation (e.g., borehole or room) in salt. Brine availability is important to the long-term repository safety case for radioactive waste disposal in salt (Kuhlman & Sevougian, 2013) because: 1) brine can facilitate transport of radionuclides off-site, 2) brine can corrode metallic and glass waste forms or waste packages, 3) chlorine in brine absorbs neutrons, reducing in-package nuclear criticality hazards, and 4) accumulated brine in an excavation undergoing creep closure can provide back-pressure that resists ultimate creep closure and sealing of a repository excavation. Future different field tests under the wider field campaign will explore other performance aspects of the long-term repository safety case that are separate from the focus of the current BATS field test.

In a generic salt repository for "hot" radioactive waste (i.e., above brine boiling temperature at the waste package surface), an area around the waste packages will dry out once water vapor is driven away. Additional bound water in hydrous evaporite minerals may become mobile upon heating, and thermal expansion of intergranular brine located away from the excavation in the host salt may cause thermal pressurization, driving brine towards lower pressure excavations. If conditions are right, a small-scale heat pipe convection process can set up in high-permeability partially liquid-saturated regions around waste (Jordan et al., 2015). The heat pipe includes salt precipitation near the waste package and salt dissolution where steam condenses as fresh water away from the heat source. The conceptual model is that eventually creep closure reconsolidates any granular salt backfill, closes gaps around waste packages, and heals the Excavation Damaged Zone (EDZ) or Excavated disturbed Zone (EdZ; the EDZ and EdZ are discussed below) associated with access drifts to create a relatively dry, low-porosity, low-permeability zone around the waste packages (Blanco-Martín et al., 2018). Knowledge of brine availability and brine composition facilitates understanding the following key performance aspects of the repository system: the

amount and distribution of brine that flows to an excavation, as well as the long-term behavior of brine around waste packages that affects transport (e.g., brine-radionuclide interactions); and the resistance to creep closure from accumulated brine that does not flow away from the repository excavation. The interplay of brine availability and complex coupled thermal-hydrological-mechanical-chemical (THMC) processes controls the extent and timing of ultimate closure.

In undisturbed geologic salt systems, the ultra-low permeability and porosity of salt (Beauheim & Roberts, 2002) provides the primary natural barrier to contain radioactive waste over performance assessment (PA) relevant time scales (10^4 to 10^6 years). However, near-field conditions (e.g., fluid pressures, liquid saturation, and chemical composition) and processes (e.g., brine and gas flow, precipitation and dissolution of salt, thermal expansion and contraction of salt and brine, and salt creep) can impact releases in disturbed scenarios and are the initial conditions for a long-term PA simulation. BATS is focused on understanding processes necessary to quantify inflow rates and brine composition in the near-field (i.e., at scales of cm to m from the heat source) with the aim to improve: 1) our understanding and observations of coupled THMC processes affecting prediction of near-field conditions; 2) conceptual models of near-field behavior that inform the safety case; and 3) the numerical models, constitutive relationships, and parameterizations that are implemented in PA models.

Brine availability in a salt repository depends on both the distribution of water in the host salt geologic formation and the flow and transport properties of the EDZ or EdZ surrounding an excavation (Kuhlman & Malama, 2013; Kuhlman, 2019). Note that we may use the generic term “water” to refer to the aqueous liquid that may range in total dissolved solids from fresh water to brine, as heating processes and condensation may alter the TDS of the aqueous liquid, and we may also use “water” to refer to the molecule itself—the specific context should make the usage clear. The EDZ is a region surrounding excavations where the salt is damaged, and both its material properties (i.e., porosity and permeability) and state or potential energy (i.e., pressure, stress, or temperature) have changed—note that the EDZ is often equivalently called the disturbed rock zone (DRZ). The EdZ is a larger region surrounding the EDZ, where only the variables in the governing equations are disturbed. The distribution of water molecules in the system includes the following: bound water that is both liquid or structural in the salt formation (i.e., brine in clay, intragranular brine, intergranular brine, and hydrous minerals; Roedder, 1984); and water in both the liquid and gas phases before and during emplacement of heat-generating radioactive waste, which is affected by heating processes, evaporation, and condensation. The primary EDZ property of interest for the BATS field test is the distribution and evolution of mechanical damage (i.e., porosity, permeability, and nature of induced fractures) around the access drift and test boreholes, which provides the primary path for flow towards the test boreholes.

1.2 BATS Phases

The preliminary “shakedown” test location of BATS was in drift E-140 of WIPP, utilizing existing boreholes. Referred to as BATS 1s (see Figure 1 and Figure 2), it was performed June 2018 through April 2019 (Boukhalfa et al., 2019; Guiltinan et al., 2020).

The BATS 1a phase began with new horizontal borehole arrays—for heated and unheated testing, respectively—drilled in the Salt Disposal Investigation (SDI) area drifts (on the south side of N-940 west of E-540; see Figure 1 and Figure 2) of WIPP. Follow-on borehole tests (e.g., BATS phase 2) are planned to use slightly different arrangements to what is presented here, based on lessons learned from the BATS 1s and BATS 1a phases of testing.

Specifically, BATS phase 1a refers to testing that occurred from January to March 2020 and involved data collection from both the heated and unheated arrays. BATS phases 1b and 1c began in January 2021 and involved addition of gas (1b) and liquid (1c) tracers in the same heated and unheated boreholes of the BATS 1a location. BATS phase 2 is being planned to use the BATS 1a unheated array, while drilling a new heated array in the same drift.

1.3 BATS Field Test Components

Several aspects of the BATS 1s field test were demonstrated and refined as part of an informal shakedown test (Boukhalifa et al., 2018; Boukhalifa et al., 2019; Guiltinan et al., 2020). These included the dry N₂ gas circulation system, the custom-fabricated borehole closure gauge, the use of Drierite desiccant to quantify water production, the LI-COR 850 CO₂/H₂O analyzer, the Stanford Research Systems (SRS) QMS-200 quadrupole mass spectrometer gas analyzer, the packer-isolated heater and gas circulation system, brine sampling techniques, the grouting of thermocouples, and several revisions of the heater design.

The western test array of BATS phase 1a is heated (heater in central HP borehole; Figure 3, bottom image) and the eastern array is a similar layout, but unheated (Figure 3, top image). Each array is configured with similar instruments in the central HP borehole and the surrounding satellite boreholes (Table 1). Temperature distribution, strain, and brine movement are monitored with thermocouples, fiber-optic distributed strain sensing (DSS) and temperature sensing (DTS), acoustic emissions (AE) monitoring and electrical resistivity tomography (ERT). To quantify parameters affecting advection of fluids, liquid and gas phase tracers were introduced and sampled from different boreholes.

Table 1. Summary of BATS phase 1a boreholes.

Type	Purpose	Boreholes per array	Diameter [in]	Length [ft]	Isolation Device
HP	Heater, packer, borehole closure, N ₂ circulation, gas sampling, gas permeability testing	1	4.8	12	Inflatable packer
D	Tracer source, gas permeability testing	1	2.1	15	Inflatable packer
SM	Liquid sampling	1	2.1	15	Mechanical packer
F	Fiber-optic temperature and strain	2	1.75	18 & 30	Grouted
E	Electrical resistivity tomography (ERT) electrodes	3	1.75	18	Grouted
AE	Acoustic emissions (AE) and ultrasonic travel-time tomography sensors	3	2.1	9	Sensors on borehole wall w/ decentralizer
T	Thermocouples	2	1.75	18	Grouted
SL	Cement seals behind mechanical packers with embedded strain gauges and thermistors	1	4.8	8	Mechanical packer

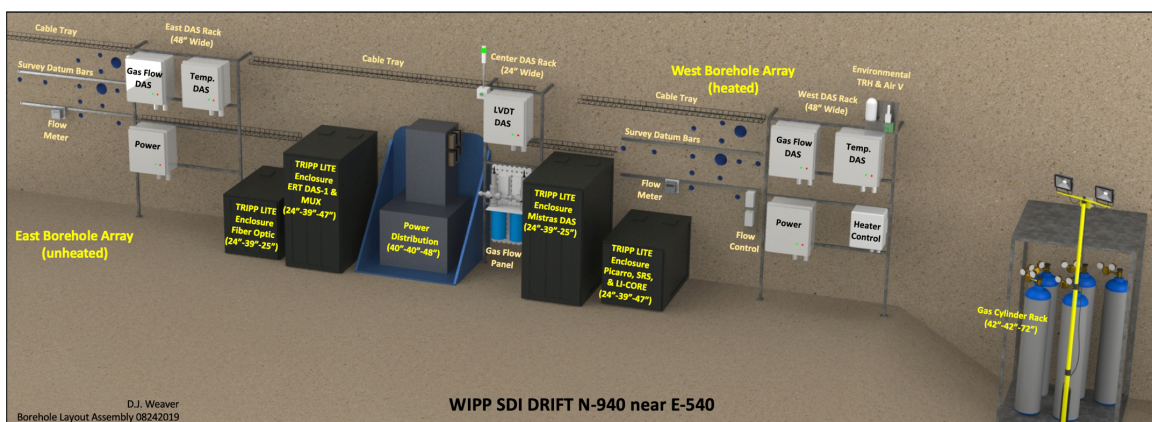


Figure 1. Layout of boreholes and in-drift equipment in N-940 (view looking south).

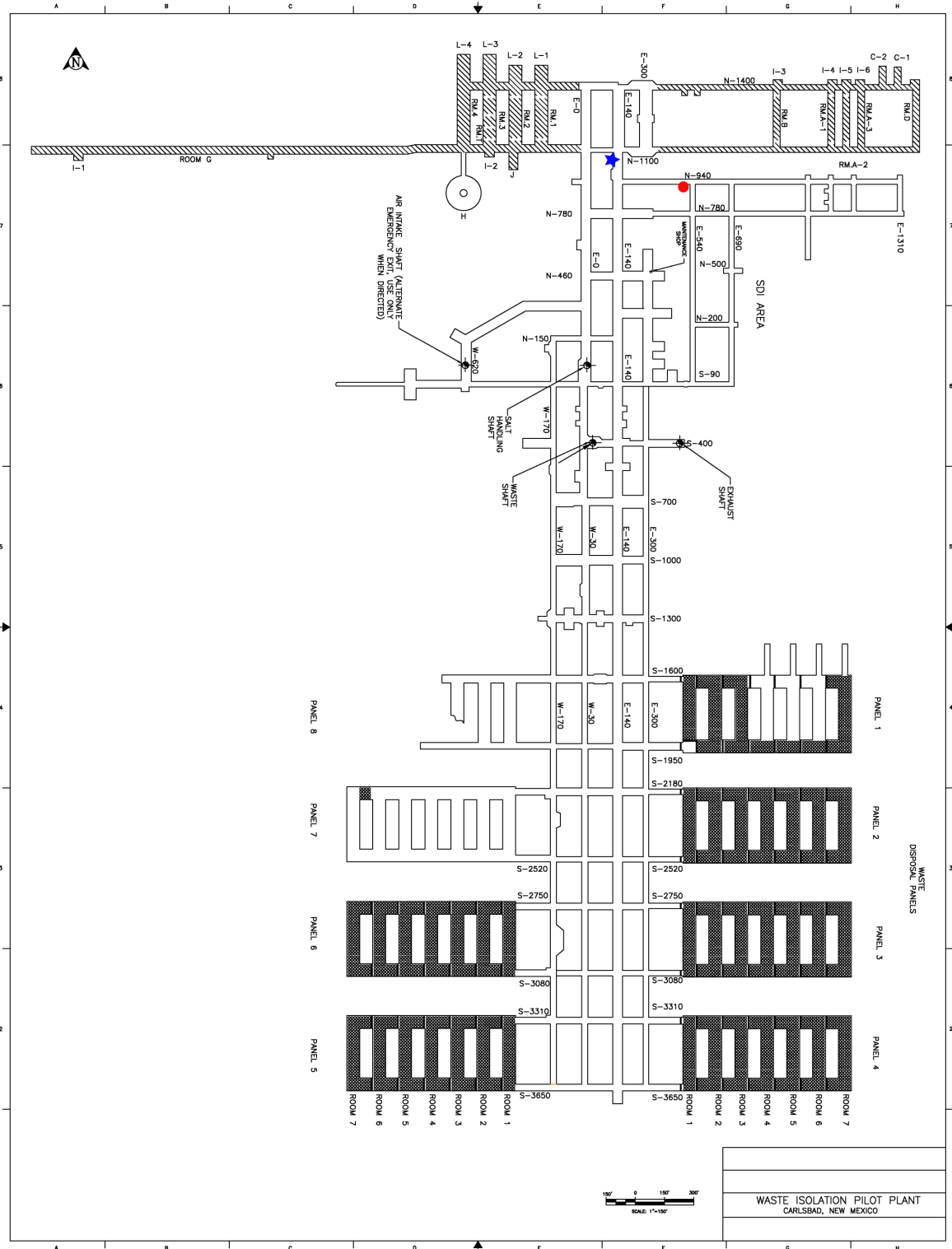


Figure 2. WIPP underground map. BATS phase 1a location indicated with red circle. BATS 1s shakedown test location indicated with blue star. Drift widths not to same scale as repository layout.

2. Test Design Details

The following testing methods relate to gas and liquid tracer testing of BATS phases 1b and 1c in the heated and unheated arrays at the BATS 1a location (see drift location in Figure 1; see Section 1.2 for discussion of the testing phases of BATS). The as-built details of the boreholes and more information on BATS phase 1a data are reported in last year's milestone report (Kuhlman et al., 2020).

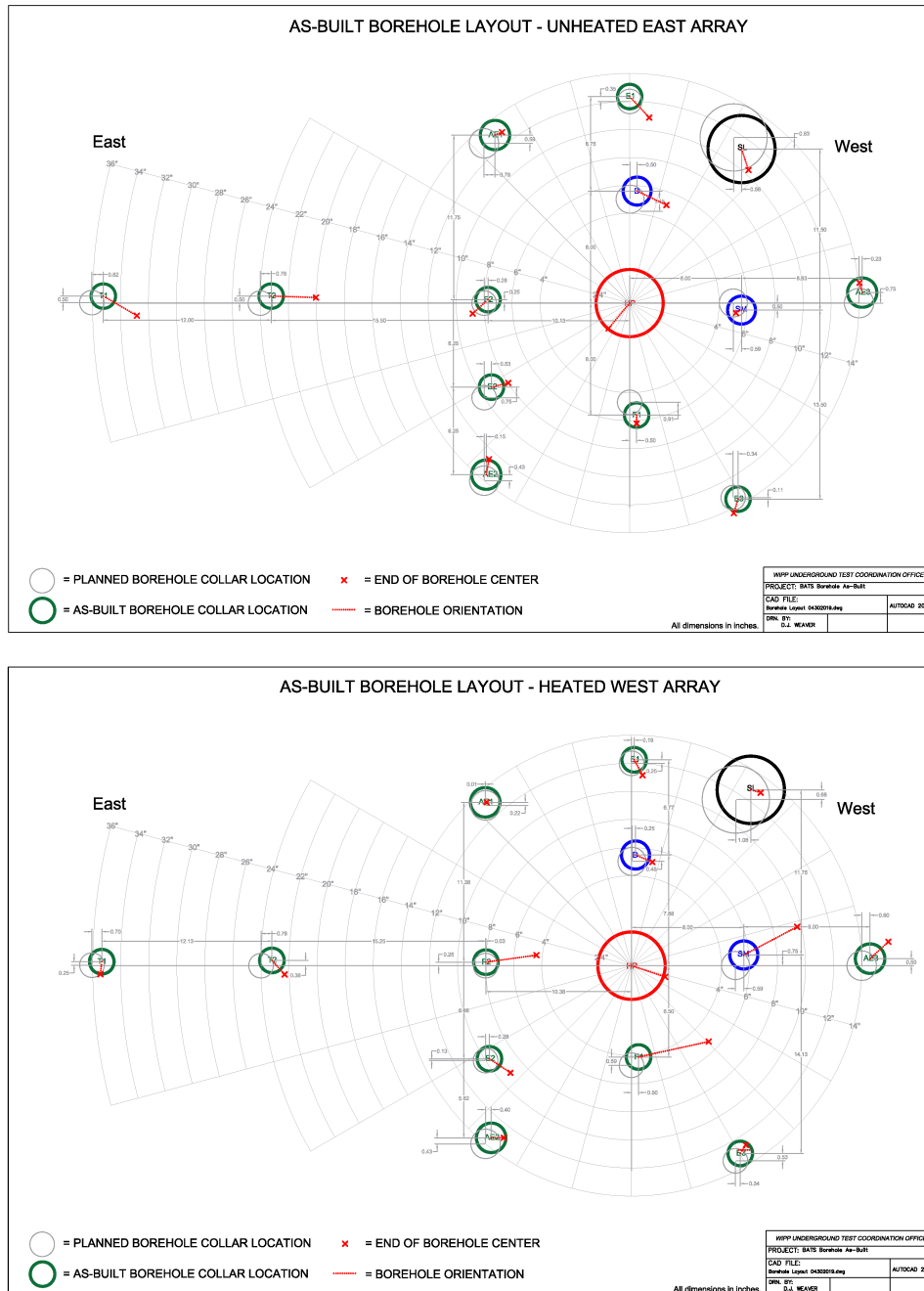


Figure 3. As-built locations and orientations of boreholes in the eastern unheated (top) and the western heated (bottom) arrays.

2.1 Heater Test Phases and Tracers

The BATS phase 1a test was conducted from January to March 2020 in the heated and unheated arrays simultaneously. This first phase heater test did not involve liquid or gas tracers. BATS phase 1a heated the salt for approximately one month (mid-January to mid-February 2020), followed by a two-week cool-down period. This heater test was cut shorter than initially planned to work around a week-long power shutdown of the WIPP underground to change power delivery infrastructure.

There was a significant limitation in access to the WIPP underground associated with the coronavirus disease of 2019 (COVID-19) pandemic. The WIPP Test Coordination Office (TCO) maintained access to the underground, but the limited ability to travel to Carlsbad and WIPP by team members from Albuquerque, Los Alamos, or Berkeley made it more difficult to execute the tests.

BATS phase 1b gas tracer testing began in January 2021. A series of unheated gas tracer tests were conducted in both the heated and unheated array locations before the second major heated test in the heated array. Pressure decay was monitored in the source borehole and gas concentrations were monitored in the gas circulation behind the central (HP) borehole.

For the subsequent (third) heater test phase (BATS phase 1c) liquid tracers were added behind the packer in the D boreholes in both arrays. First, liquid tracers were added to the unheated array, then the heated array, but the unheated test was not completed before the start of the heated tracer test. The heater was planned to be operated for approximately one month, but a power outage in the WIPP underground ended the heated liquid tracer test at approximately two weeks. Unlike the gas tracer tests, monitoring the slower liquid tracer tests were done in parallel.

2.2 D – (Tracer Source) borehole

In each array there is one 15-ft [4.6 m] (2.1-inch [5.3 cm] diameter) D borehole with an 18-inch [46 cm] long 1.9-inch [4.8 cm] diameter packer inflated in the borehole. The tracer boreholes were not actively used in the BATS phase 1a test. In BATS phase 1b and 1c, the tracer borehole and packer had two different configurations for gas and liquid tracer testing.

For gas tracer testing, the packer was set at a depth of approximately 7 feet [2.1 m] into the borehole. For liquid tracer testing, the back of the packer was set within 1.5 feet [46 cm] from the back of the borehole. The borehole gas tracer test was conducted first, then the liquid tracer test was conducted next.

2.2.1 Gas tracers

To add the gas tracers, the 1.9-inch [4.8 cm] packer was left at its initial position of approximately 7-ft [2.1 m] depth. A gas tracer mixture was added to a double-ended cylinder (DEC) through a pass-through to the interval behind the packer. Ultra-high purity (99.999%; UHP) nitrogen gas was used to purge the tracer out of the DEC and associated tubing and until the gas pressure behind the packer reached the test-design pressure, and then it was shut in (Figure 4). The pressure of the gas tracer behind the packer was monitored while it decayed, like a pressure-decay permeability test. The salt between the D and HP boreholes in each array had high enough gas permeability to require high-frequency (i.e., measurements every 2 to 5 minutes) monitoring of each tracer addition (heated and unheated) immediately following tracer addition.

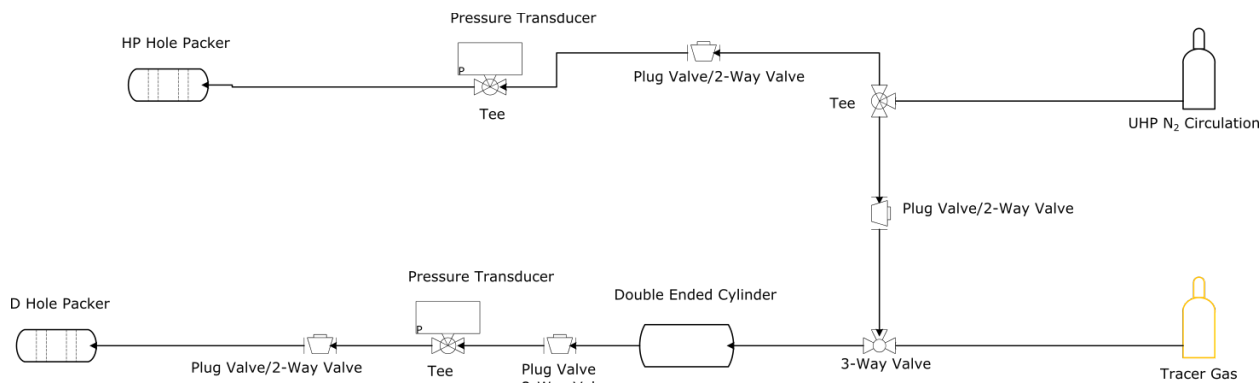


Figure 4. Gas tracer test plumbing.

The gas tracers were a mixture of Ne, Kr, and SF₆ (5% each, with the balance UHP N₂) added to the air behind the packer. Helium and argon were not added as tracers to allow possible characterization of any release of naturally-occurring geogenic noble gas isotopes—especially ⁴He (i.e., sourced from radioactive decay of naturally occurring uranium and thorium) and ⁴⁰Ar (i.e., sourced from radioactive decay of naturally occurring ⁴⁰K)—from the salt due to heating and damage accumulation (Bauer et al., 2019).

An inline SRS gas analyzer (connected to the gas stream exiting the HP borehole) reported mole fractions (i.e., partial pressures) of up to 10 gases with approximately parts-per-million sensitivity. The suite of gases and their mass monitored using the electron multiplier is CO₂ (44), O₂ (34), N₂ (19), He (4), Ar (40), H₂O (19), Ne (20), Kr (84) and SF₆ (127). For the gases of relatively high concentration (e.g., N₂, O₂ and H₂O) one of their lesser isotopologues were monitored, to prevent saturation of the electron multiplier. After the last unheated tests, tracer gas remaining behind the packer in the heated D borehole was plumbed directly into the SRS gas analyzer to better quantify the source.

2.2.2 Liquid tracers

For the liquid tracers, the 1.9-inch [4.8 cm] packer was removed, the borehole was cleaned out (i.e., scraped with tools on the end of scaling bars), and the packer was reset deeper into the borehole set to create a 1.5-ft [46 cm] long interval behind the packer. Synthetic WIPP brine with liquid-phase tracers was added to the interval behind the packer using a packer pass-through with a large syringe.

The BATS synthetic brine is designed to be similar in composition to brine collected from the BATS boreholes in Map Unit 3 (MU-3). The compositions of MU-3 brines collected from BATS boreholes are like the G-seep WIPP brine (GWB; Xiong, 2008), which has been used for geochemical experiments at the WIPP and for performance assessment calculations for the Compliance Applications Recertifications for the WIPP since 2004.

The recipe for the synthetic MU-3 synthetic brine was detailed in Kuhlman et al. (2020). The synthetic WIPP brine liquid tracers include:

- Water having a lighter stable-water isotopic signature than Salado brine (e.g., from an 8,200 ft elevation snow source near Los Alamos, NM) that was used to make the synthetic brine. The stable-water isotopic signature of completed tracer was sampled before use, since the isotopic makeup of hydrous salts used to make the brine is uncontrolled by the manufacturer.
- An organic tracer, Na-naphthionate (also known as 1-Naphthylamine-4-sulfonic acid sodium salt hydrate), which fluoresces at 325 nm (violet/blue) and was added to achieve a concentration of 2 mmol/L. This tracer has been identified as minimally mass adsorbing in saline environments (Magal et al., 2008). Fluorescent tracers are detectable in the laboratory using a fluorescent spectrometer at very low levels. An ultraviolet (i.e., black light) flashlight will be used in the field to observe the presence of the tracer during sampling and future post-test coring operations. Na-

naphthionate is light sensitive, so the tracer and any collected liquid brine samples for spectrometer analyses will be stored in amber bottles to minimize degradation.

- An anionic tracer, sodium perrhenate (NaReO_4), was added to achieve a concentration of 5 mmol/L. It is an oxyanionic form of rhenium, soluble in brine, and detectable at very low concentrations using a mass or optical emission spectrometer. Since it is anionic, it should act as a conservative tracer.

The prepared liquid tracer has been sampled and will be fully characterized in FY22 for the isotopic and dissolved makeup. The isotopic composition of water flowing into the HP borehole is being monitored via the Picarro cavity ringdown spectrometer (CRDS) attached to the exiting gas stream.

In early FY22 after the test is complete, the salt between the D and HP boreholes will be over-cored (Section 6). Black lights will be used to characterize the distribution of Na-naphthionate in the salt during follow-up post-test coring. The post-test core can be subsampled and tested in the lab to characterize the spatial distribution of tracers in the salt.

3. Summary of BATS Data: January 2020 to August 2021

The previous report (Kuhlman et al., 2020) focused on BATS 1a data from January to March 2020. In this section, we present a high-level summary of the data collected to date. In the following major section, data associated with the tracer tests are presented in greater detail.

In the following sections, the phrase “time series” is used to indicate a high-frequency dataset recorded automatically (e.g., thermocouple-based temperature observations recorded every 2 to 15 minutes), while the phrase “test results” is used to indicate a test or analysis done periodically (at least twice), but requiring manual operation or intervention (e.g., borehole permeability testing, or liquid brine sample collection). The phrase “analysis” is used to indicate something conducted once (e.g., destructive core analyses).

3.1 HP – Heater/Packer Boreholes

Dry UHP nitrogen gas is circulated through the interval isolated behind the HP packer. The inflow location is at the back of the borehole (i.e., the inlet gas is directed to the area behind both heater reflectors through a 1/4-inch [6.4 mm] stainless steel tube), and the outflow location is on the back of the packer. The mass flowrate of gas into the interval behind the packer is controlled by an Omega flow controller between the N_2 gas bottle and the packer. The flowrate of gas out of the packer-isolated interval is measured immediately downstream of the packer with an Omega multiparameter flow meter (measuring mass flowrate, temperature, and pressure). For BATS phase 1b and 1c (but not BATS phase 1a), a second LI-COR 850 $\text{CO}_2/\text{H}_2\text{O}$ analyzer was added. Both LI-COR analyzers were relocated near the multiparameter flowmeters to measure water content along with the flowrate, temperature, and pressure without the complicating effects of switching between arrays with solenoids (Figure 5). The hydrocarbon trap immediately upstream of the SRS gas analyzer was removed after BATS phase 1a.

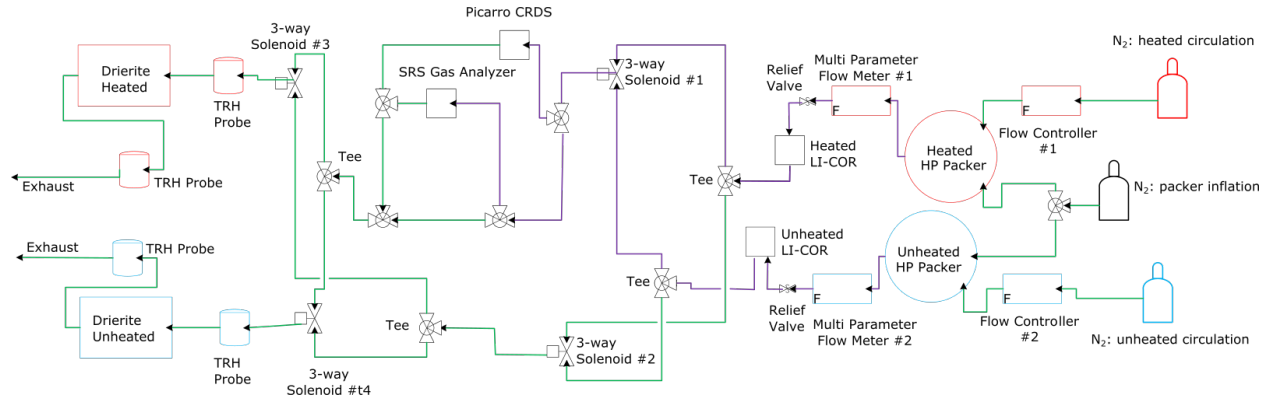


Figure 5. Gas plumbing for BATS phases 1b and 1c (removed hydrocarbon trap and moved existing LI-COR and added second LI-COR compared to BATS phase 1a).

3.1.1 Gas stream pressure and flowrate time series

Figure 6 shows the time series of gas stream mass flowrate (the flow controller upstream and mass flowmeter downstream of the packer for both heated and unheated arrays) averaged every 15 minutes on Campbell CR1000X dataloggers.

The legends and titles in this and subsequent figures use the naming convention of variables in the data spreadsheets used by the WIPP TCO. In these variables, heated or unheated array are indicated by a starting “H” or “U”. The next letters relate to the borehole (in this case “HP”), then, in the case of Figure 6, “GQUp” and “GQDown” refer to gas flowrate up and downstream of the HP packer. In the time series plots showing data since January 2020, the minor tick-marks indicate weeks (each Monday).

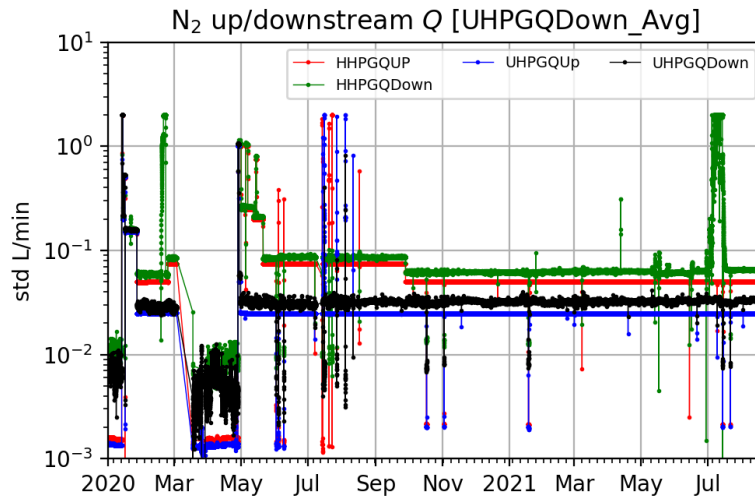


Figure 6. Gas stream mass flowrates up- and down-stream of HP packer for heated (H) and unheated (U) arrays.

March through late April 2020 the BATS heater test was in an extended shutdown mode, following a combination of the end of BATS phase 1a and a subsequent WIPP-wide power shutdown.

In Figure 6 the mass flowrates of gas upstream and downstream of the packers are close to the same (red/green or black/blue time series), except after the end of BATS phase 1a heating (late Feb 2020) and during tracer testing (July 2021) when the flowrate of gas leaving the heated HP packer rose significantly above the flowrate going behind the packer.

Differences can be observed between the upstream and downstream mass flowrate (standard liters per minute, with standard temperature for Omega equipment being 21 °C) and a non-zero flowrate was reported when gas was not being flowed (<0.01 std L/min). The reported downstream flowrate was slightly higher than the upstream flowrate. This is likely due to a difference in the accuracy or calibration of the flow controller and multiparameter flow meters at low flowrates (i.e., the gauges have a higher relative uncertainty at a small fraction of their full-scale flowrate), and not due to a continuous source of gas inside the boreholes.

Figure 7 shows the time series of pressure and temperature in the tubing downstream of the HP borehole packer (upstream of the switching solenoids), measured at the multiparameter flow meter and averaged every 15 minutes on the Campbell dataloggers. Gas pressure rose above nominal levels when the gas flowrate rose to 2 std L/min or greater (at the beginning and end of the BATS phase 1a heater test, and in July 2021 during after the heated liquid tracer test). Gas stream temperature shows effect of changes in ambient temperature, with a significant increase in temperature associated with the recent heated liquid tracer test (at the same time as the increase in gas mass outflow rate, Figure 6), which may be due to the production of steam in the borehole and possible condensation on or near the multiparameter flowmeter (which would cause a rise in temperature related to the latent heat of condensation) when liquid water flowed into the heated interval.

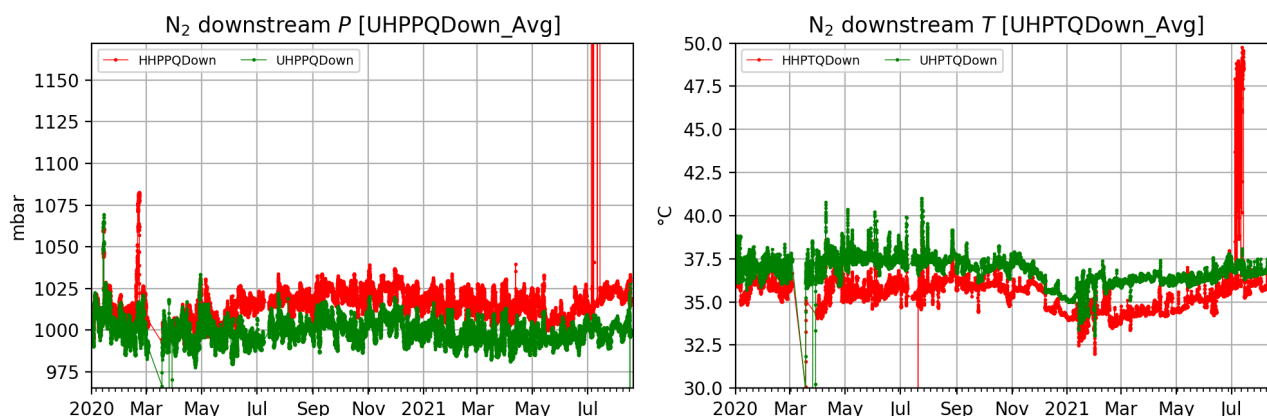


Figure 7. Gas stream pressure and temperature downstream of HP packer.

3.1.2 Water content time series

Water content is measured at multiple locations downstream of the packers. The gas flowing into the packer-isolated interval is assumed dry (UHP N₂). The flowrate of water recovered from behind the packer is determined using a combination of the gas mass flowrate and the concentration of water in the gas, now measured by two LI-COR 850 instruments (both heated and unheated). The concentration of water is also measured by the Picarro CRDS, depending on the state of the three-way solenoidal switching valves. Finally, both branches of the gas system have relative humidity probes measuring in-line humidity before and after pairs of heated and unheated desiccant canisters on each branch, which are weighed once or twice weekly as an independent check on the calculation of the total mass of water leaving the borehole system from the high-frequency flowrate data.

Figure 8 shows the water vapor concentration time series reported by the LI-COR 850, recorded as 15-minute averages by the Campbell dataloggers. During BATS phase 1a, the LI-COR 850 was located on the other branch from the Picarro and SRS gas analyzers, but since May 2020 the two LI-COR 850 sensors are located upstream of the solenoid switching, near the multiparameter flowmeters (Figure 5).

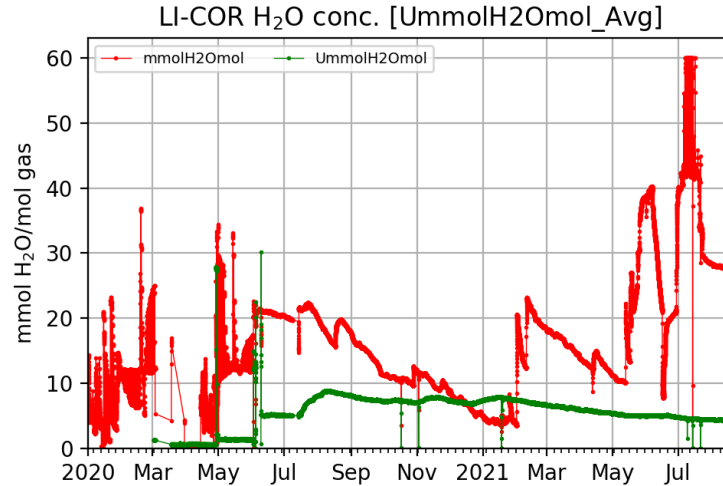


Figure 8. Raw LI-COR water concentration (Jan to Mar 2020 data are switched, after April 2020, dedicated LI-COR instruments are located before solenoids).

Relative humidity (RH) time series are measured both upstream and downstream of the Drierite desiccant canisters (Figure 9). These RH sensors are downstream of the second set of solenoid valves (Figure 5), therefore the data do not require switching as the LI-COR and Picarro data do, but the effects of switching do impact the data. The downstream RH is mostly < 1% (green curves), except during the later portions of the BATS phase 1a leak when gas flowed through the system at a high flowrate overwhelmed the desiccant. In April 2020, gas was not being flowed so the RH sensors up and downstream of the desiccant showed similar values, related to the ambient RH. Some minor increases of the downstream RH above the low background also occurred during the liquid tracer test in July 2021.

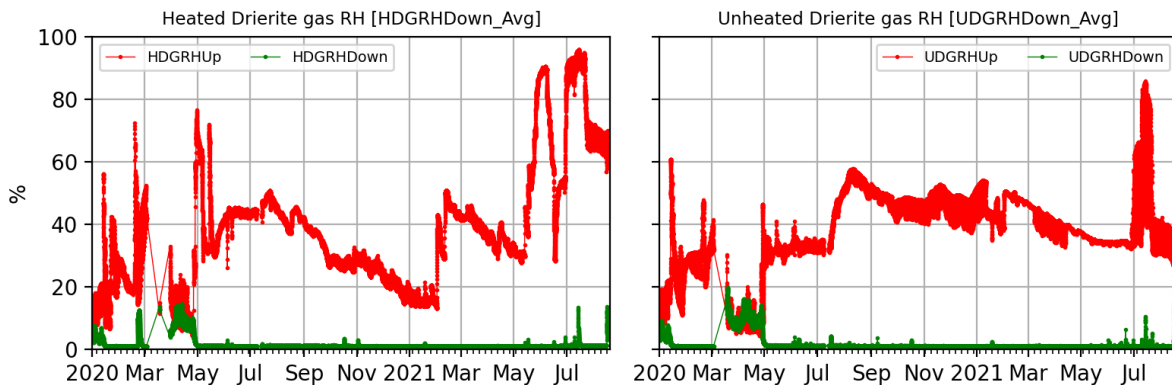


Figure 9. RH up- (red) and down-stream (green) of the heated (left) and unheated (right) desiccant.

The desiccant water production data is presented in Figure 10 and Appendix A-1 (Table 4 and Table 5). In general the unheated array has a less variable and lower production of water (the concentration is similar, but the gas flowrate is less).

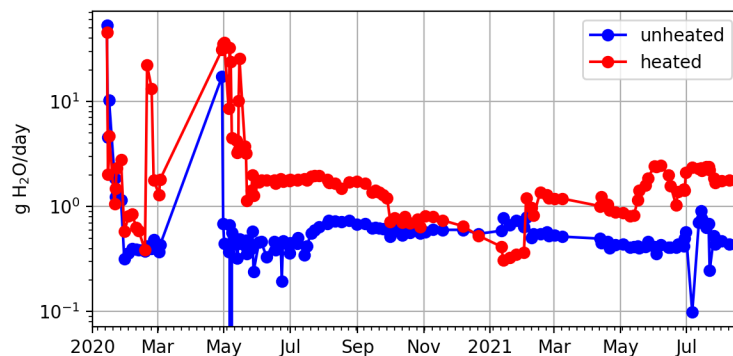


Figure 10. Desiccant water production data.

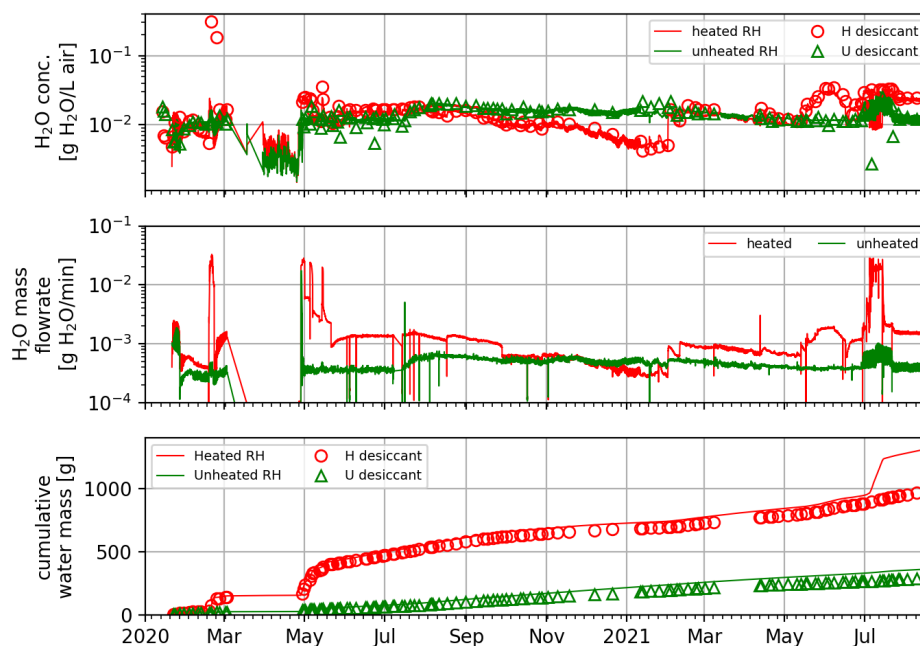


Figure 11. Water production computed from RH and gas flowrate compared to desiccant-based observations.

Figure 11 shows the average water concentration (grams H_2O per liter of air) computed using the RH sensors before the desiccant (red lines in Figure 9) plotted together with the average values computed from desiccant weighing (dots in Figure 10). The water mass flowrate, and the cumulative water production are also plotted from the same sources. There is generally good agreement between the 15-minute average data and twice-weekly desiccant observations. At the time of the July 2021 liquid tracer test, the curve (computed from the relative humidity and mass flowrate of gas) shows significantly more water production than the independent desiccant data. As explained later (Section 5.1), this may be due to anomalous mass flowrate observations at the multiparameter flowmeter related to possible condensation.

The production of water during after the April 2020 shutdown and during the July 2021 tracer test are the most significant water production events in the heated array. The unheated array produced water at a roughly constant rate since January 2020.

3.1.3 Water isotopic composition time series

The Picarro CRDS measures concentration of different isotopes in the gas stream (i.e., oxygen and hydrogen isotopes) at approximately 2-minute intervals. The raw Picarro time series (Figure 12) shows similar trends as the LI-COR 850 data (Figure 8), but the instruments are on opposite branches of the gas line. In BATS phase 1a when the Picarro was monitoring the heated array the LI-COR was monitoring the unheated array, since May 2020 there is a dedicated LI-COR on each branch.

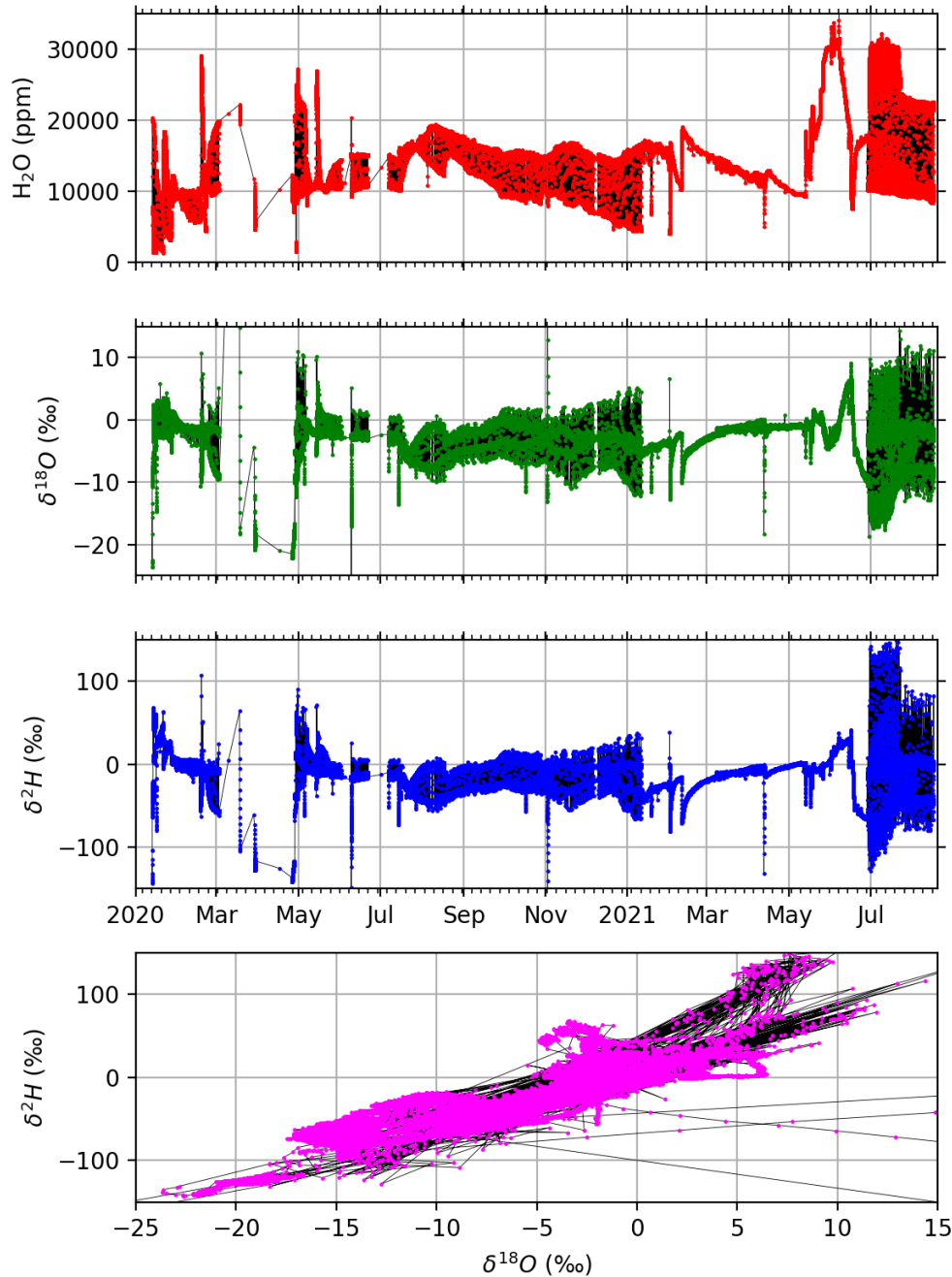


Figure 12. Picarro CRDS raw data.

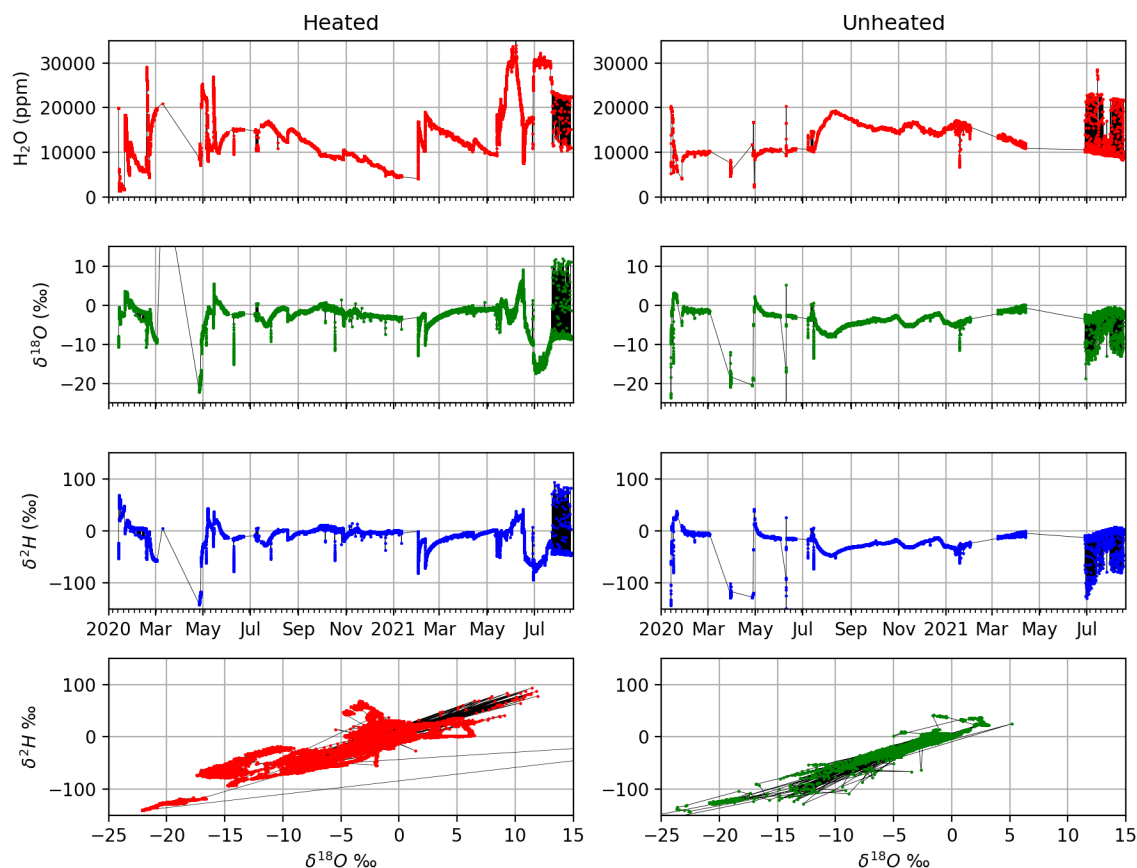


Figure 13. Heated (left) and unheated (right) array Picarro CRDS data.

Figure 13 shows the switched Picarro dataset, averaging the original 2-minute Picarro data to 15-minute intervals, to be comparable to the data recorded with the Campbell dataloggers. The upper panels show each of the variables through time, while the lower row of panels show the two water isotope ratios plotted against one another. Periods when the isotope values are very light ($\delta^{18}O \leq -10$ ‰ or $\delta^2H \leq -50$ ‰) likely corresponds to when free liquid water was present behind the packer, for example in the heated array after the March-April 2020 shutdown and during the 2021 tracer test.

More detailed analysis, including numerical modeling, of the water isotope data can be found in the 2021 LANL M3 report (Gultinan et al., 2021).

3.1.4 Gas composition time series

The gas stream from the Picarro CRDS flowed into a Stanford Research Systems Gas Analyzer (SRS QMS-200), which analyzed the gas stream for compositional changes with time. During BATS phase 1a, the gas stream was analyzed for all masses in “analog” mode with the less-sensitive Faraday cage (see Kuhlman et al., 2020). At the end of the BATS phase 1a, the vacuum pump in the gas analyzer failed, which then led to failure of the filament. Operating within the imposed travel constraints of the COVID-19 pandemic, the failed instrument was sent back to the manufacturer for repairs resulting in no data from March to August 2020. When the gas analyzer was re-installed, it was switched to “P vs. T” mode, which monitors the partial pressure of up to ten gases, using the more sensitive electron multiplier.

The SRS gas analyzer failed again (March 2021) during the unheated gas tracer test in the heated array. The second failure required replacement of the turbopump, but the instrument was back in operation in the WIPP underground by May 2021. Gas tracer tests 3 and 4 (see Section 4) occurred before and after this failure.

3.1.5 Borehole closure gauge time series

A linear variable differential transformer (LVDT) was used to measure the diameter of the HP borehole with time. Figure 14 shows the change in borehole diameter since the beginning of the test. The unheated array shows steady creep closure with minor jumps (green), while borehole closure gauge in the heated array (red) shows changes associated with the beginning and end of heating and a significant jump in closure associated with the hypothesized presence of steam in the borehole during the liquid tracer test (July 2021). The steam may have caused the salt to close suddenly, or it may have caused the spring/LVDT sensor to become unstuck (more accurately measuring closure that had already occurred). It seems physically unlikely that >1 mm borehole closure could occur so suddenly, and that it would also bring the heated borehole closure amount near that measured in the unheated borehole. A stuck LVDT sensor, loosened by moisture, seems the most likely explanation.

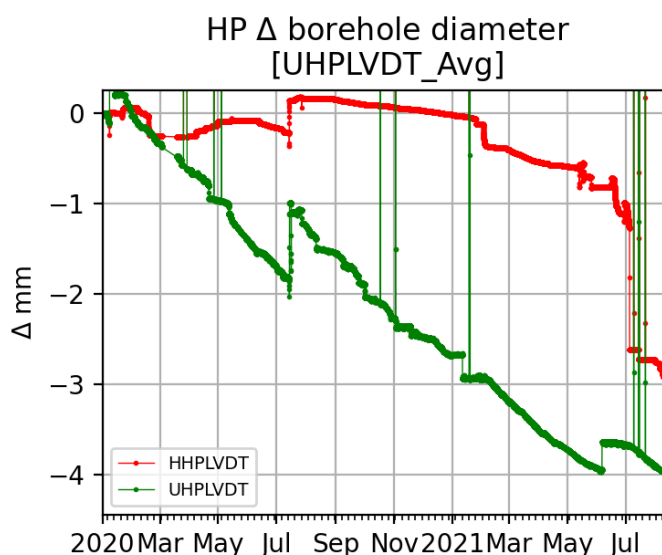


Figure 14. Change in HP borehole diameter measured by LVDT.

3.1.6 Heater power and temperature time series

The heater controller reports current, and power applied to the heater, which is critical to characterizing the applied thermal boundary condition. The controller also reports the temperature at thermocouples inside the borehole used to control and provide a high temperature safety limit for the heater (H:HP thermocouples 4 through 6). These data are used in thermal-hydrologic-mechanical models, driving the thermal response of the entire system. Only the HP borehole in the heated array is collecting this time series. Power is reported with the thermocouple data in Figure 18.

In May 2020, some short heater checks were conducted to test the system, when the heater was activated for a few hours at a time.

3.2 AE – Acoustic Emission Time Series

The piezoelectric transducers in the acoustic emission (AE) boreholes were used to passively monitor for acoustic emissions. The AE systems monitoring each array will be used to measure and locate acoustic emissions, from damage in the salt due to heating, cooling, and brine migration. The Mistras data acquisition system automatically identifies acoustic emissions, based on hits occurring on multiple channels defined by threshold crossings. During BATS phase 1a, there were two Mistras systems: the system monitoring the heated array had 8 channels; and the system monitoring the unheated array had 6 channels. For subsequent tests (BATS phase 1b, etc.), the heated array has been upgraded to monitor 16

channels and the unheated array has been upgraded to 8 channels. To reduce electrical noise and data file size, the AE dataset for the heated array has been bandpass filtered from 75 to 700 kHz with a threshold of 45 dB. Even with filtering, the heated array recorded over 443,000 AE events. The AE dataset from the unheated array has been bandpass filtered from 75 to 700 kHz with a threshold of 30 dB. The resulting dataset contains over 150,000 AE events.

After processing the data using the Mistras AE software, waveforms were imported into In-Site Lab seismic processing software for event localization. Events were defined as ≥ 4 AE hits within a 200-microsecond window. Events were located using a homogeneous isotropic velocity structure of 4600 m/sec. Arrival times were picked using the Akaike information criterion, and manually adjusted as needed. A simplex algorithm was used to locate events.

BATS phase 1a demonstrated that AE activity is much higher during increases and decreases in heater power (Kuhlman et al., 2020). Cooling of salt in the borehole area from decreased heater output results in AE activity $\sim 5\times$ larger than the initial heating phase. In this report we later present AE data from the heated borehole associated with two heating episodes during gas and liquid tracer testing from June to July 2021. We also present AE data from the unheated borehole comparing the performance of preamplification gain of 60 dB vs 40 dB. There is a desire to increase the depth of AE sensors in BATS phase 2. Currently, depth is limited by cable length of 3 m, which is due to available sensor gain. We intend to switch to a small form-factor preamplifier that could be inserted into the borehole for greater sensor depths, but this would also entail reducing the preamplifier gain from the current 60 dB to 40 dB. Gain was lowered on the unheated array to 40 dB in May 2021 to evaluate the potential of using smaller 40 dB preamplifiers and deeper sensors in BATS phase 2.

3.2.1 Unheated array – 60 versus 40 dB preamplification gain

The field-adjustable 2/4/6 Mistras preamps currently used will not fit into the 5.3 cm [2.1"] boreholes to allow for emplacement depth greater than the maximum cable length. Mistras also does not manufacture a small form factor preamplifier with greater than 40 dB gain. The small form-factor 40 dB preamplifier will fit into the borehole, allowing for greater sensor depth. In BATS phase 1a, data was collected at 60 dB gain, and software limitations prevent reprocessing data collected with different preamplifier gains, a common step in the current workflow to eliminate noise and other electrical interference. Switching to the small form factor preamplifier would require changing all the preamplifier gains from 60 dB to 40 dB. On May 3, 2021, the preamplifiers in the unheated array were switched to 40 dB gain. The data from January 11 to May 2 had 60 dB gain, bandpass filtered from 75 to 700 kHz, and had a threshold of 35 dB. The data from May 3 to July 26 had 40 dB gain, bandpass filtered from 75 to 700 kHz, and had a threshold of 32 dB.

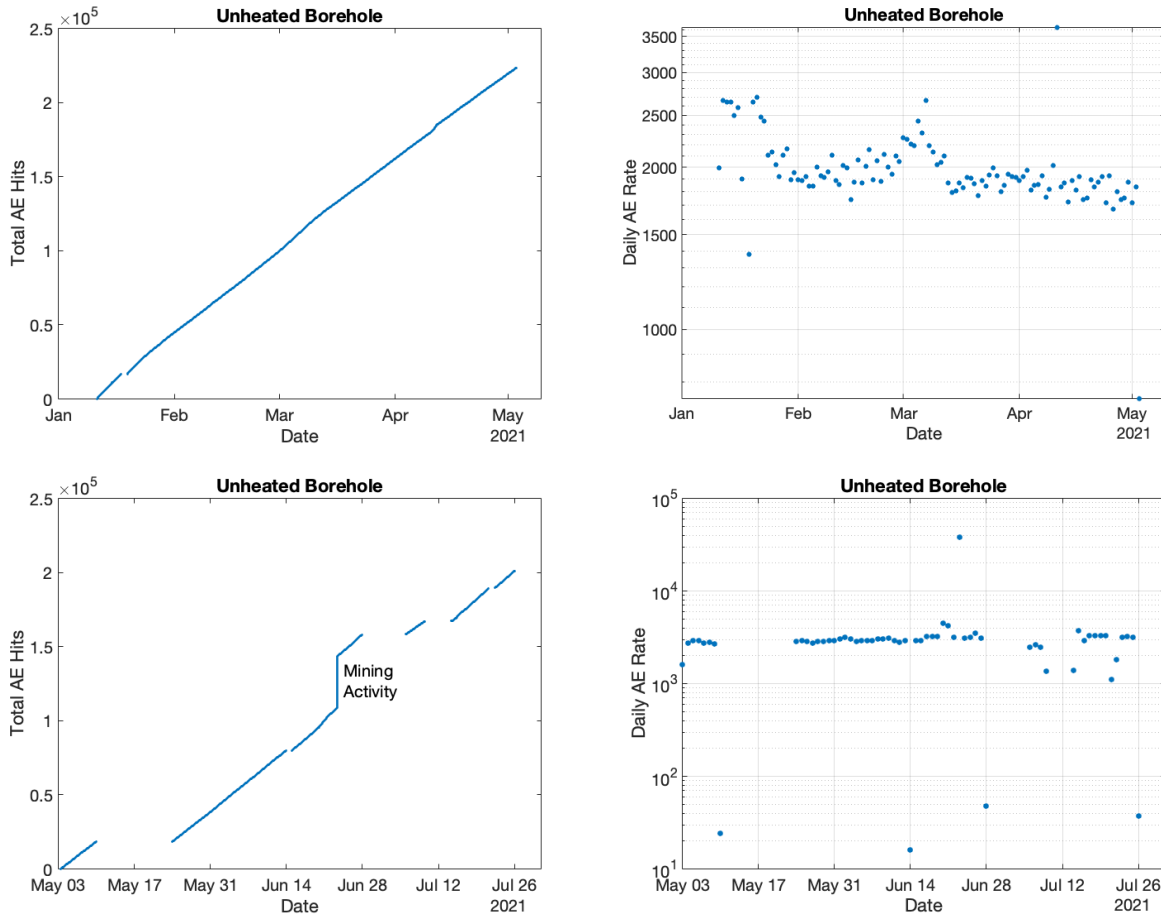


Figure 15. Total number of AE hits and daily rate per array for the unheated array. Top row is 60 dB gain. Bottom row is 40 dB gain.

Figure 15 show the cumulative AE and daily AE rates for the unheated array with the different preamplifier gains. It can be difficult to determine a priori equivalent thresholds between the different gains, but a threshold of 32 dB for the lower gain produced similar daily rates. Both gains produce consistent day-to-day rates for background behavior.

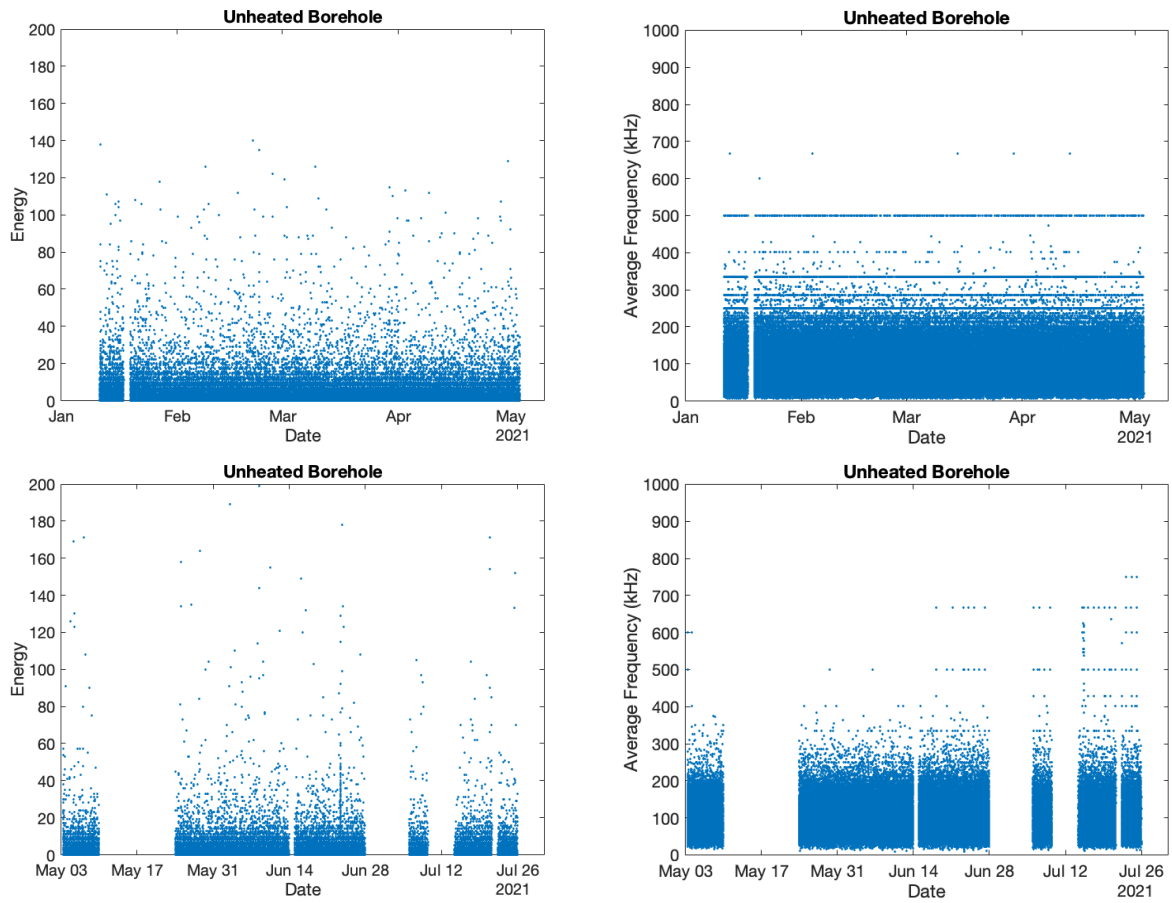


Figure 16. Energy (left) and frequency (right) content of AE from the unheated array. Top row is 60 dB gain, bottom row is 40 dB gain.

Figure 16 shows the energy and average frequency for the two data sets. Behavior is similar for both gain values.

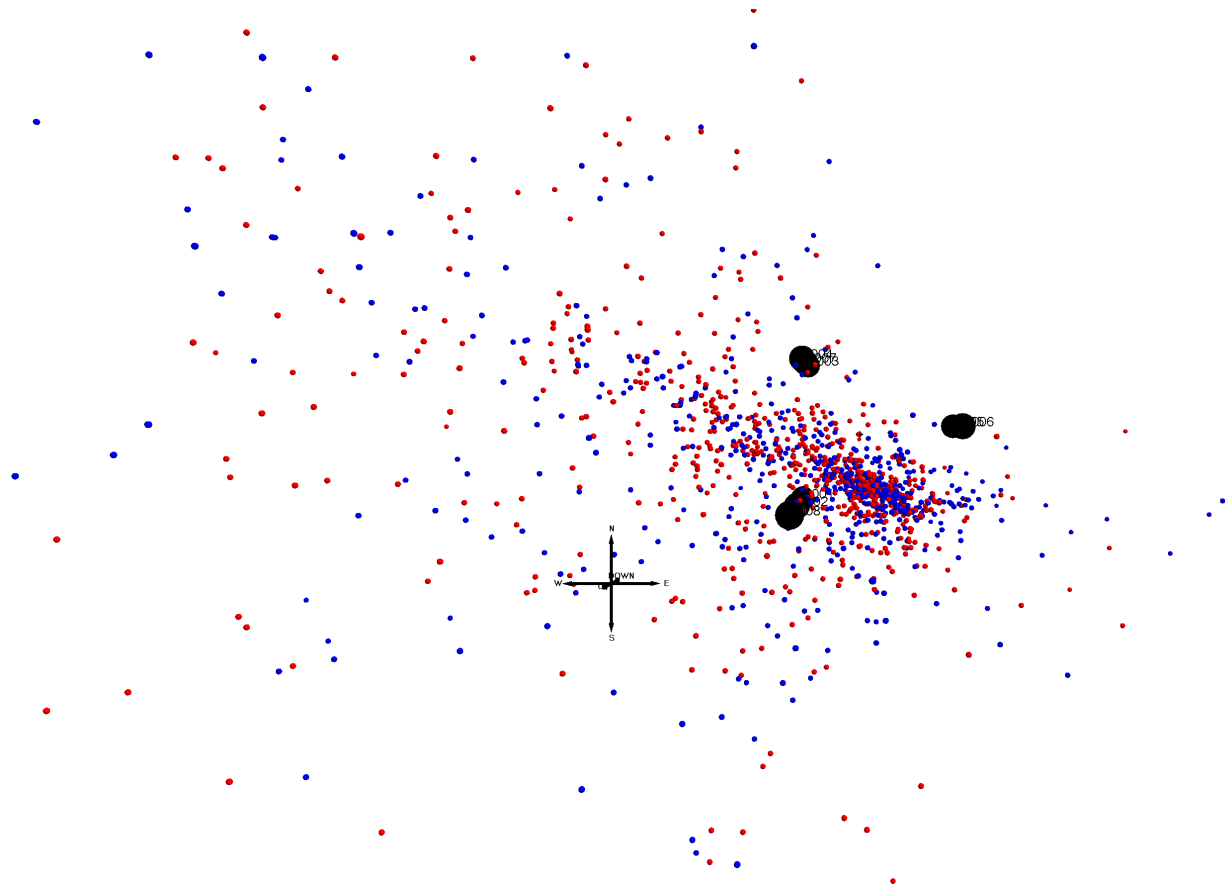


Figure 17. Located events for unheated array for April 26 to May 2 (60 dB gain), blue, and May 3 to May 10 (40 dB gain), red. The image is looking south into unheated array.

Figure 17 shows located AE events for the unheated borehole array a week before and a week after the gain switch (black dots show AE borehole locations and indicate spatial scale). This dataset was processed with different thresholds than previously: the threshold for the 60 dB dataset was 30 dB, and the threshold for the 40 dB dataset was 26 dB. This resulted in 24,106 hits for 60 dB gain, and 44,837 hits for 40 dB gain. At these threshold values, daily noise spikes are still observed, but the location algorithm can filter out the noise from real signals. Events were located using In-Site seismic processing software, resulting in 697 events for the 60 dB dataset and 820 events for the 40 dB dataset. This is only a slight increase in events for the 40 dB dataset despite a substantially higher hits, indicating higher noise in this dataset. Locations for both datasets occupy the same space.

This data set shows that the behavior of the 60 dB and 40 dB gain are essentially equivalent. Both datasets can create similar AE hits, daily rates, energy, and average frequencies. Locations generate similar results. Some drawbacks were observed while working with the lower gain data—lower signal to noise ratio and muddled waveforms, but these drawbacks are minor compared to the benefit of improved locations from deeper sensor depths. Based on this comparison, we have acquired the small form factor preamplifiers for BATS phase 2.

3.3 T – Temperature Time Series

Thirty-six sealed Type-K thermocouples are grouted into the two T boreholes, and more are co-located with other observations in other boreholes (i.e., AE, F, and E).

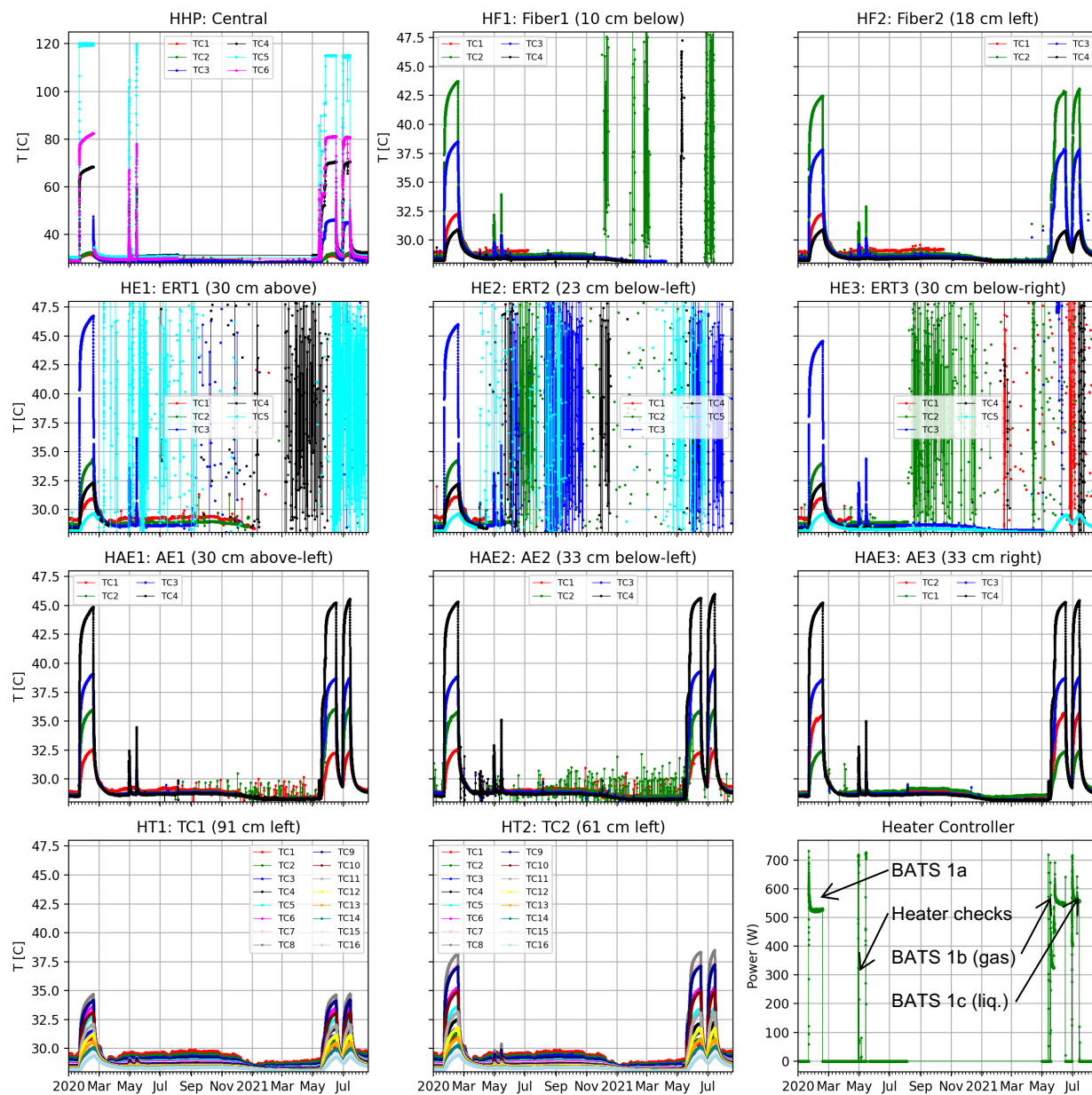


Figure 18. Thermocouple and heater power data from heated array.

Figure 18 shows the temperature data from the thermocouples in the heated array. Each panel in the plot is a different borehole, curves within each panel are for different thermocouples. The lower-right panel shows the power reported by the heater controller. The instantaneous power is that applied when the heater element is on, while the average power is time-averaged (total power \times duty cycle). Thermocouple data collected during ERT surveys are cut from the dataset (gaps in the data during ERT each night). Most of the ERT thermocouples have been reporting erratic data since summer 2020. All the temperature panels have the same temperature axis scale except the panel for the HP borehole.

Thermocouple TC5 in the heated HP borehole (top left panel of Figure 18) is the thermocouple in the middle of the heater that was used as the controlling thermocouple (set to 120 °C in BATS phase 1a). TC4 and TC6 in the heated HP borehole were located closer to the reflectors in the heated borehole.

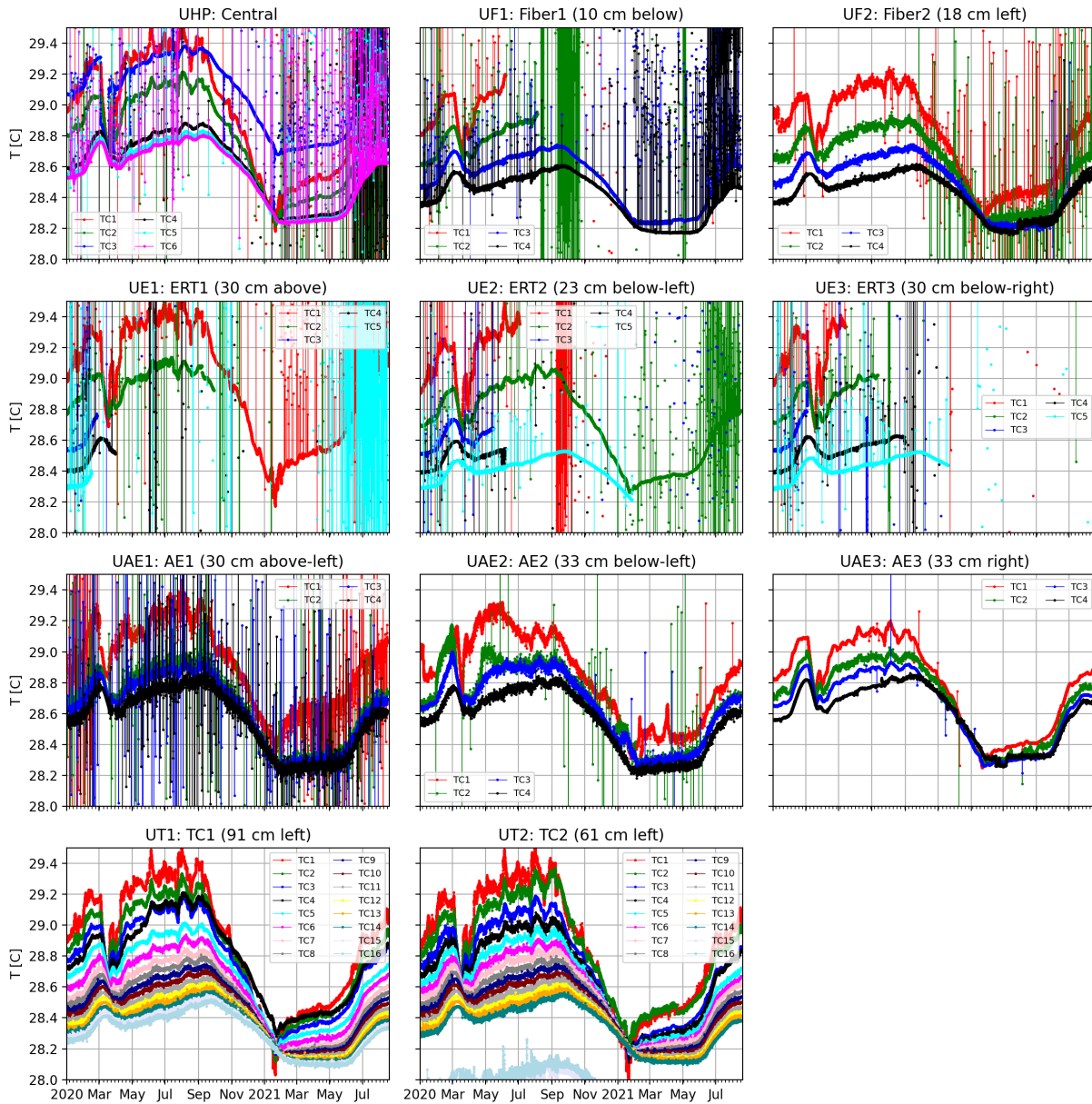


Figure 19. Thermocouple data from unheated array.

Figure 19 shows similar data for the thermocouples in the unheated array. The effects of the ERT surveys on the data appear more significant because of the stretched temperature axis scale. The thermal gradient between the drift (warmer) and deeper in the salt (cooler) is clear in these expanded temperature-scale plots (0.6 to 0.7 °C difference over 5.5 m). The shallower thermocouples also respond to changes in ambient drift air temperature, while the deeper thermocouples do not. After some delay, a temperature rise due to heating in the heated array could be seen in the thermocouples in the unheated array, but this rise was less than 0.2 °C at the end of the BATS phase 1a.

3.4 E – Apparent Resistivity Results

Starting from the end of 2019, Electrical Resistivity Tomography (ERT) data have been acquired daily throughout the BATS field test. For ERT measurements, current is injected through one pair of electrodes, and the resulting voltage measured across a separate pair of electrodes. By using numerous different

combinations of current injection and voltage measurement dipoles, the subsurface resistance is densely sampled. The measurement sequence, i.e., the selection of dipole-dipole arrangements to be measured, was obtained using an optimization approach to achieve the highest resolution possible while keeping the number of required measurements to a minimum (Uhlemann et al., 2018). A total of 1,962 resistance measurements per array were conducted each day. Data were acquired using an MPT-DAS1 electrical resistivity imaging system using a frequency of 1 Hz and a stack of 3 measurements, and injection currents of about 0.1 A. The heater in the central HP borehole of the heated array (i.e., plot P1) increased the temperature (see top panel of Figure 20). This heating occurred in January to February 2020, and again more recently (May to July 2021) after a long break with no heating taking place. The unheated array (plot P2) served as a control and remained unheated throughout the experiment.

Measured resistances (bottom panel of Figure 20) show a clear response to the heating, where increasing temperatures caused a decrease in the measured resistance. Gas permeability tests in the heated D borehole in August 2020 in the heated array seem to be related to a decrease in resistance, which remained consistent throughout the remainder of the experiment. Similarly, the unheated array experienced a strong, short-term reduction in the measured resistance in October 2020, but returned to the pre-event levels comparably quickly, and over the entire experiment showed an increasing trend.

Measurement errors (based on the stacking error obtained for each measurement, bottom panel of Figure 20) showed a generally decreasing trend within the first two months of the experiment, indicating that electrodes were settling into the formation after their installation. While for the unheated array the decrease in stacking errors continues, the events in August 2020 in the heated array have caused a slight increase in the stacking error that seems to fluctuate with activity in the array.

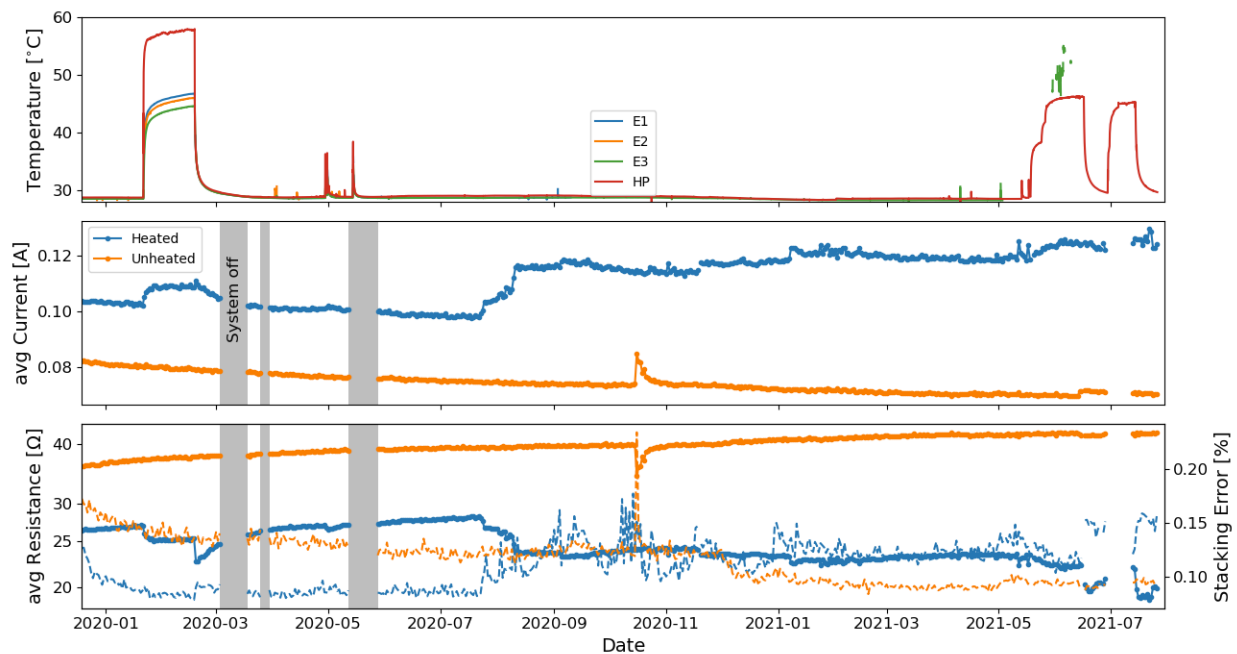


Figure 20. Data overview showing temperature in the ERT boreholes (top panel), mean injection current (central panel) and mean measured resistance (bottom panel, solid line) as well as stacking errors (dashed line). Data gaps due to interruptions in the experiment are highlighted.

3.4.1 ERT monitoring results

Figure 21 and Figure 22 show the raw monitoring data for the unheated and heated arrays, respectively. Both show stable raw resistance measurements with no obvious outliers (top left panel in both figures). Considering the change in the raw measurements over time, the unheated array shows a generally increasing trend, with measured resistances increasing over the course of the experiment by more than 50%. Only a small subset of measurements show decreasing values. This can also be seen in the distribution of the changes (bottom panel of Figure 22) as most resistance measurements are increasing. A short-term disturbance in October 2020 (~Survey 290) shows a distinct resistivity reduction, with values returning to their initial values rapidly. After this event, more changes can be observed, with some more increasing values, but also several decreasing values.

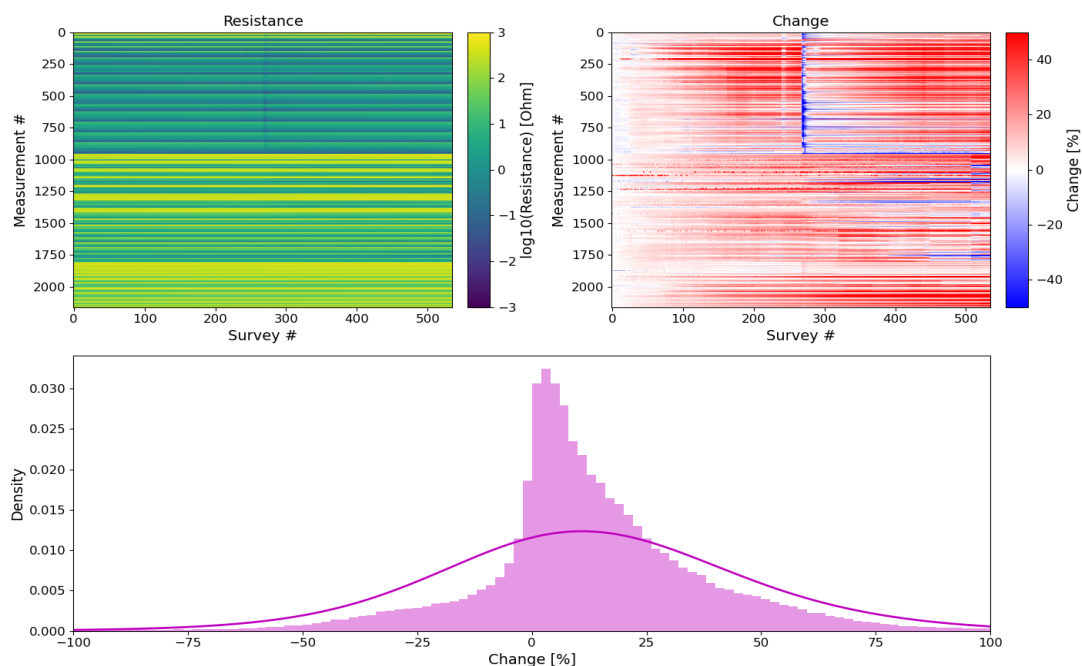


Figure 21. Raw data time-series for the unheated array. Measured resistances show stable conditions, while changes with regards to the baseline measurements highlight episodes of short-term disturbances. The entire data set (bottom panel) shows a generally increasing resistivity trend.

Monitoring data of the heated array also shows stable resistance measurements over the course of the experiment, but significantly more dynamics in response to the heating, brine leakage, and other events (top panels of Figure 22). The initial heating caused a decrease in the measured resistances throughout the measurement sequence (January to February 2020; surveys 34 to 62), while gas and brine leakage after BATS phase 1a led to a more complex change in the measurements, with some showing a significant increase, while other measurements showed a decrease in resistance. After this leak, measurements recovered and showed smaller amplitude response to short term heating events that took place at the end of April 2020 (surveys 115 to 125). From surveys 184 to 200, an initial small decrease, which in its response is like the brine leakage earlier, is followed by a large decrease in the measured resistances that remains for most of the measurements throughout the remainder of the experiment. In May 2021, additional heating was conducted, and in July 2021 a liquid tracer test was conducted. Both events caused complex changes in the measured resistances, with most measurements showing decreasing values, while others showed increasing values. Generally, the heated array shows a distribution of changes that is skewed towards decreasing values.

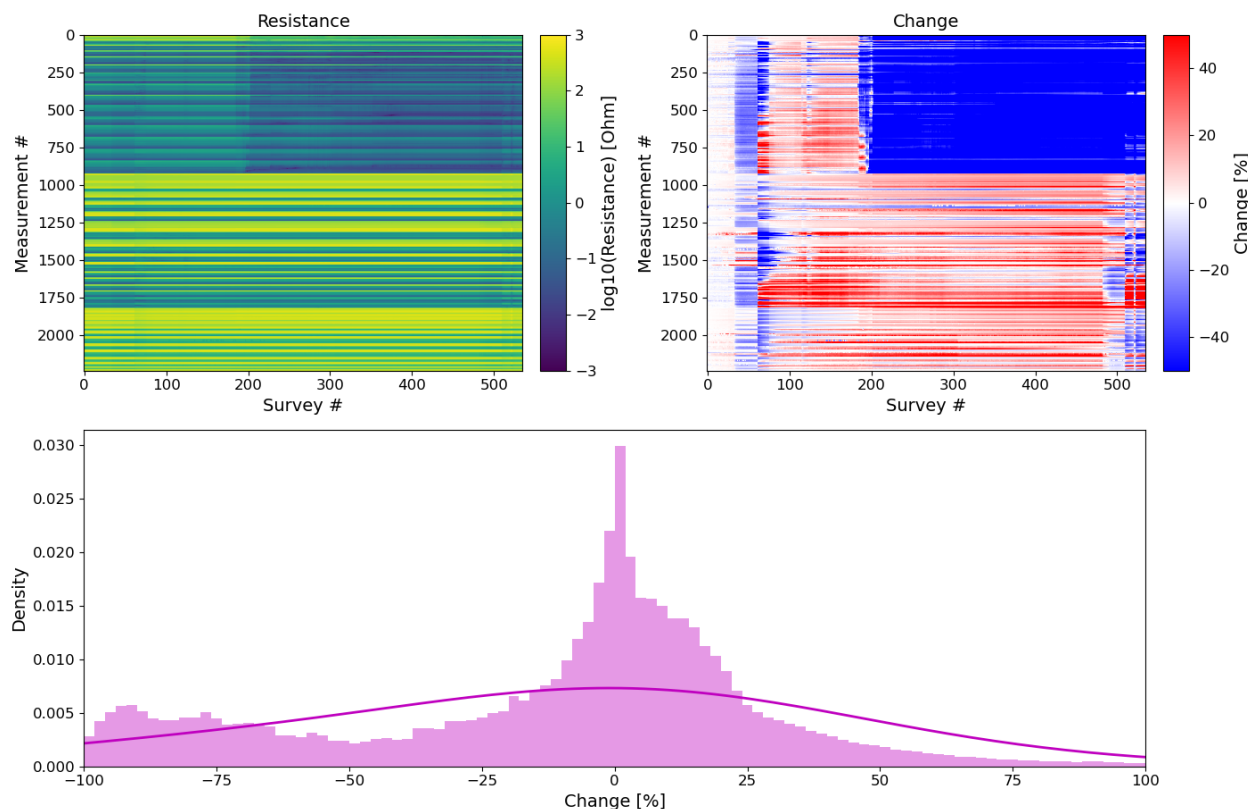


Figure 22. Raw data time-series for the heated array. Measured resistances show stable conditions, while changes with regards to the baseline measurements highlight episodes of heating and brine leakage. The strong change during the middle of the experiment relates to a period where multiple permeability tests were conducted. The entire data set (bottom panel) shows a generally decreasing resistivity trend.

3.4.2 Heating and tracer tests May to July 2021

Starting May 13, 2021, several heating experiments and tracer tests have been conducted in the heated array, while the unheated array served as reference, with both gas and liquid tracer tests but no heating. Figure 23 shows the resistivity response of both arrays (A-D), as well as the recorded change in resistivity and temperature (top panel) of the heated array. During these experiments several thermocouples were not functional, and the temperature evolution using the ERT boreholes is difficult to reconstruct (see Figure 18 for temperature data observed at other locations in the heated array). Nevertheless, the actual heating of borehole HP was recorded and is shown. The array was heated twice, and the maximum temperature was reached as liquid tracer was added to the D borehole.

However, the resistivity response of the two cycles is comparable. Heating causes a decrease in resistivity that commences in the central part of the array, showing the strongest decrease (up to -40%), which then propagates to the top, where changes become comparable towards the end of each heating period. Only negligible change was observed during the cycles in the deeper part (i.e., farthest away from the drift) of the array. This decrease is likely an aggregated response of the heating of the host rock and movement of brine, which is similar to what was observed during following BATS phase 1a heating in early 2020.

Interestingly, the decrease in resistivity is followed by a strong increase in resistivity that coincides with the shut-off of the heating elements and hence a cooling of the rock formation. If the rock remained at temperature above or equal to temperatures recorded prior to the heating, this increase in resistivity

suggests a change in the brine distribution due to its leakage into the HP hole from the formation or the liquid tracer test, or a decrease in the rock porosity. This change is focused on the central part of the borehole, which in previous experiments has shown distinct changes and can likely be associated with a fracture zone within the rock formation, through which preferential flow is taking place.

Liquid tracer was added to the D borehole when the salt was at its highest temperature. No distinct resistivity response was observed. From this and the previous observations it can be concluded that the tracer tests show no response in the resistivity distribution of the salt. The unheated array shows some smaller magnitude changes, with increasing resistivity close to the drift and decreasing resistivity towards the back of the borehole, where tracer was injected in the D borehole.

More detailed presentation of results and associated modeling can be found in the Lawrence Berkeley 2021 level-3 milestone report (Rutqvist et al., 2021). Future analysis will link those results with modelled responses to investigate likely brine migration pathways.

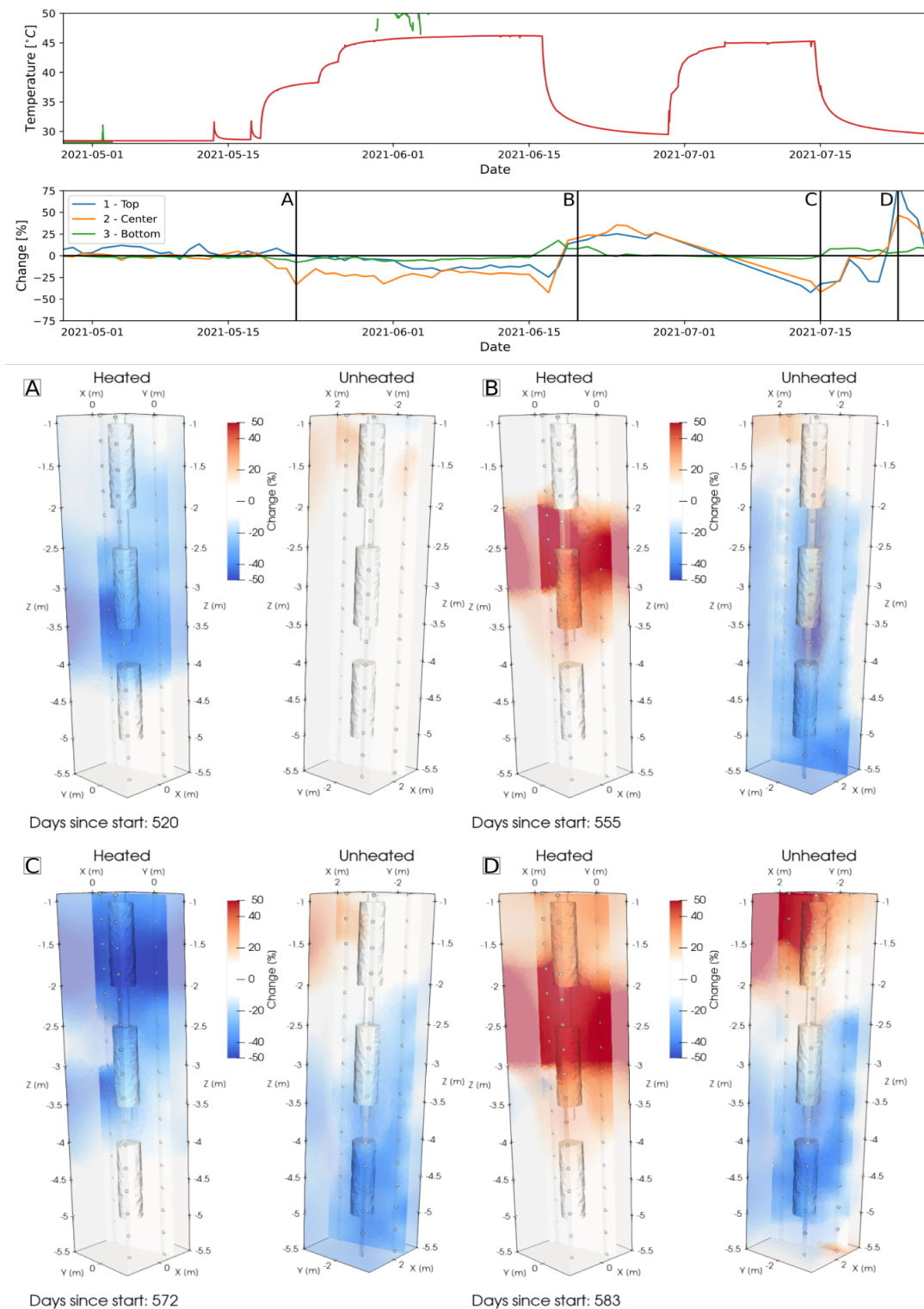


Figure 23. 3D resistivity models showing the change in both arrays during heating and tracer tests in Summer 2021. Top panel shows the resistivity variation in the heated plot for 3 different areas within the studied domain, as well as the temperature recorded in the heated borehole. The other temperature sensors failed during this experiment. A-D show 3D changes in resistivity.

3.5 SM – Liquid Sample Boreholes

3.5.1 Air temperature and RH time series

Figure 24 shows the temperature and relative humidity associated with the interval in the SM borehole behind the mechanical packer. The left panel shows the air temperature behind the packer rising during the heating portion of the test (red curve on left), while the right panel shows the relative humidity first rising during heating and then falling during cooling (red curve on right). The rise in RH behind the packer during heating may be due to brine production from the salt, while the drop in RH is likely due to gas from the leaking D borehole packer reaching the SM borehole (March 2020) or gas tracer tests (June 2021). In the unheated array there were not significant changes in the air temperature or RH observed behind the packer. RH near 75% is indicative of equilibrium between moist air and halite.

The HSMTC and USMTC thermocouples are located outside the boreholes on the drift wall. For the unheated array (black line, left panel of Figure 24) the temperature does not show similar fluctuations to the in-drift air temperature (Figure 27); the end of the thermocouple is more firmly attached to the salt that dampens its temperature response. The sharp drop and subsequent rise in humidity behind the SM packer seems to correlate to the tracer gas breakthrough associated with the heated tracer test (Figure 31), which indicates the tracer gas did not simply flow between the D and HP boreholes, but also flowed to the SM borehole.

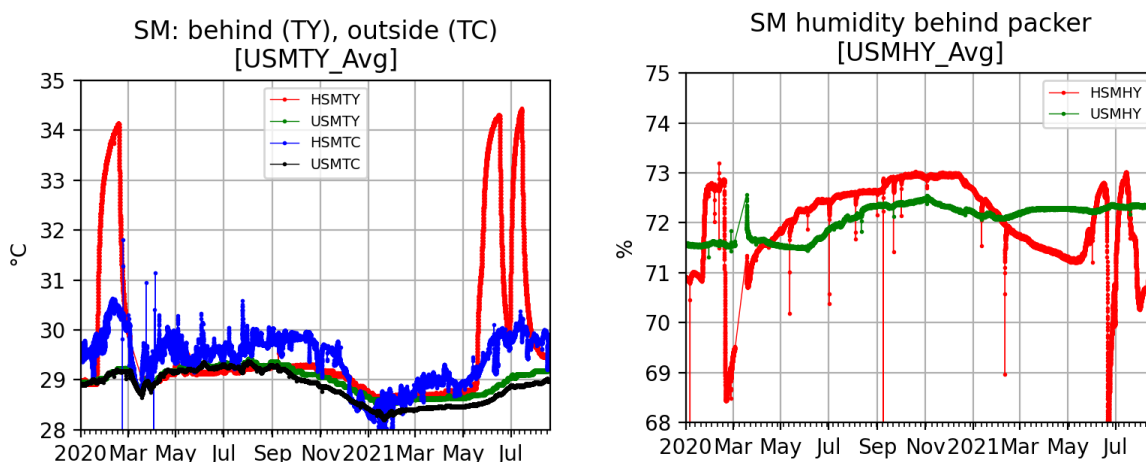


Figure 24. Air temperature (left) and relative humidity (right) for SM boreholes.

3.6 SL – Seal Borehole Time Series and Test Results

The seal portion of the experiment includes strain and temperature data collection. The cement plugs on the heated side will be over-cored in early FY22 to observe salt/cement interactions. The unheated seals will remain longer, with over-coring occurring later.

3.6.1 Air temperature and RH time series

Figure 25 shows the air temperature and relative humidity data associated with the SL boreholes. Like the SM boreholes in the previous section, the air temperature and relative humidity behind the packer rise in response to heating. In contrast with the SM borehole, the leak of gas associated with the H:D borehole packer or the gas tracer tests did not appear to impact the heated SL borehole, despite their proximity.

The in-drift thermocouples associated with SL boreholes (left panel) all show behavior like the ambient air temperature observed in the drift (Figure 27), while the measurements behind the packer in the SL boreholes do not show much change of air temperature or relative humidity.

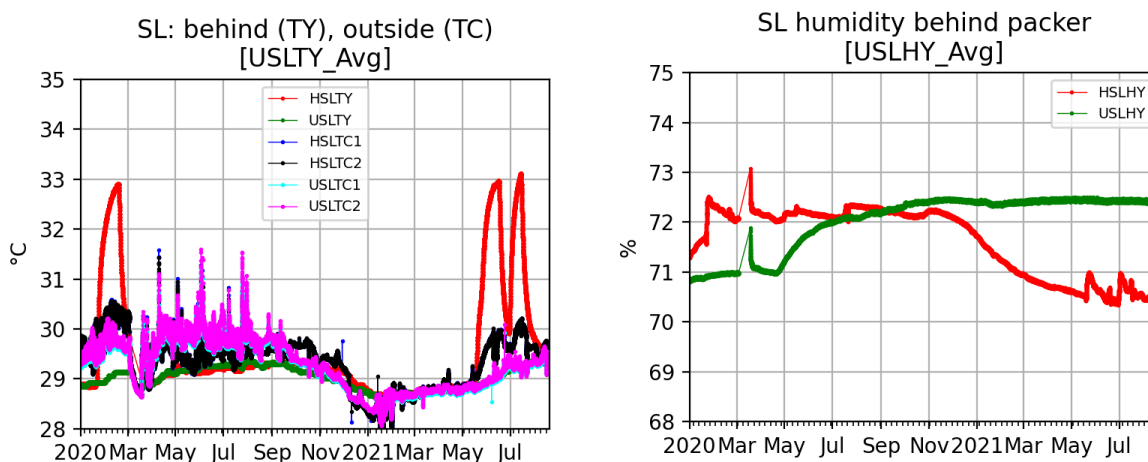


Figure 25. Air temperature (left) and relative humidity (right) for SL boreholes during BATS 1a.

3.6.2 Strain and temperature time series

The lab-constructed seals were instrumented with embedded strain gauges to observe strain in the salt once the borehole has closed in and made contact on the laboratory-fabricated cement plugs. Two types of strain gauges were implemented in the cement plugs observe three components of strain and temperature (via thermistors).

The three perpendicular Geokon strain gauges are in the sorel cement plug closer to the back of the borehole, while the VPG “waffle” strain gauge is in the salt concrete plug, closer to the front of the borehole. The VPG strain gauge in the heated seal (red curve in top right panel of Figure 26) shows the change in strain due to thermal expansion stresses related to heating, while the seal in the unheated array shows minimal strain. The data from the three-component Geokon vibrating wire strain in the sorel cement plugs do not begin until after heating started, due to a configuration issue with the equipment used to communicate with the gauges. In both the heated and unheated arrays, the three-component gauges show gauge 1 (the axial gauge at the back of the SL borehole – see Kuhlman et al. (2020) for more details about strain gauge configuration) is experiencing extension, while the two radial gauges are experiencing compression.

The upper-left panel of Figure 26 shows the temperature measured via thermistors inside the cement plugs in the SL boreholes (co-located with the Geokon strain gauges). Figure 25 shows the air temperature in the space between the cement plugs and the mechanical packers. The temperature of the cement plug in the heated SL borehole reaches a higher temperature than the air does. The three thermistors in the cement seal also reveal a temperature gradient along the length of the plug due to the relative proximity of sensors to the heater.

By May 2021, all the Geokon vibrating wire strain gauges have failed (reporting very large positive or negative strains, although their associated thermistors report consistent temperatures), while the roughly axial VPG waffle strain gauges appear to be operational. The Geokon strain gauges likely failed due to corrosion of the sensor and associated wiring in a humid salt-concrete environment. The gauges were coated in silicone by the manufacturer to hopefully make them last longer in this environment, but apparently this effort was not successful.

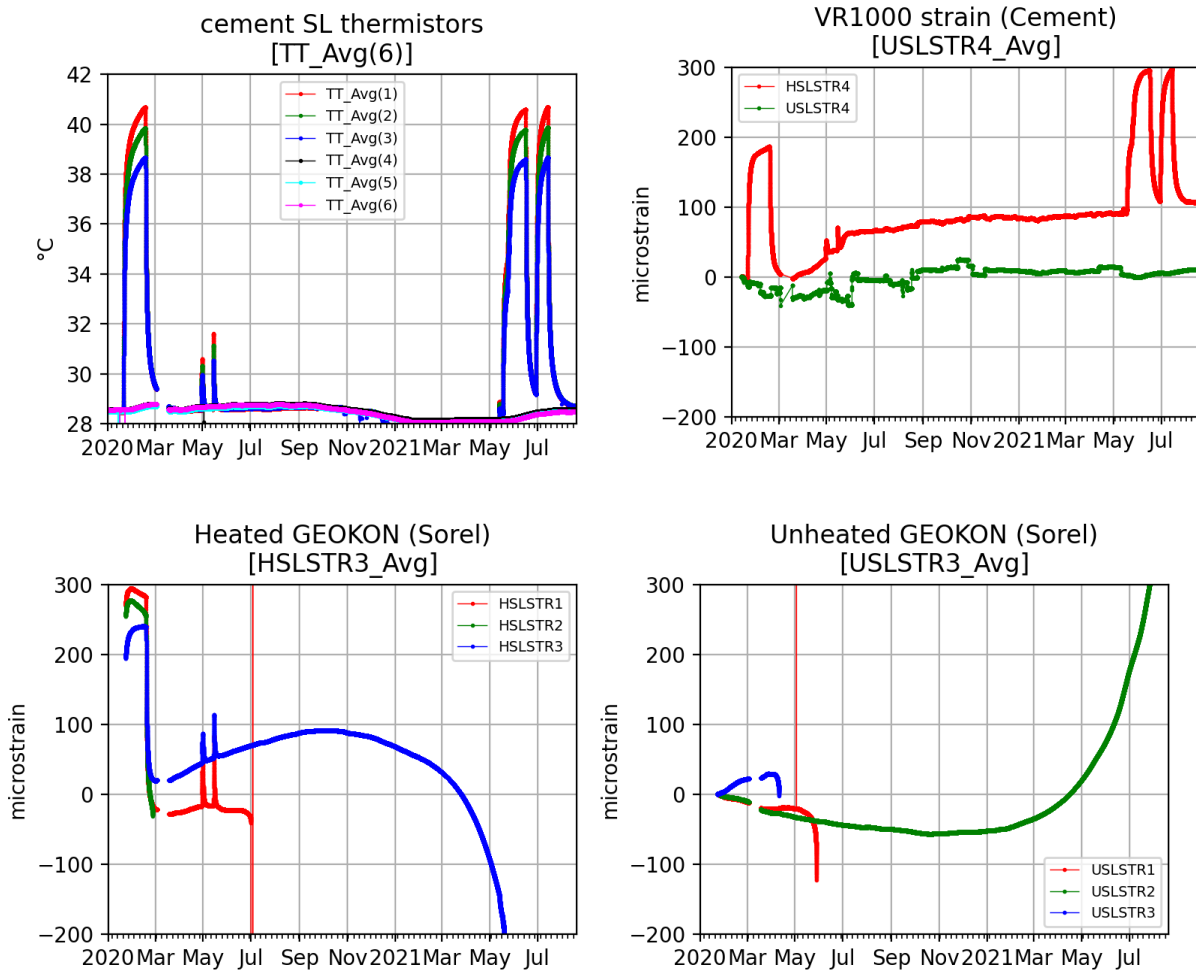


Figure 26. Strain and temperature inside cement plugs in SL borehole.

3.6.3 Salt, brine, and cementitious material interactions analysis

In FY22, before BATS phase 2, the 4.8-inch [12.2 cm] diameter heated SL borehole plugs will be over-cored with a 12-inch [30.5 cm] coring bit to examine the interaction between the cements (salt concrete and sorel cement), the intact salt surrounding the borehole, and any brine that has flowed into the borehole during the test. After removing the mechanical packer and RH sensor, any liquid brine in the borehole will be sampled for compositional analysis before over-coring. For stability reasons the rear part of the SL borehole (near the seal) will be filled with grout before over-coring. The over-cored samples will also be analyzed via computed tomography (CT) scanning at the National Energy Technology Laboratory (NETL), as the pre-test cores were analyzed (Kuhlman et al., 2020). Sub-cores of each material and across the salt-cement interfaces will be collected for petrographic (optical and scanning electron microscope analysis of thin sections), mineralogical, and micro-CT analyses. The samples will be characterized for evidence of alteration of the salt or cementitious materials. Such investigations will include examining samples as a function of distance from the salt-cement interface.

3.7 In-Drift Time Series

Weather station measurements were made in the N-940 drift. Figure 27 shows 15-minute average air temperature, relative humidity, barometric pressure, and air speed near the datalogger enclosures. Drift air temperature was relatively constant, except from April to September 2020 when the drift air temperature

peaked 3 to 4 degrees higher several times and some days in January and February 2021 when the drift air temperature decreased 1 to 2 degrees several times. The relative humidity in the winter (roughly November to April) was generally below 25%, while summer RH was 40 to 50% in the summer of 2020 and 50 to 60% in the summer of 2021. Changes in ventilation air speeds are likely due to changes in routing of ventilation in the WIPP underground, which is due to ventilation needs and proximity of other activities in WIPP (e.g., mining or rock bolting). Lower ventilation air speeds occur at night when fewer personnel are underground at WIPP. Small fluctuations in air temperature appear to correlate with daily changes in drift ventilation. Barometric pressure fluctuations generally stay between 960 and 980 mbar, with higher-amplitude fluctuations in the winter and spring months.

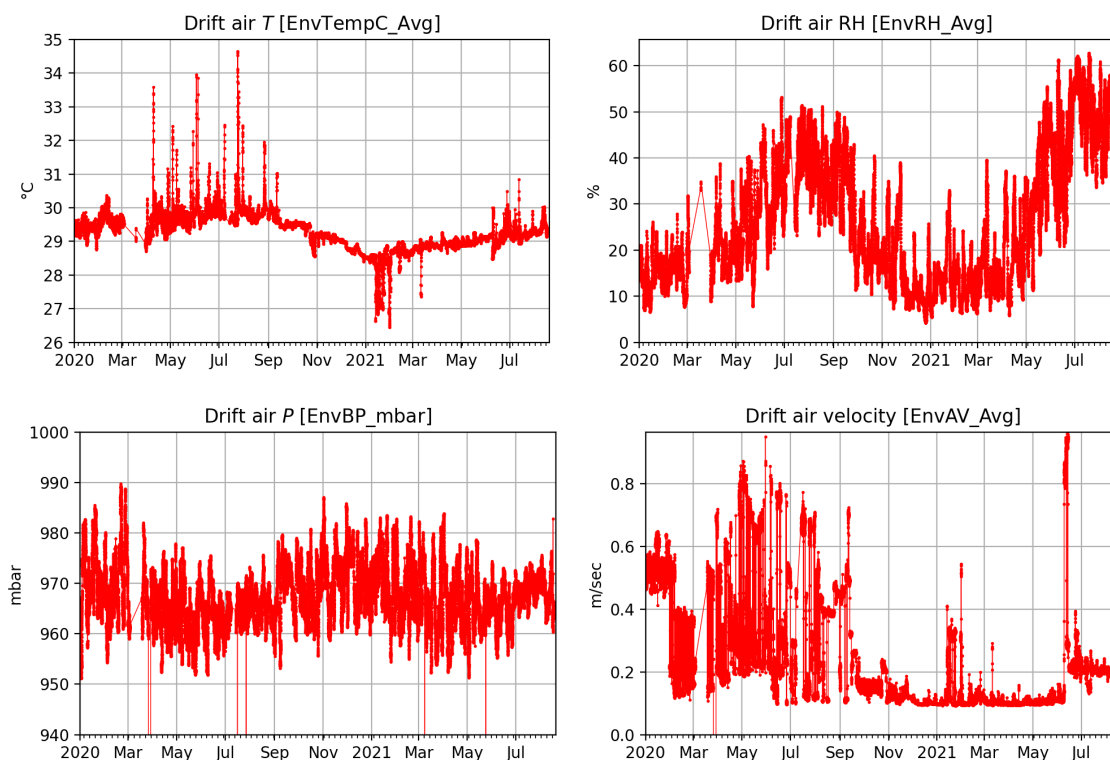


Figure 27. In-drift air temperature (top left), relative humidity (top right), barometric pressure (bottom left), and air speed (bottom right).

4. BATS Phase 1b Gas Tracer Tests: January to June 2021

The gas tracer tests were conducted first, with the unheated gas tracer tests conducted before the heated one. The unheated gas tracer test was first conducted in the unheated array. A small source bottle of tracer gas was purchased from Matheson with the composition 5% Kr, 5% Ar, 5% SF₆, 85% N₂. This was plumbed with a double-ended cylinder (DEC) as shown in Figure 4, to allow filling the interval behind the D packer with tracer gas. Neither the packed-off interval nor the DEC was evacuated before pressurizing with tracer gas, so it was a mixture of added gas at the specified pressure with existing gas at atmospheric pressure (i.e., air for the first tracer test, and remnant of tracer gas from the preceding test for follow-on tracer tests). The solenoids on the gas circulation system were set to only monitor one array at a time (no switching), to reduce the chance of missing the gas breakthrough with the SRS gas analyzer.

Table 2 lists key statistics regarding the gas tracer tests. As part of BATS phase 1b, an unheated array gas tracer test was conducted first in the unheated array (test 1), then three unheated tracer tests were conducted in the heated array (tests 2 through 4), and finally a heated gas tracer test was conducted in the heated array (test 5).

Table 2. Gas tracer test statistics.

Test	Array	Heated	Begin Date, Time	Source Pressure (bars gauge)	Notes
1	U	No	Jan 11, 10:29 AM	3.144	
2	H	No	Feb 1, 8:42 AM	1.073	No gas breakthrough observed
3	H	No	Feb 10, 8:52 AM	2.038	Gas analyzer turbopump failed
4	H	No	May 13, 10:29 AM	2.064	
5	H	Yes	Jun 3, 8:43 AM	2.115	Gas breakthrough after heat off

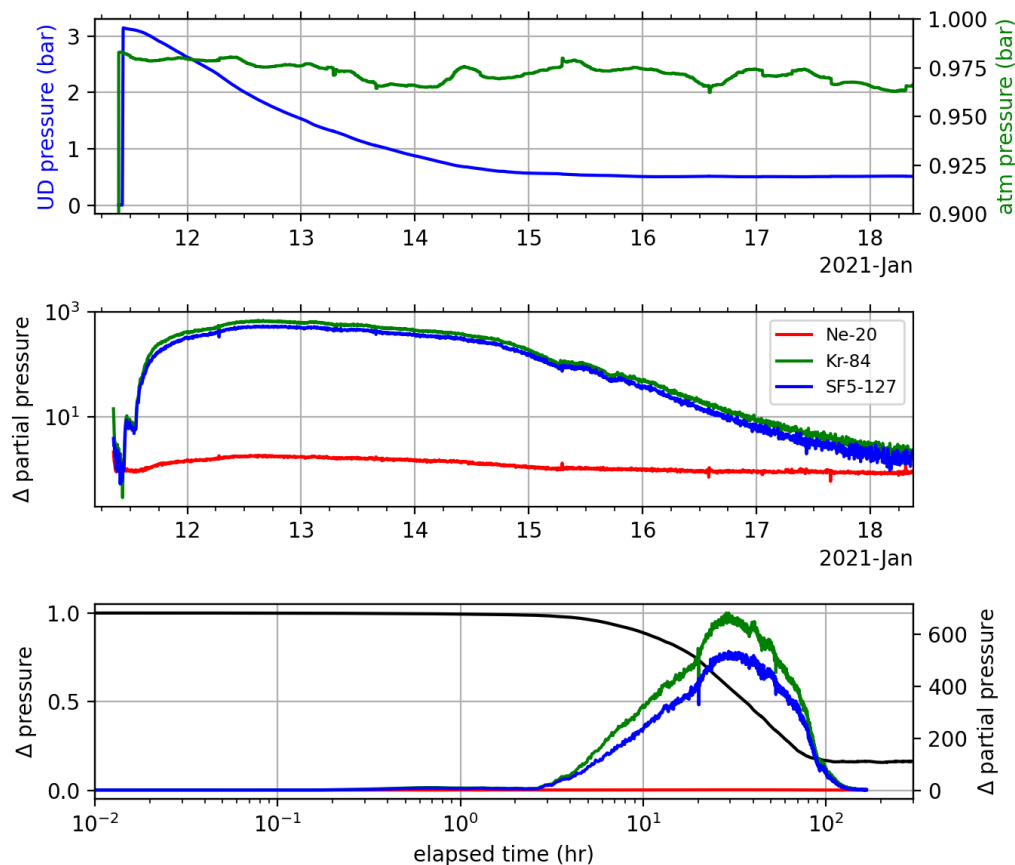


Figure 28. Gas tracer test 1 results in unheated array.

In Figure 28 the top panel shows the pressure decline observed in the source (unheated D) borehole and the middle panel shows change in tracer partial pressures illustrating breakthrough observed in the gas circulation of the unheated HP borehole. The bottom panel shows the same data (relative change in source pressure and the relative change in partial pressure of tracer gases) against log-scale elapsed time from when the interval behind the packer was shut in. Tracer test 1 showed a clear rise in tracer partial pressure after approximately three hours, a peak at approximately 30 hours, and subsequent decrease in tracer partial pressure over several days, like a classical diffusion of gas through the salt, as would be expected in a single-phase medium.

A residual tracer gas pressure of almost 0.5 bars remained behind the D packer after more than 100 hours.

Based on previous permeability testing, it was believed the packer-isolated interval in the D borehole in the heated array could not hold 3 bars pressure, so the first test in the heated array was only pressurized to approximately 1 bar pressure (test 2 – not shown in an individual figure, pressure response is shown with other tests in Figure 33). The pressure of the tracer gas added behind the heated D packer declined quickly to essentially no residual pressure, but no tracer gas was observed in the HP circulation.

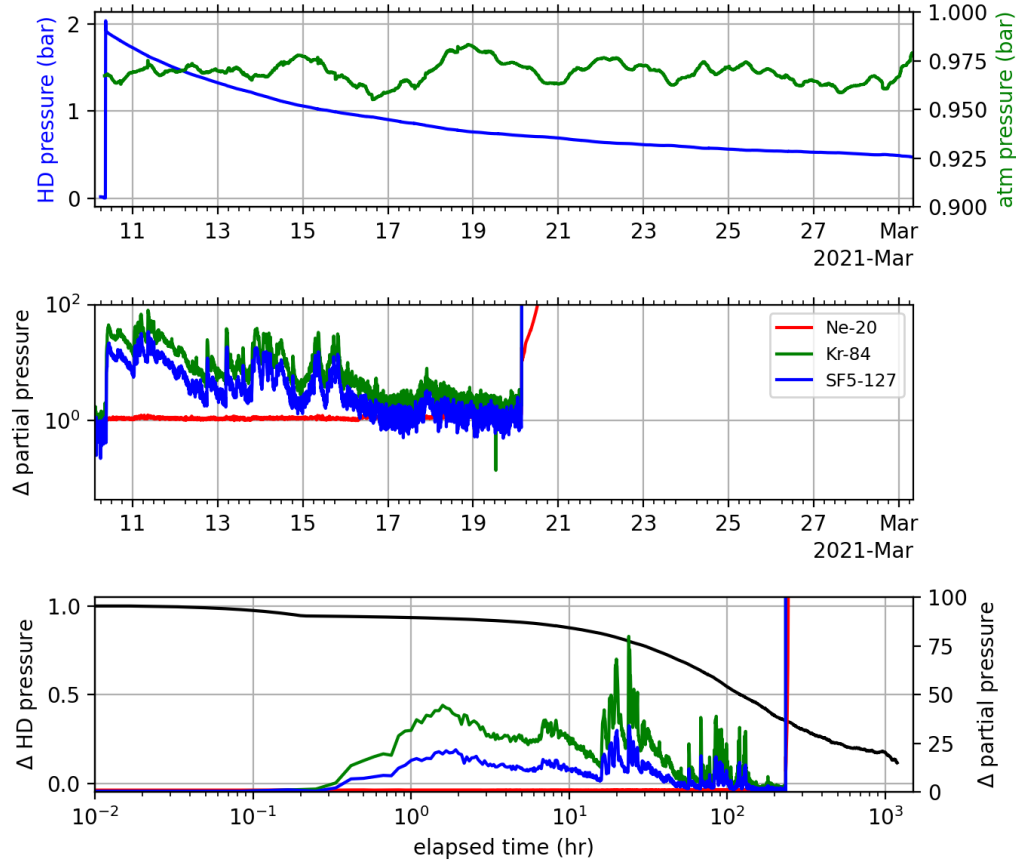


Figure 29. Gas tracer test 3 results (unheated) in heated array.

In Figure 29 the top panel shows the pressure decline observed in the heated D source borehole during tracer test 3 (no heating), when the source pressure was increased to 2 bars. The gas breakthrough in the heated HP circulation system (middle panel) showed an almost immediate rise, and a more complex or jagged breakthrough decline curve. On March 20, the turbopump on the SRS gas analyzer failed, requiring the instrument to be sent back to the manufacturer for repairs.

Like test 1 in the unheated array, a residual pressure behind the D packer of almost 0.5 bars remained out to 1000 hours after the start of the test.

The pressure in the source interval showed a very rapid early time drop (first 0.1 hours; see bottom panel of Figure 29) immediately preceding early tracer began to breakthrough (approximately 0.3 hours). Tracer increased in the HP borehole until about 2 hours, with another increase at 7 hours and more increases at 15 and 30 hours, followed by an irregular decrease through the rest of the test. Despite the jagged tracer breakthrough, the decline in pressure was mostly smooth (aside from the early-time rapid drop before 0.1 hours). The barometric pressure in the drift is plotted in the top panel (green line). It appears there may be some weak correlation between the later peaks of gas breakthrough and barometric pressure measured in the drift, but not all the fluctuations in the concentration data can be clearly associated with changes in barometric pressure.

There may be several contributing mechanisms contributing to this irregular breakthrough behavior, including two-phase flow (i.e., gas bubbling into brine-filled fractures), a network of discrete fractures (i.e., combinations of shorter and longer pathways between the boreholes leading to both early- and late-

time flow), and contributions from barometric pumping (i.e., a variable air pressure in the drift, differentially impacting both the source and destination boreholes in a delayed manner).

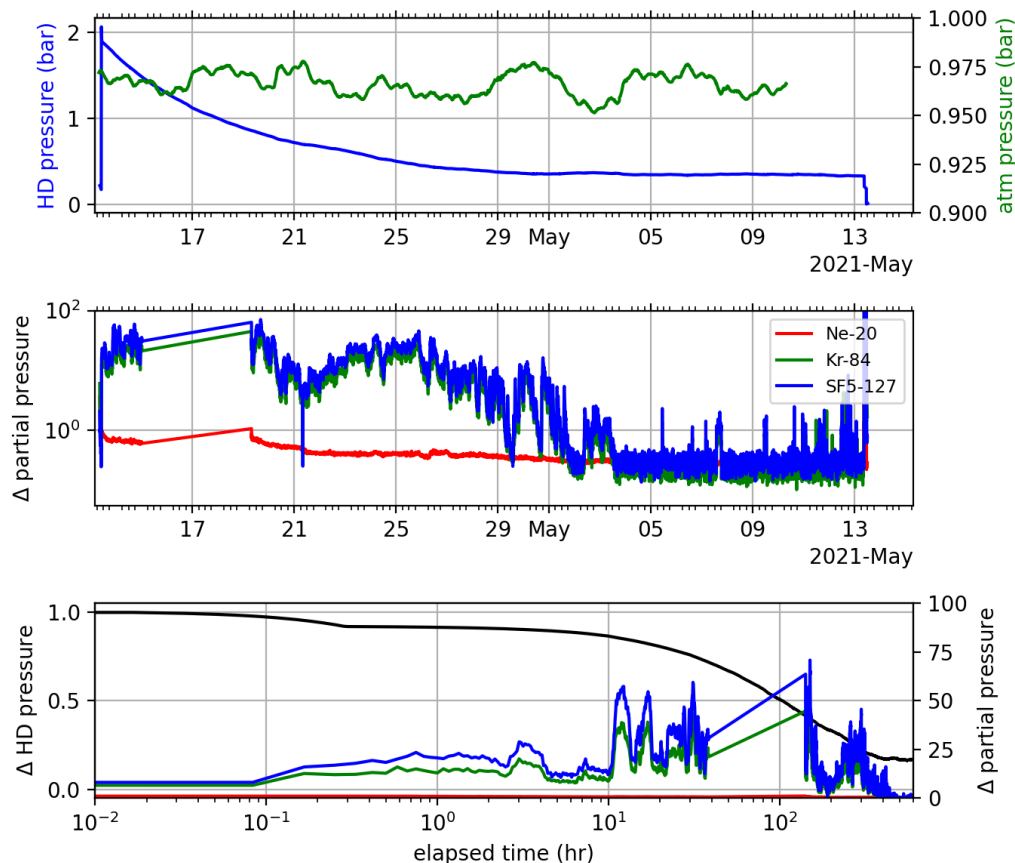


Figure 30. Gas tracer test 4 results (unheated) in heated array.

After the repair of the SRS gas analyzer, test 4 was essentially a repeat of test 3 (same source pressure and configuration). An even earlier fast breakthrough of gases was observed (approximately 0.1 hours) associated with a similar rapid early time drop in pressure (bottom panel Figure 30), followed by a gentler decline in source interval pressure and a similar complex irregular breakthrough of gases.

The gap in the gas analyzer data around May 16 to 20 is due to an issue with an internal safety sensor turning the mass spectrometer sensor off. When WIPP TCO next came underground, the sensor was turned back on, and the rest of the breakthrough was observed as planned.

There may be some weak correlation between the small peaks in the tracer gas partial pressures and the drift barometric pressure, but it is also clear that all the fluctuations cannot be explained by this alone. After approximately 500 hours, a residual pressure less than 0.5 bars remained behind the D packer. Like test 3, there may be multiple explanations for the observed tracer breakthrough behavior.

Test 4 is the only gas tracer test where the SF₆ breakthrough was at a higher level than the Kr breakthrough, but the reason for this difference is not immediately clear.

At the end of tracer test 4, the gas remaining behind the heated D packer was connected directly to the SRS gas analyzer to check the source concentration. Kr-84 and SF₅-127 were observed at partial pressures 68,000× and 62,000× higher than the background concentration (Kr-84 signal being higher), which is significantly higher than the concentrations observed in any of the tracer test breakthrough (i.e., 500× and

600× in tracer test 1 – Figure 28). Some of this difference is due to the very low mass recovery expected in this test (i.e., only a small fraction of the gas is expected to make it to the interval behind the HP packer), and secondly the gas flowing into the HP borehole is further diluted by the UHP N₂ stream that circulates it out of the borehole to the detector.

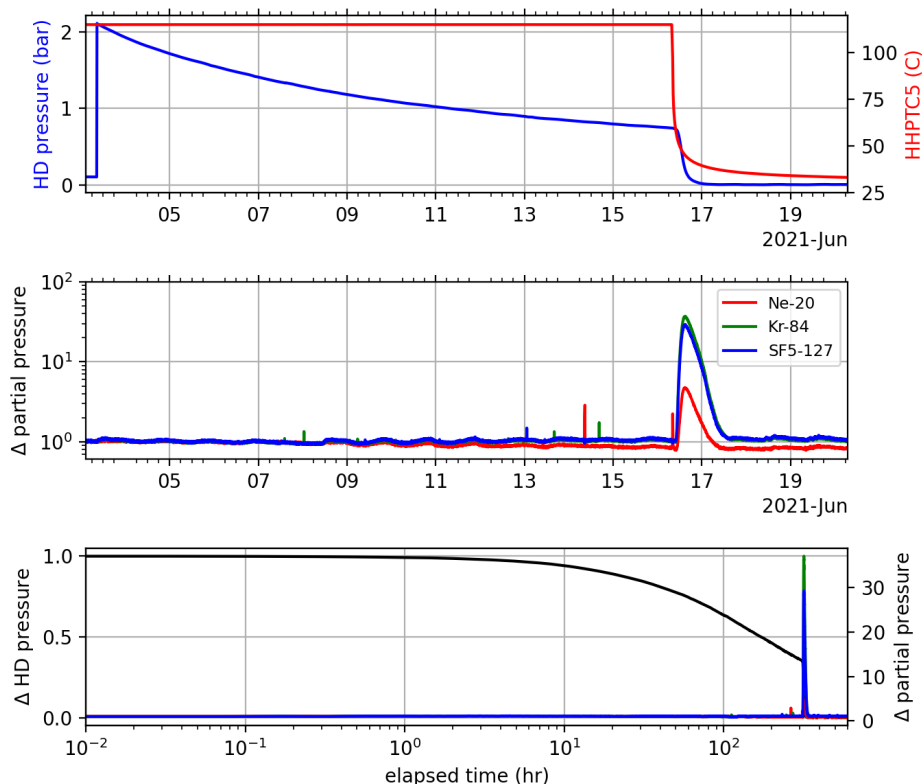


Figure 31. Gas tracer test 5 results (heated) in heated array.

Figure 31 shows the results of tracer test 5, which was conducted after turning on the heat (May 18), allowing the salt between the HP and D boreholes to heat up. Gas tracer was added Jun 3. Although the pressure declined in the source borehole, no tracer breakthrough was observed in the HP borehole until after the heat was turned off on June 16. The controlling thermocouple (located in the middle of the heated interval in the HP borehole) is shown on the right-hand y-axis in the top panel. The tracer breakthrough to the HP borehole occurred very rapidly after turning off the heater, and the tracer breakthrough was smooth.

The pressure response in the source borehole also does not show the same early-time rapid drop in pressure observed in tracer tests 3 and 4 at approximately 0.1 hours.

Figure 32 shows RH observations made behind the mechanical packer in the SM boreholes. This data was plotted previously over a longer time in Figure 24. From May 18 to June 16 the RH in this borehole increased from just over 71 to almost 73% during heating. After the heat was turned off June 16, the RH rapidly declined to 67% over the course of 3 to 4 days, possibly due to the migration of tracer gas through the salt after cooling. The RH observations in the SM borehole are only an indirect measurement, but they do give evidence that the tracer gas flowed throughout the salt, and not just flowed through a single fracture linking the HP and D boreholes. The RH in this borehole also decreased at the end of the BATS 1a heater test, in response to the leak of packer inflation gas into the formation.

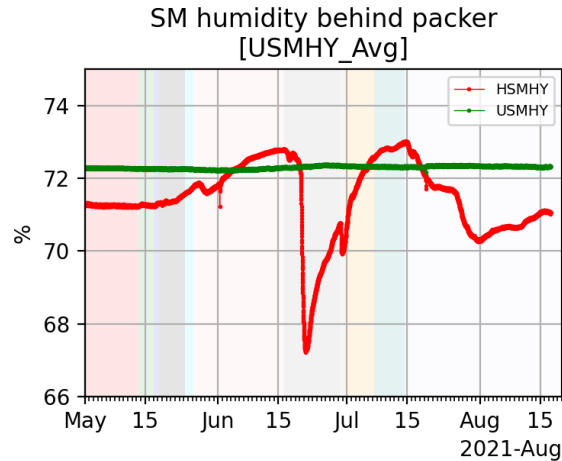


Figure 32. RH observed in SM boreholes during tracer testing activities

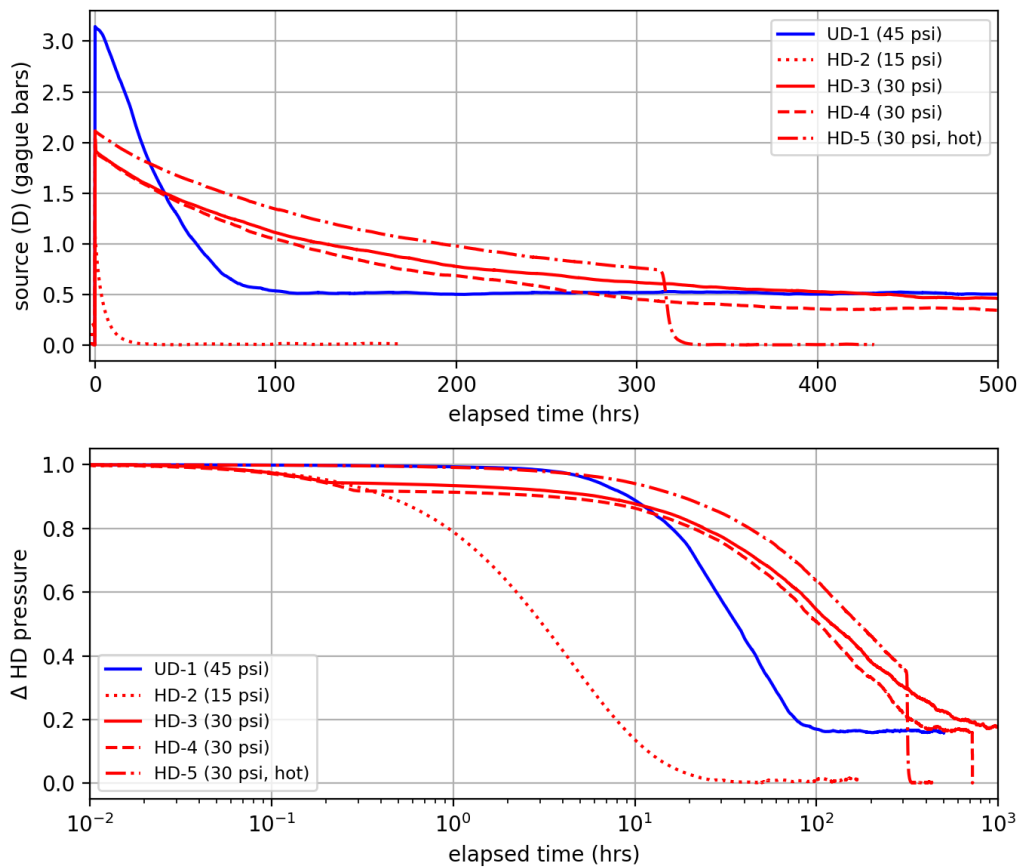


Figure 33. All gas tracer test source borehole pressure responses.

Figure 33 shows the source borehole pressure responses from all five gas tracer tests plotted on a common elapsed time abscissa. The unheated array tracer test is blue, the heated array tracer tests are red, with different line types signifying the different tests. The upper panel shows the responses in terms of gauge pressure (i.e., pressure above atmospheric), as they are measured. The lower panel shows the same responses scaled to the make the peak pressures all of unit height and a log elapsed time axis.

The pressure response of tests 3 and 4 are quite similar, despite the tracer breakthrough having different irregular shapes. When scaled, the low-pressure tracer test with no gas breakthrough (test 2) follows tests 3 and 4 at early time in the lower panel. The heated test (5) does not show the same early-time rapid drop, but instead roughly parallels the later-time behavior of tests 3 and 4, at a higher pressure. This early time drop in pressure (not seen in the heated test) may be associated with a liquid-filled fracture near the HP borehole that was closed off due to thermal expansion from heating.

Despite being apparently more permeable than the unheated array at ambient temperature, during heating the heated array held gas at a higher pressure for a longer period than the unheated array.

Test 2 showed a very fast decline in pressure (considered to possibly be a leaky packer at the time) and held no significant residual pressure after approximately 100 hours. The other three unheated tests (tests 1, 3 and 4) all reached approximately the same late-time scaled pressure behind the packer.

5. BATS Phase 1c Liquid Tracer Tests: July to August 2021

In this section we discuss the heated liquid tracer test results, which are preliminary since this portion of the test is still ongoing. Some of the data are also relevant to the heated gas tracer test (test 5).

5.1 Water Production Data During Heating

Figure 34 shows temperatures observed in some of the thermocouples in the heated array during the two heating events in June and July 2021 (thermocouples in ERT boreholes are not plotted, since they have almost all failed by this time). Shading in the background of these figures indicates key events, summarized in Table 3 (these select events and many more are listed in the comprehensive event catalog given in the Appendix, Table 6). These results are a zoomed in to show additional detail associated with the heating events, but this data was also shown in Figure 18. In these zoomed-in figures, the minor tick-marks indicate individual days.

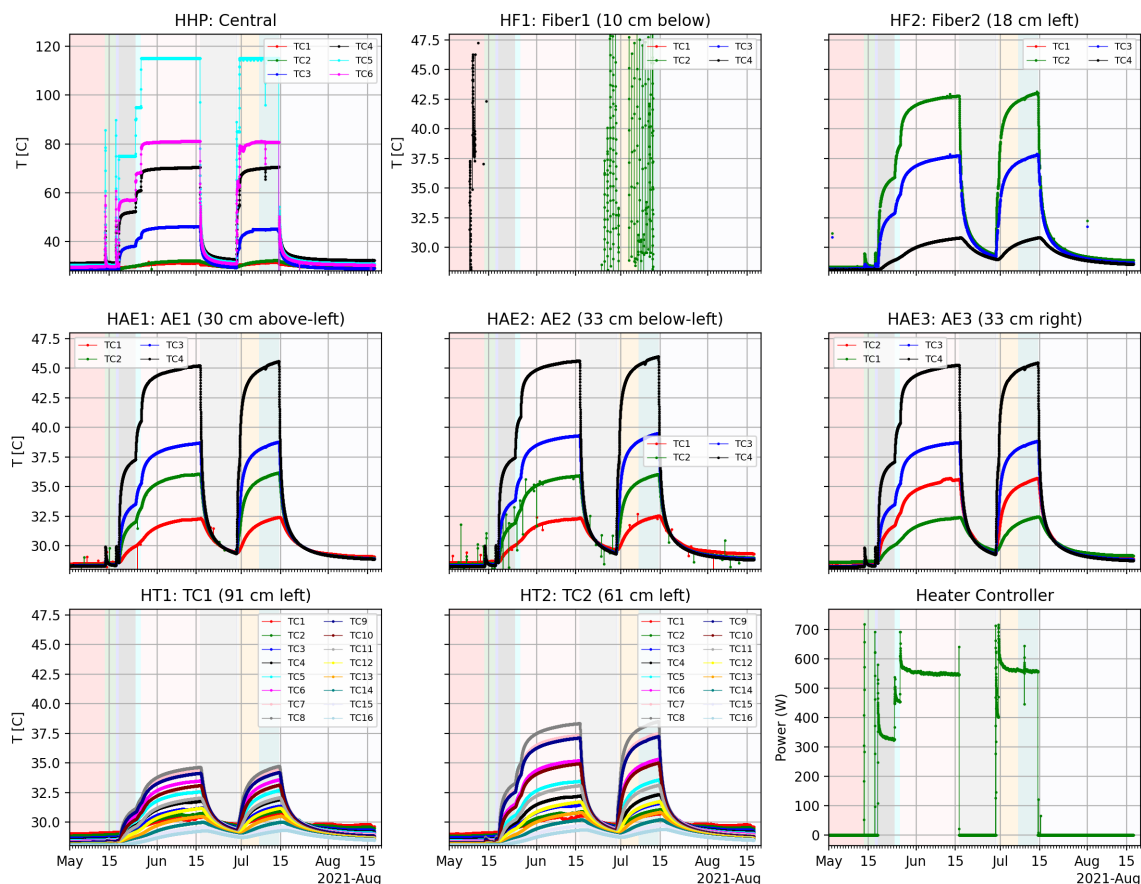


Figure 34. Temperature response of thermocouples in heated array during heated tracer test.

Before the heated gas tracer test, two attempts (May 13 and 17) were made to start the heater by programming it directly to its final desired setpoint, but in both cases the heater controller turned off after a few hours. On May 18, the heater was turned on at a lower setpoint (75 °C), which was then increased stepwise to the target setpoint (115 °C) by May 26. The heater was then turned off on June 16, leading to the rapid breakthrough of gases into the HP borehole shown in Figure 31 and decrease in RH in the SM borehole seen in Figure 32.

Table 3. Key events during 2021 heated tracer tests.

Date Time	Event
May 13, 11:10 AM	Failed heating attempt 1
May 17, 07:10 AM	Failed heating attempt 2
May 18, 07:36 AM	Heater on at 75 °C (gas tracer test 5)
May 24, 07:07 AM	Heater setpoint increased to 90 °C
May 26, 07:24 AM	Heater setpoint increased to 110 °C
May 26, 08:01 AM	Heater setpoint increased to 115 °C
June 16, 07:53 AM	Heater off
June 29, 07:35 AM	Heater on at 50 °C (liquid tracer test)
June 29, 10:17 AM	Heater triggered off (was set at 100 °C)
June 29, 10:20 AM	Heater restarted at 85 °C
June 30, 07:48 AM	Heater setpoint increased to 95 °C
June 30, 09:37 AM	Heater setpoint increased to 115 °C
July 7, 09:40 AM	Liquid tracers added to heated D borehole
July 14, 12:24 PM	Heater off

After two weeks of cool-down, on June 29 the heater was re-started as part of the liquid tracer test. The heater setpoint was more rapidly adjusted stepwise up to the final desired temperature of 115 °C by June 30.

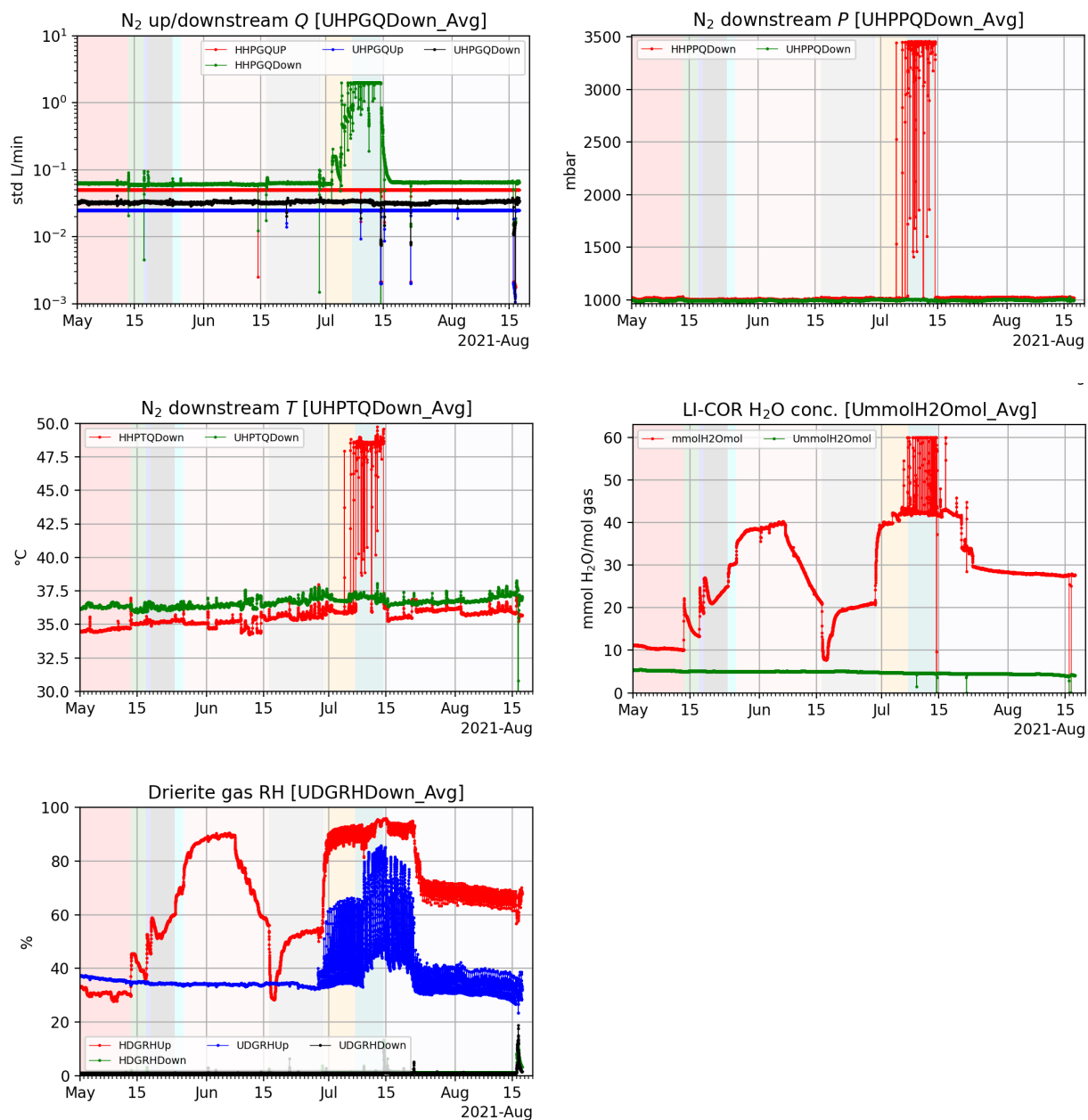


Figure 35. Multiparameter flowmeter, LI-COR 850, and RH data during heated gas and liquid tracer tests

Figure 35 shows observations from the multiparameter flowmeters downstream of the HP packer, the LI-COR 850 observations of water concentration, and the relative humidity (RH) both up- and downstream of the desiccant. Like the temperature data, these were already shown in earlier figures, but are plotted again at a scale to allow closer discussion of details relevant to the heated gas and liquid tracer tests.

Starting on June 30, when the heat was turned back on after a two-week cooldown period, brine production surged (see LI-COR and desiccant humidity data). The flowrate, pressure, and temperature measured by the multiparameter flowmeter all began to rise above ambient levels just before the addition of liquid brine in the heated D borehole on July 7. This might be due to the heater converting standing

water in the HP borehole, associated with the previous on/off heater cycle, into steam. The phase change would increase the flowrate (which apparently maxed out the flowmeter at 2 std L/min) as well as the pressure (likely reporting the instrument maximum of 50 psi) and temperature. The high temperature may be due to a combination of heat convecting down the ¼” tubing and the latent heat of condensation on or near the multiparameter flow meter. When brine was added to the D borehole on July 7, the brine production only increased.

The LI-COR 850 and Picarro CRDS are different instruments that also show the increase in water content during the liquid tracer test, but the mass flowrate of gas reported by the multiparameter flow meter may be erroneous (i.e., associated with conditions beyond the instrument’s accurate range).

The unheated desiccant (blue curve in lower subplot of Figure 35) also rose, because these sensors are downstream of two solenoid-switched valves. High humidity (and possibly condensation) in the tubing takes some time to clear out at the low flowrates in the unheated array (25 std mL/min).

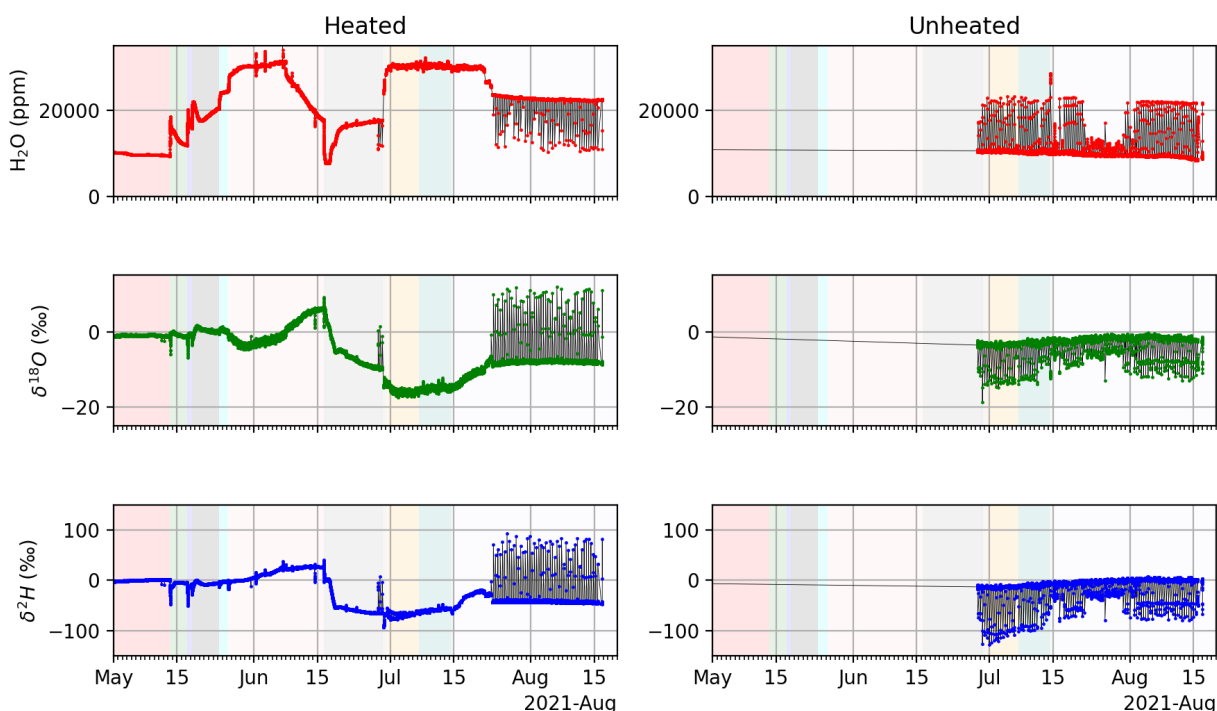


Figure 36. Picarro CRDS data during heated tracer tests.

Figure 36 shows the Picarro CRDS results for the same period shown in the previous two figures. The same relative profiles of water production are observed between the Picarro, the LI-COR 850, and the desiccant (although each of the results are in different units).

The oxygen and hydrogen isotopes after the beginning of July support the idea that liquid water was standing in the borehole when the heater was on (causing evaporation and fractionation), leading to very light ($\delta^{18}O \leq -10 \text{ ‰}$ or $\delta^2H \leq -50 \text{ ‰}$) readings. When water production decreased in later July, the isotopic signature also got heavier, possibly indicating the system was drying out. The liquid tracer was made with an isotopically light snowmelt source, but the confluence of both standing liquid water and the tracer source is hard to disentangle at this moment. After more data collection (including over-coring of the HP packer), the interpretation of these data may become clearer.

5.2 AE Observations During May to Aug 2021 Heating Events

During the heating events listed in Table 3, the acoustic emission system was observing many events. Gaps in the data do occur on June 7, June 14, June 28 to July 6, July 9 to 14, and July 21 to 22. The threshold was raised to 45 dB during postprocessing to manage file size.

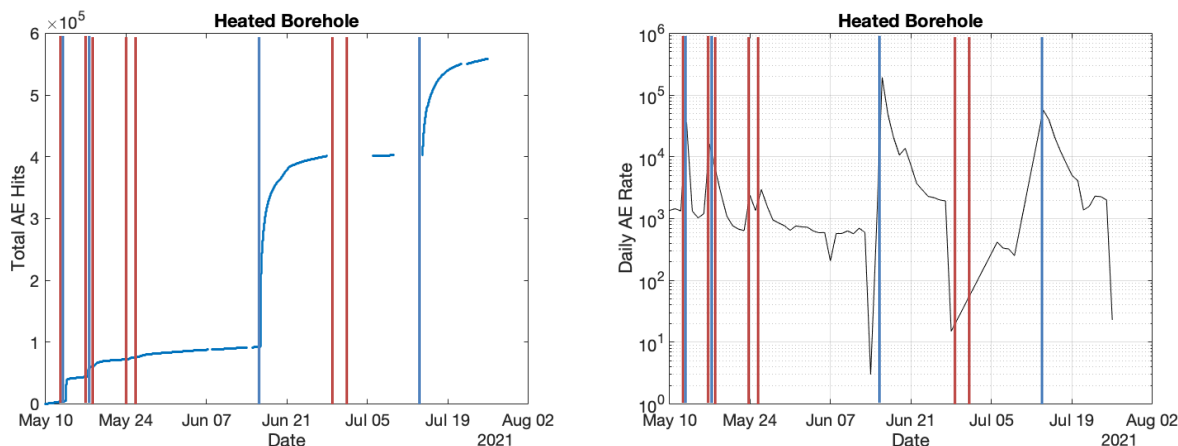


Figure 37. Total number of AE hits and daily rate per array during May to July 2021 heater test. Orange lines represent heating phases in the borehole; blue lines represent cooling phases.

Figure 37 shows the cumulative AE behavior and the daily AE rates. Increases can be seen for both heating and cooling phases, but far greater activity is associated with cooling periods. Pulses of AE activity can be seen on May 13 and May 17 for heater on/off events. Raising the temperature on May 24 and 26 also create surges in AE activity. Turning the heater off on June 16 after a long heating phase has a daily rate an order of magnitude higher than any other day. Turning the heater off on July 14 creates another surge in AE activity, but not as great as the previous cooling activity. We hypothesize that the June 16 cooling event is greater than the July 14 cooling event because of the longer heated period prior to the June 16 shutdown. This longer heating event would have created a larger thermally disturbed interval around the borehole to create hits during cooling. Another possibility would be the Kaiser effect, a phenomenon in metals where AE is not observed in reloads until the previous maximum load is reached. From this data, this does not fully explain the behavior. The borehole is subjected to similar thermal loading as BATS phase 1a, and there is a reduction in activity. The total numbers of AE hits are very close for the heater test in January to February 2020 and May to June 2021, despite the May to June 2021 test have double the number of sensors as BATS phase 1a. The Kaiser effect would indicate that no AE should be observed for similar (thermal) loading paths, but the Kaiser effect is a manifestation of accumulating damage—it is likely that heated salt is able to heal damage that occurred previously and negate the Kaiser effect during cooling.

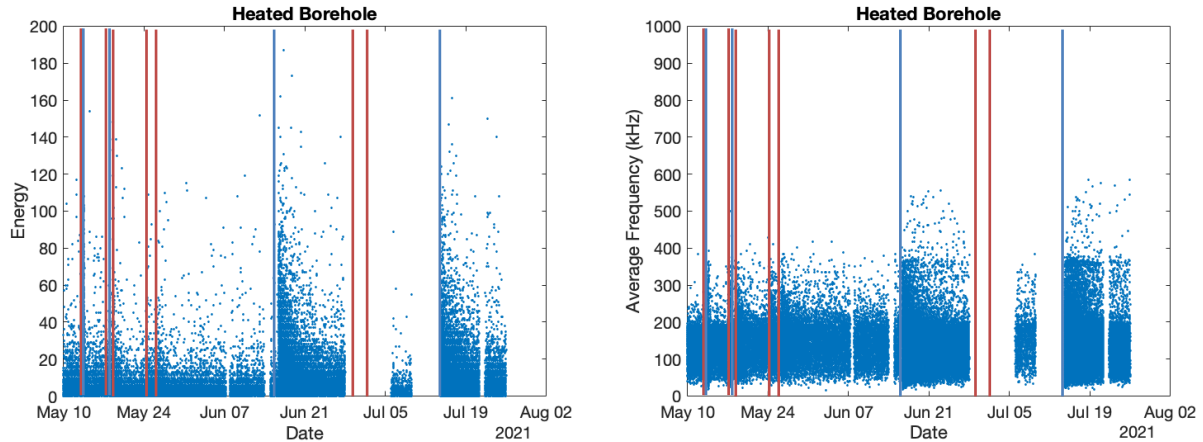


Figure 38. Energy (left) and frequency (right) content of AE from May to July 2021 heater test.

Figure 38 shows energy (10 μ volt-sec/count) and frequency content for AE during the May to July 2021 heater test. BATS phase 1a demonstrated that the energy and average frequencies of AE increase at the beginning of heating and cooling. In this test, similar behavior is observed. Large increases in energy and average frequency occur during cooling periods. Smaller increases can be observed with heating, but they are not as distinct as the increases associated with heating in BATS 1a.

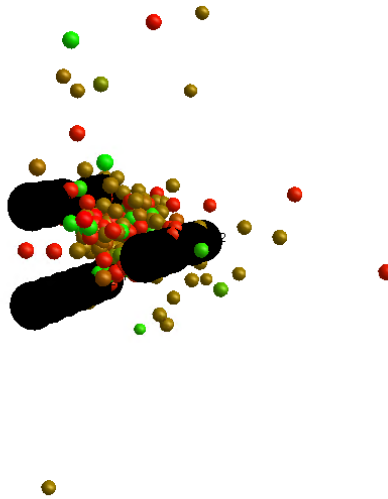


Figure 39. Event localizations of May to July 2021 heater test showing sensors, black cones, and event, colored spheres. Color scale shows time progression, with red colors representing May 10 and green representing July 26.

Figure 39 shows located AE events from the May to July 2021 heater tests (black AE boreholes indicate spatial scale). Events are clustered around the heated borehole in a tight cloud, primarily located within the AE boreholes. Red and green events are randomly distributed and collocated. Brown events correspond to the cooling phase on June 16, and these form a broader cloud due to the higher number of events and larger thermally stresses volume around the heater. As opposed to the tracer tests, these events are located at the borehole array due to the centralized thermal stress source, as well as the higher threshold reducing background events.

6. Planned Post-Test Analyses

Several destructive post-test analyses are planned for the heated array. These will be completed in FY22 before drilling the new BATS phase 2 array nearby.

6.1 Borehole Precipitate Analysis

After removing the packer from the HP borehole but before over-coring it, the salt precipitate and any liquid present in the borehole will be scraped out, and both solids and liquids will be sampled. Borehole video and still cameras will be used to document the condition of the borehole and the distribution of solids and liquids before collecting discrete samples and performing bulk salt removal. Several samples will be collected from each type of salt deposit (salt near the heater should be different from salt at the end of the borehole near the N₂ inlet, due to differences in temperature). Samples will be visually inspected by a geologist upon collection (difference between precipitate, recrystallized, original Salado salt, and salt impacted by metal corrosion products). Samples will be preserved and labeled in the field to reduce damage and contamination.

Precipitate samples will be analyzed using bulk X-ray diffraction to estimate the mineral phases present and bulk X-ray fluorescence (XRF) to determine the elemental composition of the precipitated salt. Thermal gravimetric analysis (TGA) may also be used to further help identify any hydrous minerals formed in the borehole through their characteristic dehydration temperature. The water phase driven off during TGA may be analyzed isotopically to further constrain the fractionation models proposed to explain the stable water isotope time series collected in the HP boreholes. The isotopic makeup of hydrous salts is possibly a point of significant uncertainty in isotope fractionation models (Krause, 1983; Clynne et al. 1981).

The precipitated salts will be analyzed after washing the salts with a series of solutions: saturated Na-Cl brine (to dissolve minerals more soluble than halite) and deionized water (to remove all soluble minerals). It is not expected that significant carbonate or sulfate minerals will precipitate in the borehole, but if there are, they can be analyzed like the bulk salt.

Any liquid phases present in boreholes at the end of the test will be sampled and their composition will be analyzed. These solid and liquid compositional data will be used to constrain geochemical models that predict the mineral phases that would precipitate under the observed conditions.

6.2 Salt Sampling via Over-Core

After the packer is removed from the heated HP borehole, a large-diameter (12 inch [30.5 cm]) horizontal core will be collected around the HP borehole to quantify the effects of heating and map the distribution of liquid tracers in the salt. The heated SL borehole will also be over-cored.

To reduce damage to the salt near the boreholes during the over-coring process, the boreholes will be grouted to stabilize the salt surrounding the borehole, hopefully minimizing damage from coring and handling.

Any core collected after the test in the region where tracers were added will be checked for fluorescent tracer by ultraviolet flashlight and will be preserved in a similar manner to the way the pre-test core was collected and preserved. This core will also be sent to NETL for CT imaging and documentation. The borehole from over-coring should also be documented with borehole logging using a black-light light source.

The ERT, DSS, DTS, and AE sensors must be disconnected, and in-drift enclosures will need to be moved before drilling the post-test core. The measurements in the unheated array will continue if possible, or at least will be re-connected after over-coring and drilling of the new BATS 2 heated array is complete.

After both pre-test and post-test cores have been analyzed via non-destructive whole-core methods, the cores will be sub-cored and sampled for laboratory microscopic (e.g., thin section petrography) and compositional analyses.

7. Summary

This updated report on the Brine Availability Test in Salt (BATS) field test in the underground at the Waste Isolation Pilot Plant (WIPP) presented the motivation and technical background for creating coupled process field experiments in salt, along with data collected from tracer tests in BATS phase 1b and 1c. Brine is important to radioactive waste disposal safety as brine leads to corrosion of waste packages and waste forms, is the primary offsite transport vector, can resist final elimination of excavation porosity by creep closure, and presents a high chlorine concentration environment enabling reduced risk of in-package nuclear criticality. The main goals of the BATS field test are to collect data that lead to better understanding and possible confirmation of model predictions related to brine availability in bedded salt and to train a new generation of scientists and technicians on the use of underground research labs in the US for radioactive waste disposal.

The BATS phase 1a test array in N-940 has 14 boreholes in each array. Seven of the boreholes in each array have instrumentation grouted into them (T1, T2, E1, E2, E3, F1, F2), while four of the remaining boreholes are isolated with inflatable or mechanical packers (HP, D, SM, SL). The three AE boreholes are not grouted or sealed with packers.

In each array, electrical resistivity electrodes in the three E boreholes are used to interrogate changes in apparent resistivity through time due to brine migration and temperature variation. The ERT system has shown a sensitivity to the migration and distribution of brine during and after heating. The three AE boreholes contain decentralized piezoelectric transducers for monitoring and triangulating the source of acoustic emissions in the salt. Significant numbers of AE events were observed during the heating and cool-down phases, associated with the tensile fracture of salt during cooling. Many thermocouples are in the two T boreholes for monitoring the spatial and temporal variability of temperature around the heater. Aside from some interactions between the ERT system and the thermocouples (which may have led to premature failure of most of the thermocouples in the ERT boreholes), the thermocouples have proven to be generally robust in the salt environment. The SL borehole includes a laboratory-created composite seal (salt concrete and sorel cement), instrumented with strain gauges behind a mechanical packer. Over-coring of the heated SL borehole will be conducted before drilling the BATS phase 2 heated array to retrieve the cement seals and inspect the salt/cement/brine interactions that have occurred under heated conditions. The D boreholes were used for adding liquid and gas tracers. The central HP borehole contains a 750-watt heater used to heat a 69-cm interval of the borehole, while moisture is removed with flowing dry nitrogen for in-drift analyses of gas and water isotope composition.

The gas tracer tests confirmed the previous observation from packer testing that the heated array is more permeable than the unheated array, but during heating the heated array held pressure better than the unheated array (i.e., thermal expansion closes fractures reducing permeability). The response of the liquid tracer test is still ongoing and will be reported on after samples from post-test over-coring reveal the spatial distribution of tracers around the D and HP boreholes in the heated array.

Since March 2020, limited travel to WIPP has been allowed due to COVID-19 travel restrictions. The WIPP Test Coordination Office has maintained access to the WIPP underground, despite the limitations on travel from Albuquerque, Los Alamos, or Berkeley. Drilling of new boreholes for a new heated array (BATS phase 2) will be coordinated to occur when post-test core is being collected from the heated BATS phase 1a array, at the beginning of FY22. Additional laboratory analyses will be performed to characterize the native salt, tracers, and precipitated salts in boreholes. The unheated BATS phase 1a array will continue to collect passive data once over-coring and mining operations are complete.

8. References

- Bauer, S.J., W.P. Gardner & H. Lee, 2019. Noble gas release from bedded rock salt during deformation, *Geofluids*, 2871840:1-12.
- Beauheim, R.L. & R.M. Roberts, 2002. Hydrology and hydraulic properties of a bedded evaporite formation, *Journal of Hydrology*, 259(1-4):66-68.
- Boukhalfa, H., P.J. Johnson, D. Ware, D.J. Weaver, S. Otto, B.L. Dozier, P.H. Stauffer, M.M. Mills, E.N. Matteo, M.B. Nemer, C.G. Herrick, K.L. Kuhlman, Y. Wu & J. Rutqvist, 2018. *Implementation of Small Diameter Borehole Thermal Experiments at WIPP*, (70 p.) M3SF-18LA010303014, LA-UR-29203. Los Alamos, NM: Los Alamos National Laboratory.
- Boukhalfa, H., E. Gultinan, T. Rahn, D. Weaver, B. Dozier, S. Otto, P.H. Stauffer, M. Mills, K. Kuhlman, E. Matteo, C. Herrick, M. Nemer, J. Heath, Y. Xiong, C. Lopez, J. Rutqvist, Y. Wu & M. Hu, 2019. *2019 LANL Experiments and Simulations in Support of Salt R&D*, (34 p.) M3SF-19LA010303014, LA-UR-19-29830, Los Alamos, NM: Los Alamos National Laboratory.
- Clynne, M.A., R.W. Potter & L.D. White, 1981. *Analytical Results of Tagged Synthetic Brine Migration Experiments at Avery Island, Louisiana*, (16 p.) USGS Open File Report 81-1137. Menlo Park, CA: US Geological Survey.
- Gultinan, E.J., K.L. Kuhlman, J. Rutqvist, M. Hu, H. Boukhalfa, M. Mills, S. Otto, D.J. Weaver, B. Dozier & P.H. Stauffer, 2020. Temperature response and brine availability to heated boreholes in bedded salt, *Vadose Zone Journal*, 19(1):e20019.
- Gultinan, E., H. Boukhalfa, M. Dangelmayr, M. Janicke, O. Marina, S. Otto, T. Rahn, B. Dozier, D. Ware, D. Weaver, P.H. Stauffer, K.L. Kuhlman, M. Mills, R. Jayne, E. Matteo, C. Herrick, M. Nemer, J. Heath, Y. Xiong, C. Choens, M. Paul, J. Rutqvist, Y. Wu, M. Hu, 2021. *2021 LANL Contributions to the BATS Test in WIPP*, (62 p.) LA-UR-21-28130. Los Alamos, NM: Los Alamos National Laboratory.
- Jordan, A.B., H. Boukhalfa, F.A. Caporuscio; B.A. Robinson & P.H. Stauffer, 2015. Hydrous mineral dehydration around heat-generating nuclear waste in bedded salt formations, *Environmental Science & Technology*, 5:1-13.
- Kuhlman, K.L., S. Otto, P. Stauffer & Y. Wu, 2021. *Brine Availability Test in Salt (BATS) Extended Plan for Experiments at the Waste Isolation Pilot Plant (WIPP)*, (25 p.) SAND2021-3497R. Albuquerque, NM: Sandia National Laboratories.
- Kuhlman, K.L., 2019. *Processes in Salt Repositories*, (41 p.) SAND19-6441R, Albuquerque, NM: Sandia National Laboratories.
- Kuhlman, K.L. & B. Malama, 2013. *Brine Flow in Heated Geologic Salt*, (128 p.) SAND2013-1944, Carlsbad, NM: Sandia National Laboratories.
- Kuhlman, K.L. & S.D. Sevougian, 2013. *Establishing the Technical Basis for Disposal of Heat-Generating Waste in Salt*, (100 p.) SAND2013-6212P, FCRD-UFD-2013-000233. Albuquerque, NM: Sandia National Laboratories.
- Kuhlman, K.L., M.M. Mills & E.N. Matteo, 2017. *Consensus on Intermediate Scale Salt Field Test Design*, (95 p.) SAND2017-3179R, Albuquerque, NM: Sandia National Laboratories.
- Kuhlman, K.L., C.M. Lopez, M.M. Mills, J.M. Rimsza & D.C. Sassani, 2018. *Evaluation of Spent Nuclear Fuel Disposition in Salt (FY18)*, (83 p.) M2SF-18SN010303031, SAND2018-11355R, Albuquerque, NM: Sandia National Laboratories.

- Kuhlman, K., M. Mills, R. Jayne, E. Matteo, C. Herrick, M. Nemer, J. Heath, Y. Xiong, C. Choens, P. Stauffer, H. Boukhalfa, E. Guiltinan, T. Rahn, D. Weaver, B. Dozier, S. Otto, J. Rutqvist, Y. Wu, M. Hu, S. Uhlemann, J. Wang, 2021. *FY20 Update on Brine Availability Test in Salt*, (107 p.) SAND2020-9034R. Albuquerque, NM: Sandia National Laboratories.
- Magal, E., N. Weisbrod, A. Yakirevich & Y. Yechieli, 2008. The use of fluorescent dyes as tracers in highly saline groundwater. *Journal of Hydrology*, 358(1–2), 124–133.
- Roedder, E., 1984. The fluids in salt. *American Mineralogist*, 69(5–6):413–439.
- Rutqvist, J., M. Hu, H. Tounsi, Y. Wu, C. Steefel, S. Uhlemann, J. Wang & J. Birkholzer, 2021. *Salt Coupled THMC Processes Research Activities at LBNL: FY21 Progress* (114 p.) M3SF-21LB010303031, Berkeley, CA: Lawrence Berkeley National Laboratory.
- Sandia National Laboratories (SNL), LANL & LBNL, 2020. *Project Plan: Salt in situ Heater Test*, (20 p.) SAND2020-1251R.
- Stauffer, P.H., A.B. Jordan, D.J. Weaver, F.A. Caporuscio, J.A. Ten Cate, H. Boukhalfa, B.A. Robinson, D.C. Sassani, K.L. Kuhlman, E.L. Hardin, S.D. Sevougian, R.J. MacKinnon, Y. Wu, T.A. Daley, B.M. Freifeld, P.J. Cook, J. Rutqvist & J.T. Birkholzer, 2015. *Test Proposal Document for Phased Field Thermal Testing in Salt*, (104 p.) LA-UR-15-23154, FCRD-UFD-2015-000077. Los Alamos, NM: Los Alamos National Laboratory.
- Stauffer, P.H., E.J. Guiltinan, S.M. Bourret & G.A. Zyvoloski, 2019. *Salt Thermal Testing in Heated Boreholes: Experiments and Simulations*, (25 p.) M2SF-19LA010303011, LA-UR-19-22729, Los Alamos, NM: Los Alamos National Laboratory.
- Uhlemann, S., P.B. Wilkinson, H. Maurer, F.M. Wagner, J.C. Johnson & J.E. Chambers, 2018. Optimized survey design for electrical resistivity tomography: combined optimization of measurement configuration and electrode placement. *Geophysical Journal International* 214(1):108–121.
- Xiong, Y., 2008. *WIPP Procedure SP-20-4: Preparing Synthetic Brines for Geochemical Experiments, Revision 2*. Carlsbad, NM: Sandia National Laboratories.

A-1. Appendix: Tabular Data

Additional data, summarized or exemplified in figures in the main text, is presented here in tabular form. Tables listing borehole construction details are given in the appendix of the FY20 report (Kuhlman et al., 2020).

Table 4. Desiccant water production data for heated array.

Date Time Start	Date Time End	Delta Time [day]	Change in H ₂ O weight [g]	Change H ₂ O weight rate [g/day]	Upstream gas mass flow rate [std mL/min]
1/13/20 09:38	1/14/20 07:14	0.9000	40.67	45.189	2000
1/14/20 07:33	1/15/20 07:16	0.9882	2.01	2.034	200
1/15/20 07:16	1/16/20 07:23	1.0049	4.71	4.687	500
1/16/20 07:35	1/21/20 08:45	5.0486	5.35	1.060	150
1/21/20 08:56	1/22/20 07:29	0.9396	1.39	1.479	150
1/22/20 07:36	1/23/20 07:35	0.9993	2.34	2.342	150
1/23/20 07:35	1/27/20 07:10	3.9826	11.08	2.782	150
1/27/20 07:25	1/30/20 07:40	3.0104	1.74	0.578	50
1/30/20 07:40	2/3/20 07:14	3.9819	3.23	0.811	50
2/3/20 07:14	2/6/20 07:27	3.0090	2.56	0.851	50
2/6/20 07:27	2/10/20 07:45	4.0125	2.55	0.636	50
2/10/20 07:45	2/12/20 12:24	2.1938	1.29	0.588	50
2/12/20 12:24	2/18/20 08:18	5.8292	2.26	0.388	50
2/18/20 08:18	2/20/20 07:53	1.9826	43.90	22.142	50
2/20/20 08:11	2/24/20 11:13	4.1264	54.93	13.312	50
2/24/20 11:13	2/26/20 08:18	1.8785	3.37	1.794	75
2/26/20 08:18	3/2/20 07:14	4.9556	6.41	1.293	75
3/2/20 07:10	3/3/20 07:37	1.0188	1.85	1.816	75
4/28/20 09:22	4/29/20 08:03	0.9451	29.35	31.054	1000
4/29/20 08:07	4/30/20 08:14	1.0049	35.70	35.527	1000
4/30/20 08:20	5/1/20 07:33	0.9674	35.35	36.543	1000
5/1/20 07:39	5/5/20 07:43	4.0028	34.56	8.634	250
5/5/20 08:14	5/6/20 07:46	0.9806	31.67	32.298	1000
5/6/20 07:50	5/7/20 08:04	1.0097	23.94	23.709	1000
5/7/20 08:11	5/8/20 08:21	1.0069	4.56	4.529	250
5/8/20 08:21	5/12/20 08:03	3.9875	16.95	4.251	250
5/12/20 08:03	5/13/20 08:38	1.0243	3.36	3.280	200
5/13/20 08:38	5/14/20 07:58	0.9722	3.34	3.435	200
5/14/20 07:58	5/14/20 14:01	0.2521	2.55	10.116	200
5/14/20 14:01	5/15/20 08:03	0.7514	19.25	25.619	750
5/15/20 08:08	5/20/20 08:28	5.0139	18.91	3.772	200
5/20/20 08:28	5/21/20 07:58	0.9792	3.14	3.207	200
5/21/20 07:58	5/22/20 07:42	0.9889	1.12	1.133	75
5/22/20 07:46	5/26/20 07:43	3.9979	5.71	1.428	75
5/26/20 07:43	5/27/20 08:15	1.0222	2.05	2.005	75
5/27/20 08:15	5/28/20 07:31	0.9694	1.23	1.269	75
5/28/20 07:31	6/2/20 08:17	5.0319	8.64	1.717	75
6/2/20 10:55	6/4/20 07:52	1.8729	3.34	1.783	75
6/4/20 13:50	6/9/20 08:10	4.7639	8.47	1.778	75
6/9/20 11:27	6/16/20 08:04	6.8590	12.15	1.771	75
6/16/20 08:04	6/17/20 08:40	1.0250	1.70	1.659	75
6/17/20 08:40	6/22/20 07:31	4.9521	9.13	1.844	75
6/22/20 07:31	6/23/20 08:10	1.0271	1.84	1.791	75
6/23/20 08:20	6/24/20 08:26	1.0042	1.75	1.743	75
6/24/20 08:26	6/29/20 08:57	5.0215	9.01	1.794	75
6/29/20 08:57	6/30/20 08:19	0.9736	1.70	1.746	75
6/30/20 08:19	7/1/20 07:46	0.9771	1.76	1.801	75
7/1/20 07:46	7/7/20 08:16	6.0208	10.81	1.795	75
7/7/20 08:16	7/8/20 08:05	0.9924	1.79	1.804	75

7/8/20 08:14	7/14/20 07:40	5.9764	11.01	1.842	75
7/14/20 12:03	7/16/20 08:12	1.8396	3.30	1.794	75
7/16/20 08:12	7/20/20 07:40	3.9778	7.69	1.933	75
7/20/20 08:08	7/23/20 07:47	2.9854	5.89	1.973	75
7/23/20 07:47	7/27/20 08:30	4.0299	7.98	1.980	75
7/27/20 08:30	8/4/20 08:31	8.0007	14.49	1.811	75
8/4/20 08:31	8/5/20 07:37	0.9625	1.65	1.714	75
8/5/20 07:37	8/6/20 08:03	1.0181	1.71	1.680	75
8/6/20 08:03	8/11/20 08:11	5.0056	8.30	1.658	75
8/11/20 08:11	8/17/20 07:53	5.9875	8.88	1.483	75
8/17/20 12:10	8/24/20 08:05	6.8299	11.68	1.710	75
8/24/20 08:05	8/31/20 08:10	7.0035	12.20	1.742	75
8/31/20 08:10	9/8/20 07:35	7.9757	13.18	1.653	75
9/8/20 07:35	9/14/20 07:39	6.0028	8.22	1.369	75
9/14/20 07:49	9/17/20 07:40	2.9938	4.28	1.430	75
9/17/20 07:40	9/21/20 07:37	3.9979	5.46	1.366	75
9/21/20 07:37	9/24/20 08:15	3.0264	3.91	1.292	75
9/24/20 08:15	9/28/20 07:45	3.9792	4.79	1.204	75
9/28/20 07:45	10/1/20 07:43	2.9986	2.16	0.720	50
10/1/20 07:43	10/5/20 07:46	4.0021	3.10	0.775	50
10/5/20 07:58	10/12/20 09:26	7.0611	4.98	0.705	50
10/12/20 09:26	10/14/20 08:00	1.9403	1.56	0.804	50
10/14/20 08:00	10/19/20 07:49	4.9924	3.49	0.699	50
10/19/20 07:49	10/26/20 08:08	7.0132	5.29	0.754	50
10/26/20 08:08	10/28/20 11:55	2.1576	1.38	0.640	50
10/28/20 11:55	11/2/20 08:30	4.8576	3.93	0.809	50
11/2/20 08:30	11/9/20 08:13	6.9882	5.58	0.798	50
11/9/20 08:25	11/18/20 09:50	9.0590	6.70	0.740	50
11/18/20 09:50	12/7/20 08:10	18.9306	12.30	0.650	50
12/7/20 08:10	12/21/20 08:32	14.0153	7.42	0.529	50
12/21/20 08:32	1/11/21 08:20	20.9917	8.73	0.416	50
1/11/21 08:20	1/13/21 07:08	1.9500	0.60	0.308	50
1/13/21 07:08	1/19/21 07:52	6.0306	1.97	0.327	50
1/19/21 07:52	1/25/21 07:40	5.9917	2.11	0.352	50
1/25/21 07:40	2/1/21 07:45	7.0035	2.55	0.364	50
2/1/21 07:45	2/3/21 07:35	1.9931	2.41	1.209	50
2/3/21 07:35	2/8/21 07:52	5.0118	4.91	0.980	50
2/8/21 07:52	2/10/21 07:58	2.0042	1.66	0.828	50
2/10/21 07:58	2/16/21 07:40	5.9875	8.19	1.368	50
2/16/21 07:40	2/22/21 07:32	5.9944	7.73	1.290	50
2/22/21 07:41	2/24/21 07:52	2.0076	2.41	1.200	50
2/24/21 07:52	3/1/21 07:35	4.9882	5.89	1.181	50
3/1/21 07:35	3/8/21 07:50	7.0104	8.36	1.193	50
3/8/21 07:50	4/12/21 10:50	35.1250	35.44	1.009	50
4/12/21 11:01	4/13/21 10:30	0.9785	1.22	1.247	50
4/13/21 10:30	4/19/21 08:07	5.9007	6.14	1.041	50
4/19/21 08:07	4/21/21 09:55	2.0750	1.90	0.916	50
4/21/21 09:55	4/26/21 08:14	4.9299	4.37	0.886	50
4/26/21 08:14	5/3/21 08:14	7.0000	6.13	0.876	50
5/3/21 08:22	5/10/21 07:47	6.9757	5.69	0.816	50
5/10/21 07:47	5/13/21 09:53	3.0875	2.54	0.823	50
5/13/21 09:53	5/17/21 07:30	3.9007	4.52	1.159	50
5/17/21 07:30	5/18/21 07:54	1.0167	1.45	1.426	50
5/18/21 07:54	5/24/21 07:21	5.9771	9.53	1.594	50
5/24/21 07:21	5/26/21 07:39	2.0125	3.74	1.858	50
5/26/21 07:44	6/1/21 08:31	6.0326	14.62	2.423	50
6/1/21 08:31	6/3/21 07:57	1.9764	4.74	2.400	50
6/3/21 07:57	6/7/21 07:52	3.9965	9.88	2.472	50
6/7/21 07:52	6/14/21 09:33	7.0701	14.02	1.983	50

6/14/21 09:38	6/16/21 08:10	1.9389	3.06	1.578	50
6/16/21 08:10	6/21/21 08:45	5.0243	5.19	1.033	50
6/21/21 08:45	6/23/21 10:08	2.0576	2.87	1.395	50
6/23/21 10:08	6/28/21 08:30	4.9319	7.20	1.460	50
6/28/21 08:40	6/29/21 07:40	0.9583	1.36	1.419	50
6/29/21 07:40	6/30/21 08:30	1.0347	2.18	2.107	50
6/30/21 08:30	7/6/21 07:45	5.9688	14.05	2.354	50
7/6/21 07:50	7/12/21 09:24	6.0653	14.01	2.310	50
7/12/21 09:24	7/14/21 07:37	1.9257	4.47	2.321	50
7/14/21 07:37	7/15/21 07:48	1.0076	2.22	2.203	50
7/15/21 07:48	7/19/21 08:04	4.0111	9.61	2.396	50
7/19/21 08:04	7/21/21 07:40	1.9833	4.75	2.395	50
7/21/21 07:47	7/22/21 09:00	1.0507	2.35	2.237	50
7/22/21 09:00	7/26/21 07:56	3.9556	7.33	1.853	50
7/26/21 07:56	7/27/21 12:52	1.2056	2.03	1.684	50
7/27/21 12:52	8/2/21 07:55	5.7937	10.25	1.769	50
8/2/21 07:55	8/9/21 08:26	7.0215	12.47	1.776	50
8/9/21 08:33	8/17/21 09:53	8.0556	13.33	1.655	50
8/17/21 09:53	8/19/21 12:06	2.0924	3.68	1.759	50
8/19/21 12:06	8/23/21 08:15	3.8396	6.77	1.763	50

Table 5. Desiccant water production data for unheated array.

Date Time Start	Date Time End	Delta Time [day]	Change in H ₂ O weight [g]	Change H ₂ O weight rate [g/day]	Upstream gas mass flow rate [std mL/min]
1/13/20 09:38	1/14/20 07:14	0.9000	40.67	45.189	2000
1/14/20 07:33	1/15/20 07:16	0.9882	2.01	2.034	200
1/15/20 07:16	1/16/20 07:23	1.0049	4.71	4.687	500
1/16/20 07:35	1/21/20 08:45	5.0486	5.35	1.060	150
1/21/20 08:56	1/22/20 07:29	0.9396	1.39	1.479	150
1/22/20 07:36	1/23/20 07:35	0.9993	2.34	2.342	150
1/23/20 07:35	1/27/20 07:10	3.9826	11.08	2.782	150
1/27/20 07:25	1/30/20 07:40	3.0104	1.74	0.578	50
1/30/20 07:40	2/3/20 07:14	3.9819	3.23	0.811	50
2/3/20 07:14	2/6/20 07:27	3.0090	2.56	0.851	50
2/6/20 07:27	2/10/20 07:45	4.0125	2.55	0.636	50
2/10/20 07:45	2/12/20 12:24	2.1938	1.29	0.588	50
2/12/20 12:24	2/18/20 08:18	5.8292	2.26	0.388	50
2/18/20 08:18	2/20/20 07:53	1.9826	43.90	22.142	50
2/20/20 08:11	2/24/20 11:13	4.1264	54.93	13.312	50
2/24/20 11:13	2/26/20 08:18	1.8785	3.37	1.794	75
2/26/20 08:18	3/2/20 07:14	4.9556	6.41	1.293	75
3/2/20 07:10	3/3/20 07:37	1.0188	1.85	1.816	75
4/28/20 09:22	4/29/20 08:03	0.9451	29.35	31.054	1000
4/29/20 08:07	4/30/20 08:14	1.0049	35.70	35.527	1000
4/30/20 08:20	5/1/20 07:33	0.9674	35.35	36.543	1000
5/1/20 07:39	5/5/20 07:43	4.0028	34.56	8.634	250
5/5/20 08:14	5/6/20 07:46	0.9806	31.67	32.298	1000
5/6/20 07:50	5/7/20 08:04	1.0097	23.94	23.709	1000
5/7/20 08:11	5/8/20 08:21	1.0069	4.56	4.529	250
5/8/20 08:21	5/12/20 08:03	3.9875	16.95	4.251	250
5/12/20 08:03	5/13/20 08:38	1.0243	3.36	3.280	200
5/13/20 08:38	5/14/20 07:58	0.9722	3.34	3.435	200
5/14/20 07:58	5/14/20 14:01	0.2521	2.55	10.116	200
5/14/20 14:01	5/15/20 08:03	0.7514	19.25	25.619	750
5/15/20 08:08	5/20/20 08:28	5.0139	18.91	3.772	200
5/20/20 08:28	5/21/20 07:58	0.9792	3.14	3.207	200
5/21/20 07:58	5/22/20 07:42	0.9889	1.12	1.133	75
5/22/20 07:46	5/26/20 07:43	3.9979	5.71	1.428	75
5/26/20 07:43	5/27/20 08:15	1.0222	2.05	2.005	75
5/27/20 08:15	5/28/20 07:31	0.9694	1.23	1.269	75
5/28/20 07:31	6/2/20 08:17	5.0319	8.64	1.717	75
6/2/20 10:55	6/4/20 07:52	1.8729	3.34	1.783	75
6/4/20 13:50	6/9/20 08:10	4.7639	8.47	1.778	75
6/9/20 11:27	6/16/20 08:04	6.8590	12.15	1.771	75
6/16/20 08:04	6/17/20 08:40	1.0250	1.70	1.659	75
6/17/20 08:40	6/22/20 07:31	4.9521	9.13	1.844	75
6/22/20 07:31	6/23/20 08:10	1.0271	1.84	1.791	75
6/23/20 08:20	6/24/20 08:26	1.0042	1.75	1.743	75
6/24/20 08:26	6/29/20 08:57	5.0215	9.01	1.794	75
6/29/20 08:57	6/30/20 08:19	0.9736	1.70	1.746	75
6/30/20 08:19	7/1/20 07:46	0.9771	1.76	1.801	75
7/1/20 07:46	7/7/20 08:16	6.0208	10.81	1.795	75
7/7/20 08:16	7/8/20 08:05	0.9924	1.79	1.804	75
7/8/20 08:14	7/14/20 07:40	5.9764	11.01	1.842	75
7/14/20 12:03	7/16/20 08:12	1.8396	3.30	1.794	75
7/16/20 08:12	7/20/20 07:40	3.9778	7.69	1.933	75
7/20/20 08:08	7/23/20 07:47	2.9854	5.89	1.973	75
7/23/20 07:47	7/27/20 08:30	4.0299	7.98	1.980	75
7/27/20 08:30	8/4/20 08:31	8.0007	14.49	1.811	75

8/4/20 08:31	8/5/20 07:37	0.9625	1.65	1.714	75
8/5/20 07:37	8/6/20 08:03	1.0181	1.71	1.680	75
8/6/20 08:03	8/11/20 08:11	5.0056	8.30	1.658	75
8/11/20 08:11	8/17/20 07:53	5.9875	8.88	1.483	75
8/17/20 12:10	8/24/20 08:05	6.8299	11.68	1.710	75
8/24/20 08:05	8/31/20 08:10	7.0035	12.20	1.742	75
8/31/20 08:10	9/8/20 07:35	7.9757	13.18	1.653	75
9/8/20 07:35	9/14/20 07:39	6.0028	8.22	1.369	75
9/14/20 07:49	9/17/20 07:40	2.9938	4.28	1.430	75
9/17/20 07:40	9/21/20 07:37	3.9979	5.46	1.366	75
9/21/20 07:37	9/24/20 08:15	3.0264	3.91	1.292	75
9/24/20 08:15	9/28/20 07:45	3.9792	4.79	1.204	75
9/28/20 07:45	10/1/20 07:43	2.9986	2.16	0.720	50
10/1/20 07:43	10/5/20 07:46	4.0021	3.10	0.775	50
10/5/20 07:58	10/12/20 09:26	7.0611	4.98	0.705	50
10/12/20 09:26	10/14/20 08:00	1.9403	1.56	0.804	50
10/14/20 08:00	10/19/20 07:49	4.9924	3.49	0.699	50
10/19/20 07:49	10/26/20 08:08	7.0132	5.29	0.754	50
10/26/20 08:08	10/28/20 11:55	2.1576	1.38	0.640	50
10/28/20 11:55	11/2/20 08:30	4.8576	3.93	0.809	50
11/2/20 08:30	11/9/20 08:13	6.9882	5.58	0.798	50
11/9/20 08:25	11/18/20 09:50	9.0590	6.70	0.740	50
11/18/20 09:50	12/7/20 08:10	18.9306	12.30	0.650	50
12/7/20 08:10	12/21/20 08:32	14.0153	7.42	0.529	50
12/21/20 08:32	1/11/21 08:20	20.9917	8.73	0.416	50
1/11/21 08:20	1/13/21 07:08	1.9500	0.60	0.308	50
1/13/21 07:08	1/19/21 07:52	6.0306	1.97	0.327	50
1/19/21 07:52	1/25/21 07:40	5.9917	2.11	0.352	50
1/25/21 07:40	2/1/21 07:45	7.0035	2.55	0.364	50
2/1/21 07:45	2/3/21 07:35	1.9931	2.41	1.209	50
2/3/21 07:35	2/8/21 07:52	5.0118	4.91	0.980	50
2/8/21 07:52	2/10/21 07:58	2.0042	1.66	0.828	50
2/10/21 07:58	2/16/21 07:40	5.9875	8.19	1.368	50
2/16/21 07:40	2/22/21 07:32	5.9944	7.73	1.290	50
2/22/21 07:41	2/24/21 07:52	2.0076	2.41	1.200	50
2/24/21 07:52	3/1/21 07:35	4.9882	5.89	1.181	50
3/1/21 07:35	3/8/21 07:50	7.0104	8.36	1.193	50
3/8/21 07:50	4/12/21 10:50	35.1250	35.44	1.009	50
4/12/21 11:01	4/13/21 10:30	0.9785	1.22	1.247	50
4/13/21 10:30	4/19/21 08:07	5.9007	6.14	1.041	50
4/19/21 08:07	4/21/21 09:55	2.0750	1.90	0.916	50
4/21/21 09:55	4/26/21 08:14	4.9299	4.37	0.886	50
4/26/21 08:14	5/3/21 08:14	7.0000	6.13	0.876	50
5/3/21 08:22	5/10/21 07:47	6.9757	5.69	0.816	50
5/10/21 07:47	5/13/21 09:53	3.0875	2.54	0.823	50
5/13/21 09:53	5/17/21 07:30	3.9007	4.52	1.159	50
5/17/21 07:30	5/18/21 07:54	1.0167	1.45	1.426	50
5/18/21 07:54	5/24/21 07:21	5.9771	9.53	1.594	50
5/24/21 07:21	5/26/21 07:39	2.0125	3.74	1.858	50
5/26/21 07:44	6/1/21 08:31	6.0326	14.62	2.423	50
6/1/21 08:31	6/3/21 07:57	1.9764	4.74	2.400	50
6/3/21 07:57	6/7/21 07:52	3.9965	9.88	2.472	50
6/7/21 07:52	6/14/21 09:33	7.0701	14.02	1.983	50
6/14/21 09:38	6/16/21 08:10	1.9389	3.06	1.578	50
6/16/21 08:10	6/21/21 08:45	5.0243	5.19	1.033	50
6/21/21 08:45	6/23/21 10:08	2.0576	2.87	1.395	50
6/23/21 10:08	6/28/21 08:30	4.9319	7.20	1.460	50
6/28/21 08:40	6/29/21 07:40	0.9583	1.36	1.419	50
6/29/21 07:40	6/30/21 08:30	1.0347	2.18	2.107	50

Salt Heater Test (FY21)

August 2021

53

6/30/21 08:30	7/6/21 07:45	5.9688	14.05	2.354	50
7/6/21 07:50	7/12/21 09:24	6.0653	14.01	2.310	50
7/12/21 09:24	7/14/21 07:37	1.9257	1.76	0.914	25
7/14/21 07:37	7/15/21 07:48	1.0076	0.78	0.774	25
7/15/21 07:48	7/19/21 08:04	4.0111	2.53	0.631	25
7/19/21 08:04	7/21/21 07:40	1.9833	1.36	0.686	25
7/21/21 07:47	7/22/21 09:00	1.0507	0.26	0.247	25
7/22/21 09:00	7/26/21 07:56	3.9556	2.08	0.526	25
7/26/21 07:56	7/27/21 12:52	1.2056	0.53	0.440	25
7/27/21 12:52	8/2/21 07:55	5.7937	2.73	0.471	25
8/2/21 07:55	8/9/21 08:26	7.0215	3.07	0.437	25
8/9/21 08:33	8/17/21 09:53	8.0556	3.28	0.407	25
8/17/21 09:53	8/19/21 12:06	2.0924	0.91	0.435	25
8/19/21 12:06	8/23/21 08:15	3.8396	1.48	0.385	25

Table 6. BATS TCO Events through July 2021

Date	Time	Event	Description
1/21/20	12:09	Heating	Turn on heater - 120 °C set point.
2/18/20	08:15	Heating	Turned off heater
4/29/20	08:53	Heating	Start heater for oscilloscope measurements of power controller.
4/29/20	11:30	Heating	Turn heater off.
4/30/20	08:53	Heating	Start heater for oscilloscope measurements of power controller.
4/30/20	12:15	Heating	Turn heater off.
5/14/20	08:21	Heating	Heater set to 70 °C @ 100% power datalogger = 5.58 A, scope = 6.22 to 6.23 A, fluke = 6.35 A, scope = 118 to 119 V AC. (scope measurements for 6 peaks)
5/14/20	08:37	Heating	Heater set point of 70 °C reached.
5/14/20	09:39	Heating	Heater set point changed to 120 °C.
5/14/20	13:37	Heating	Heater reached 120 °C
5/14/20	14:15	Heating	Heater set point changed to 28 °C and heater unplugged from Watlow controller.
7/14/20	08:47	Permeability	Permeability testing in H-HP borehole. Leak checks of the packer assembly found leaks. Permeability test is suspect.
7/14/20	09:18	Permeability	Permeability testing in H-D borehole. Rapid pressure loss. Permeability test is suspect.
7/14/20	09:55	Permeability	Deflate H-D packer for leak checks. Move packer to front/top of borehole and inflate. Start circulation flow and leak check. No obvious leaks found, but leak checking is suspect since pressure behind packer is minimal due to DRZ.
7/14/20	11:00	Permeability	Permeability testing in Unheated HP borehole. Leak checks of the packer assembly did not show any leaks.
7/14/20	11:51	Permeability	Permeability testing in Unheated D borehole. Leak checks of the packer assembly did not show any leaks.
7/16/20	08:30	Permeability	Start permeability testing unheated array.
7/20/20	07:47	Permeability	Start permeability testing Heated D.
7/23/20	07:49	Permeability	Start permeability testing to Heated D borehole, testing interval 9.00 to 15.00 ft.
7/23/20	08:26	Permeability	End permeability testing to H-D borehole. Note - the pressure was set to ~20 psi for this test and the borehole pressure remained <5.6 psi indicating a leak or significant permeability.
7/27/20	05:10	Permeability	Review of Heated D permeability test suggests there is a leak related to the inflation pressure, most likely the Heated D packer. Inflation pressure started slowly decreasing on 7/22/2020 @ ~8:45.
7/27/20	09:12	Permeability	Start of Unheated D permeability test at ~15 psi.
7/27/20	14:00	Permeability	Data review of inflation pressures to packers shows that the psi decreased to ~38 psi which supports the packers in the HP boreholes remained inflated and the vapor testing data were not impacted. Following the inflation tank cylinder change and removal of the Heated D leaking packer the inflation pressure to the HP packers is ~78 psi.
8/4/20	08:37	Permeability	Close unheated circulation valve to Unheated HP and open valve to Unheated D at ~30 psi for Unheated D permeability test.
8/17/20	07:50	Permeability	Open HC flow valve to Heated D - start of Heated D permeability test at ~20 psi.
9/24/20	na	Tracer	Tracer testing plumbing, parts/pieces, and instrumentation added to experiment.
10/1/20	10:20	Tracer	Leak tested DEC and tracer testing equipment.
11/2/20	12:48	Permeability	Start permeability test of UD borehole at 20 psi.
12/21/20	09:15	Permeability	UD borehole psi equilibrium reached (~19.5 psi) and then gas circulation flow ended for start of permeability test.
1/11/21	09:15	Permeability	Ended UD perm test by releasing pressure behind UD packer.
1/11/21	10:09	Tracer	Started tracer test in UD borehole. Note - GA and AE systems were started and collecting data today, prior to starting the tracer test.
1/11/21	10:29	Tracer	Ended tracer test in UD borehole by closing N ₂ circulation. Pressure was ~45.6 psi. Tracer and nitrogen are in UD borehole for GA monitoring for break-through.
1/25/21	07:56	Heating	Turn on heater with a set point 35 °C.
1/25/21	08:00	Heating	Turn off heater when set point 35 °C was reached.
2/1/21	08:30	Tracer	Start tracer test for the heated D borehole. 30 psi for the DEC and chased with 15 psi N ₂ .
2/1/21	08:42	Tracer	End tracer test, D borehole ~15.56 psi at end of N ₂ chasing.
2/1/21	na	Tracer	Flow controller located outside the heated D borehole did not work for tracer test.
2/10/21	08:34	Tracer	Start tracer test, fill DEC to 60 psi (actual psi was ~61 at end of filling DEC) and chase with 30 psi of N ₂ .
2/10/21	08:42	Tracer	When starting N ₂ chasing, a small amount of tracer/N ₂ activated the unheated circulation tank regulator pressure relief valve for ~5 seconds.
2/10/21	08:52	Tracer	End N ₂ chasing of tracer into HD borehole. Pressure at end of gas flow was ~29.56 psi.
4/13/21	10:02	Tracer	Started filling DEC with tracer gas @ 60 psi.
4/13/21	10:09	Tracer	End time for filling DEC with tracer gas.
4/13/21	10:11	Tracer	Open valves to allow flow of tracer gas from DEC to heated D borehole.
4/13/21	10:12	Tracer	Started chasing tracer gas with nitrogen to heated D borehole @ 30 psi.
4/13/21	10:20	Tracer	Tracer gas after tracer test at 1850 psi.
4/13/21	10:21	Tracer	Ended nitrogen chasing/flow to heated D borehole. Pressure 29.94 psi before valve closed.
5/13/21	11:10	Heating	Start heater in the heated HP borehole. Set point was set to 120 °C.
5/13/21	12:20	Heating	Temperature in the heated HP borehole was 70 °C.
5/17/21	07:10	Heating	Check of heated HP heater showed that the heater was off. Heater power controller re-started (hard/unplug re-start) and set point set to 120 °C.
5/17/21	07:38	Heating	Check of heater showed that the temperature in the heated HP borehole was 50 °C.
5/18/21	07:35	Heating	HP heater is off due to automatic shutdown. Hard reset the heater power controller.
5/18/21	07:36	Heating	Re-start HP heater with a set point of 75 °C.
5/18/21	08:02	Heating	Heater check showed temperature 46 °C.
5/18/21	09:08	Heating	Heater check showed temperature 75 °C and power at ~70%.
5/24/21	07:07	Heating	Change heater set point to 90 °C.
5/26/21	07:24	Heating	Change heater set point to 110 °C.
5/26/21	07:51	Heating	Heater at 110 °C and power at 95%.
5/26/21	07:52	Heating	Change heater set point to 113 °C.
5/26/21	07:57	Heating	Heater at 113 °C and power at 97%.
5/26/21	08:00	Heating	Heater at 113 °C and power at 92%.
5/26/21	08:01	Heating	Change heater set point to 115 °C.
5/26/21	08:04	Heating	Heater at 115 °C and power at 99%.

5/26/21	08:15	Heating	Heater at 115 °C and power at 90%.
5/26/21	09:45	Heating	Heater at 115 °C and power at 83.5%.
6/1/21	07:52	Heating	Heater at 115 °C and power at 75%.
6/3/21	08:25	Tracer	Started filling DEC with tracer gas @ 60.5 psi.
6/3/21	08:32	Tracer	End time for filling DEC with tracer gas.
6/3/21	08:33	Tracer	Open valves to allow flow of tracer gas from DEC to heated D borehole.
6/3/21	08:35	Tracer	Started chasing tracer gas with nitrogen to heated D borehole @ 30 psi.
6/3/21	08:36	Tracer	Tracer gas after tracer test at 1840 psi.
6/3/21	08:43	Tracer	Ended nitrogen chasing/flow to heated D borehole. Pressure at 30.67 psi before valve closed.
6/16/21	07:53	Heating	Set heater set point to 28 °C (turn off heater).
6/16/21	08:06	Heating	Unplug heater from heater controller.
6/29/21	07:33	Heating	Hard reset of power controller.
6/29/21	07:35	Heating	Power controller set point set to 50 °C. Temperature of borehole at start was ~32 °C.
6/29/21	07:58	Heating	Heater set point changed to 75 °C. Heater was at 44 °C.
6/29/21	08:07	Heating	Heater set point changed to 90 °C. Heater was at 49 °C.
6/29/21	08:13	Heating	Heater power output at 55%.
6/29/21	08:14	Heating	Heater set point changed to 100 °C. Heater was at 52 °C.
6/29/21	10:17	Heating	Heater check that the heater shutdown automatically at ~92 °C and the power output was 100%.
6/29/21	10:20	Heating	Re-start heater with an 85 °C set point.
6/29/21	11:37	Heating	Heater at 85 °C and 86% power.
6/30/21	07:48	Heating	Heater check showed temperature 85 °C and 54% power. Heater set point changed to 95 °C.
6/30/21	07:57	Tracer	Open air bleed-off valve for the pass thru in the unheated D borehole packer and start brine tracer injection in the 2nd pass thru.
6/30/21	08:05	Tracer	Finish brine tracer injection in the unheated D borehole. 1000 mL of brine tracer injected. Air valve closed.
6/30/21	08:06	Heating	Heater at 94 °C and 81% power. Set point changed to 105 °C.
6/30/21	08:27	Heating	Heater at 105 °C and 96% power. Set point changed to 108 °C.
6/30/21	08:39	Heating	Heater at 109 °C and 94% power. Set point changed to 112 °C.
6/30/21	08:51	Heating	Heater at 112 °C and 98% power.
6/30/21	09:29	Heating	Heater at 112 °C and 89% power. Set point changed to 115 °C.
6/30/21	09:37	Heating	Heater at 115 °C and 99% power.
6/30/21	09:41	Heating	Heater at 115 °C and 96.5% power.
6/30/21	10:45	Heating	Heater at 115 °C and 90% power.
7/6/21	07:45	Heating	Heater stable at 115 °C.
7/7/21	09:35	Tracer	Measured remaining brine tracer solution and noted that 950 ml was available for brine injection.
7/7/21	09:40	Tracer	Connected brine injection apparatus to fill valve. Started brine injection into heated D borehole.
7/7/21	09:50	Tracer	Completed brine injection into heated D borehole. 950mL of brine tracer injected. Closed air valve.
7/14/21	12:24	Heating	Changed the heater set point to 28 °C and unplugged the heater from the power controller to end the heating of the heated HP borehole.

APPENDIX E

NFCSC DOCUMENT COVER SHEET¹

Name/Title of Deliverable/Milestone/Revision No. Brine Availability Test in Salt (BATS) FY21 Update

Work Package Title and Number Salt Disposal R&D – SNL

Work Package WBS Number SF-21SN01030305

Responsible Work Package Manager Kris Kuhlman  (Name/Signature)

Date Submitted _____

Quality Rigor Level for Deliverable/Milestone ²	<input type="checkbox"/> QRL-1 <input type="checkbox"/> Nuclear Data	<input type="checkbox"/> QRL-2	<input checked="" type="checkbox"/> QRL-3	<input type="checkbox"/> QRL-4 Lab QA Program ³
--	---	--------------------------------	---	---

This deliverable was prepared in accordance with Sandia National Laboratories (*Participant/National Laboratory Name*) QA program which meets the requirements of

DOE Order 414.1 NQA-1 Other

This Deliverable was subjected to:

Technical Review

Peer Review

Technical Review (TR)

Peer Review (PR)

Review Documentation Provided

Review Documentation Provided

Signed TR Report or,

Signed PR Report or,

Signed TR Concurrence Sheet or,

Signed PR Concurrence Sheet or,

Signature of TR Reviewer(s) below

Signature of PR Reviewer(s)

below

Name and Signature of Reviewers

Jason Heath



NOTE 1: Appendix E should be filled out and submitted with the deliverable. Or, if the PICS:NE system permits, completely enter all applicable information in the PICS:NE Deliverable Form. The requirement is to ensure that all applicable information is entered either in the PICS:NE system or by using the NFCSC Document Cover Sheet.

- In some cases there may be a milestone where an item is being fabricated, maintenance is being performed on a facility, or a document is being issued through a formal document control process where it specifically calls out a formal review of the document. In these cases, documentation (e.g., inspection report, maintenance request, work planning package documentation or the documented review of the issued document through the document control process) of the completion of the activity, along with the Document Cover Sheet, is sufficient to demonstrate achieving the milestone.

NOTE 2: If QRL 1, 2, or 3 is not assigned, then the QRL 4 box must be checked, and the work is understood to be performed using laboratory QA requirements. This includes any deliverable developed in conformance with the respective National Laboratory / Participant, DOE or NNSA-approved QA Program.

NOTE 3: If the lab has an NQA-1 program and the work to be conducted requires an NQA-1 program, then the QRL-1 box must be checked in the work Package and on the Appendix E cover sheet and the work must be performed in accordance with the Lab's NQA-1 program. The QRL-4 box should not be checked.